Cosmic Microwave Background: Foregrounds and Secondary Anisotropies

arXiv: 1811.02310
arXiv: 1112.1862
arXiv:1212.1075
arXiv:1511.04335
arXiv:1312.2462
arXiv:1303.5081

(Secondary) CMB anisotropies:
Polarization
Reionization
Sunyaev Zeldovich Effect

arXiv: 1811.02310
arXiv: 1112.1862
arXiv:1212.1075
arXiv:1511.04335
arXiv:1312.2462
arXiv:1303.5081

CMB

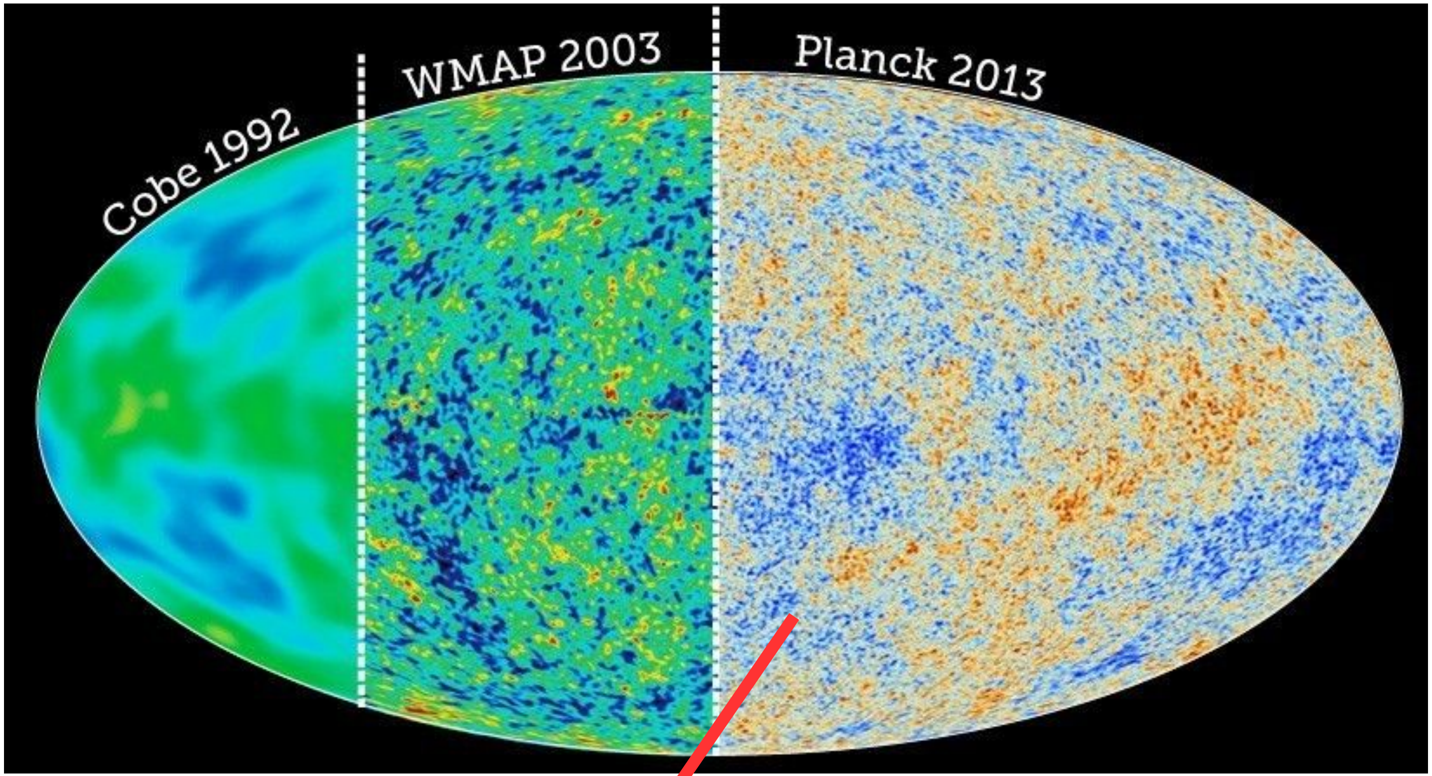

TT Power Spectrum information is sample-variance limited

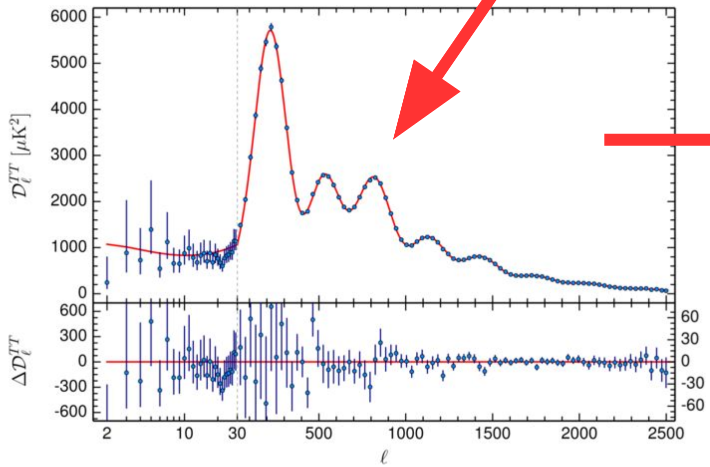

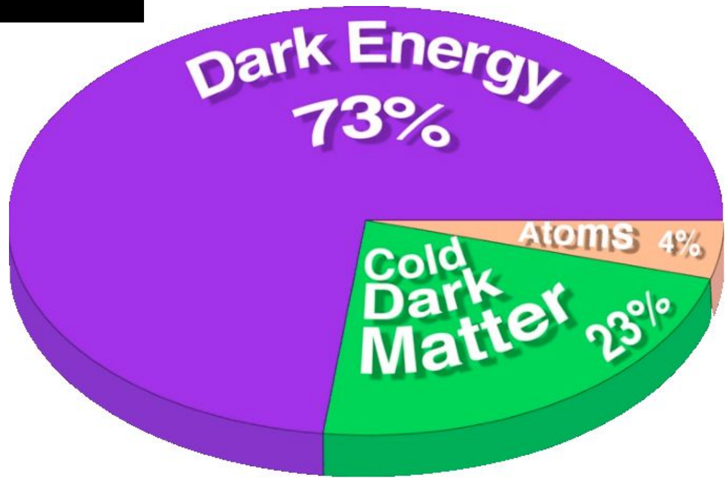

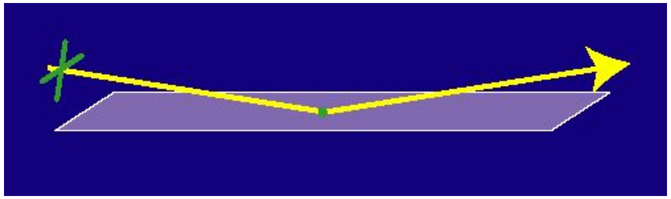

Polarization

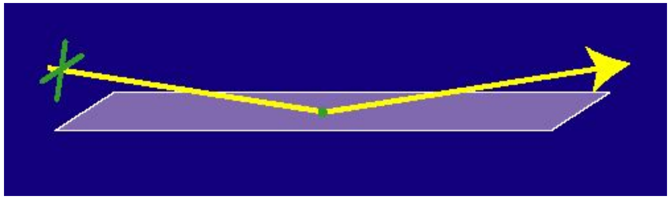

Polarization

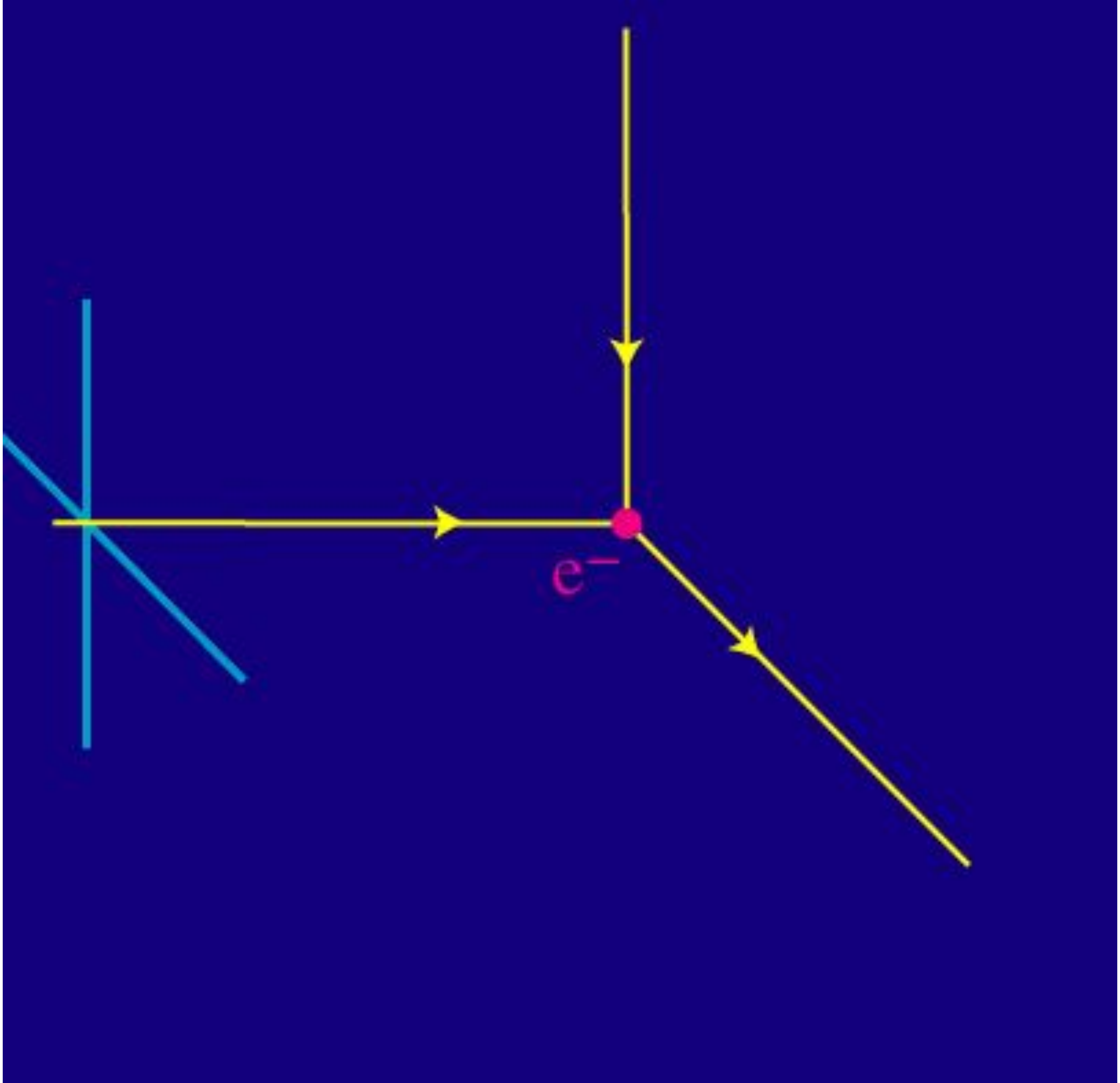
e^-

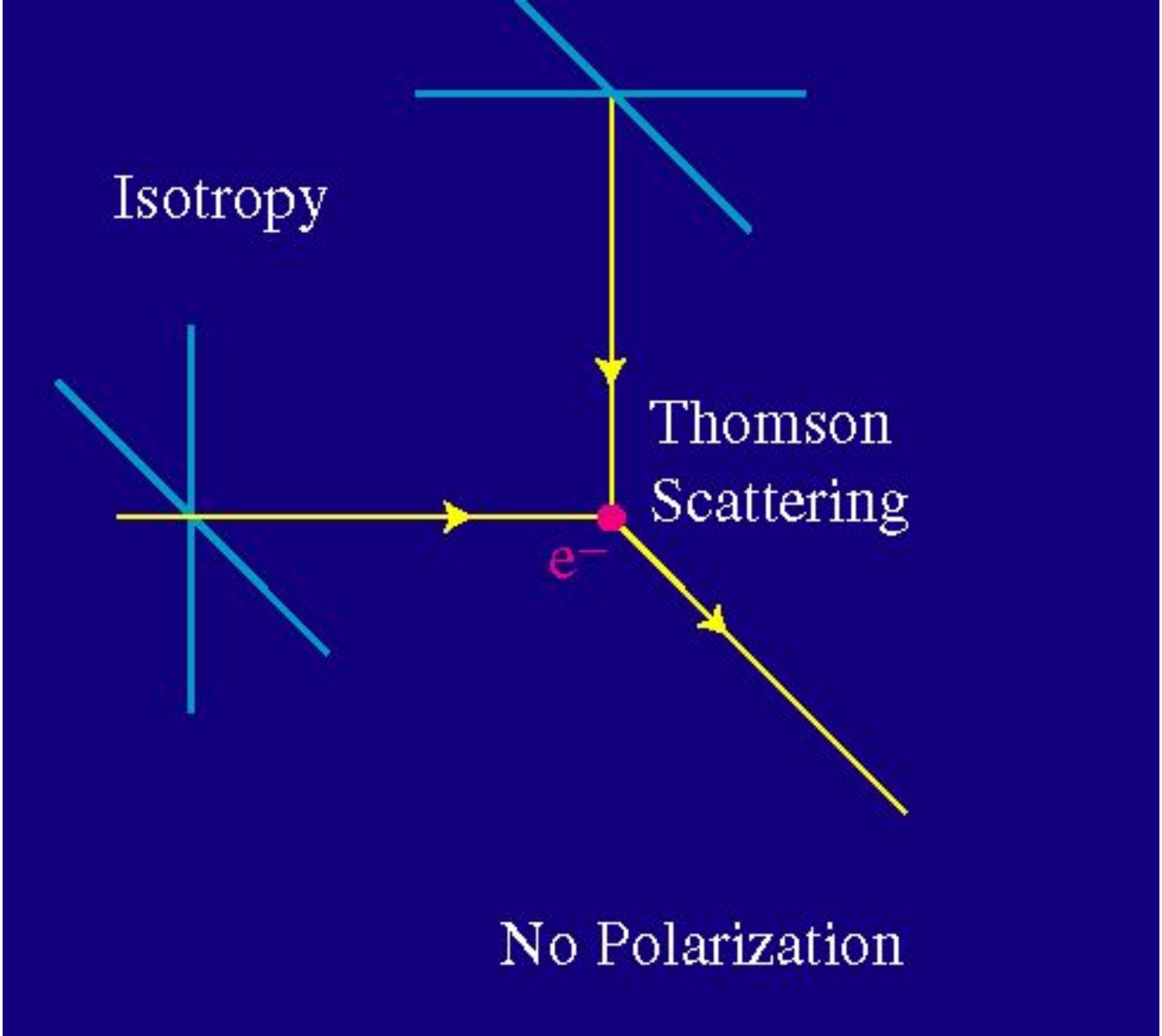
Isotropy
Thomson
Scattering
e⁻
No Polarization

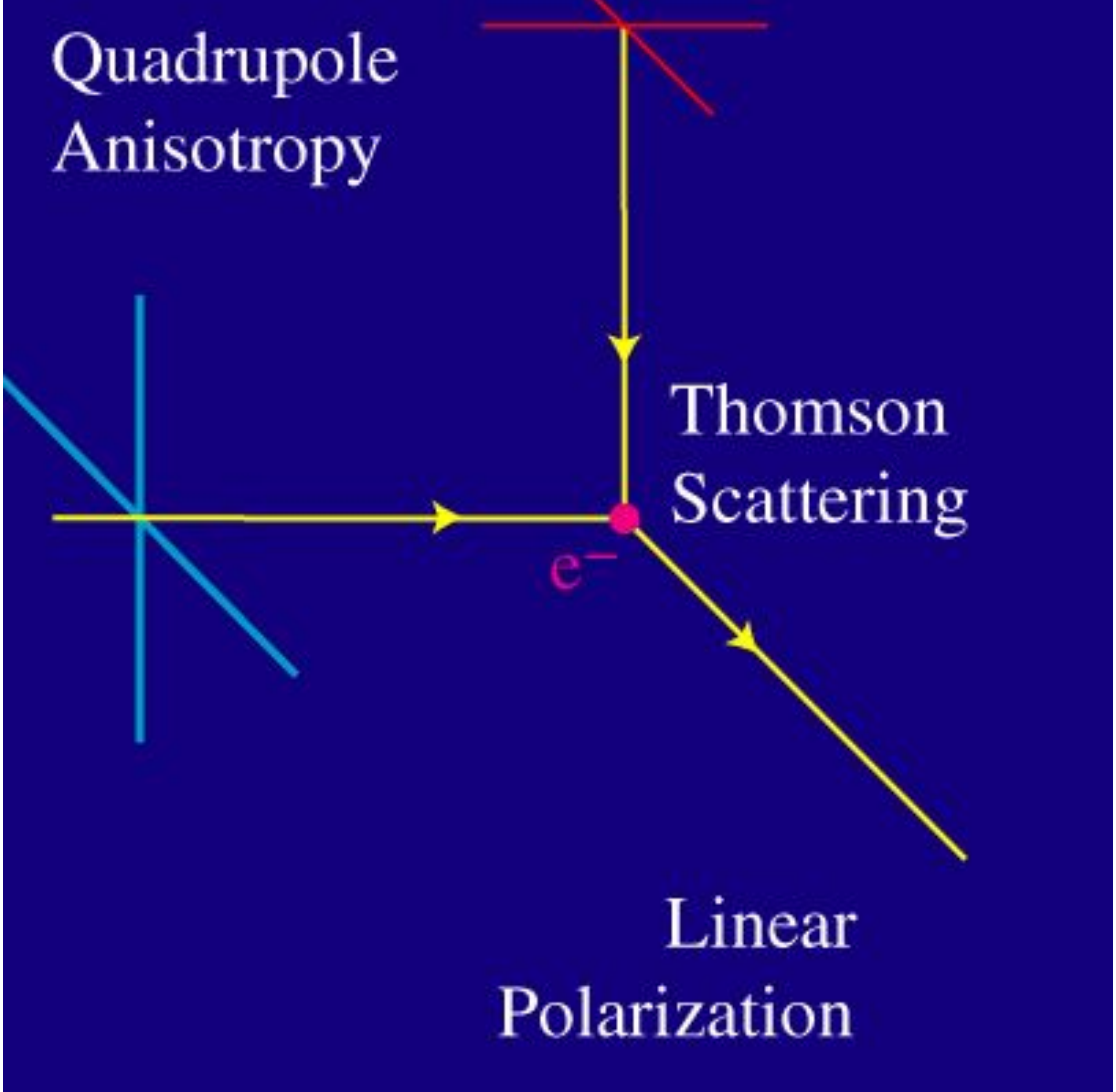
Quadrupole
Anisotropy
Thomson
Scattering
e⁻
Linear
Polarization

CMB polarization: scattering from sound waves

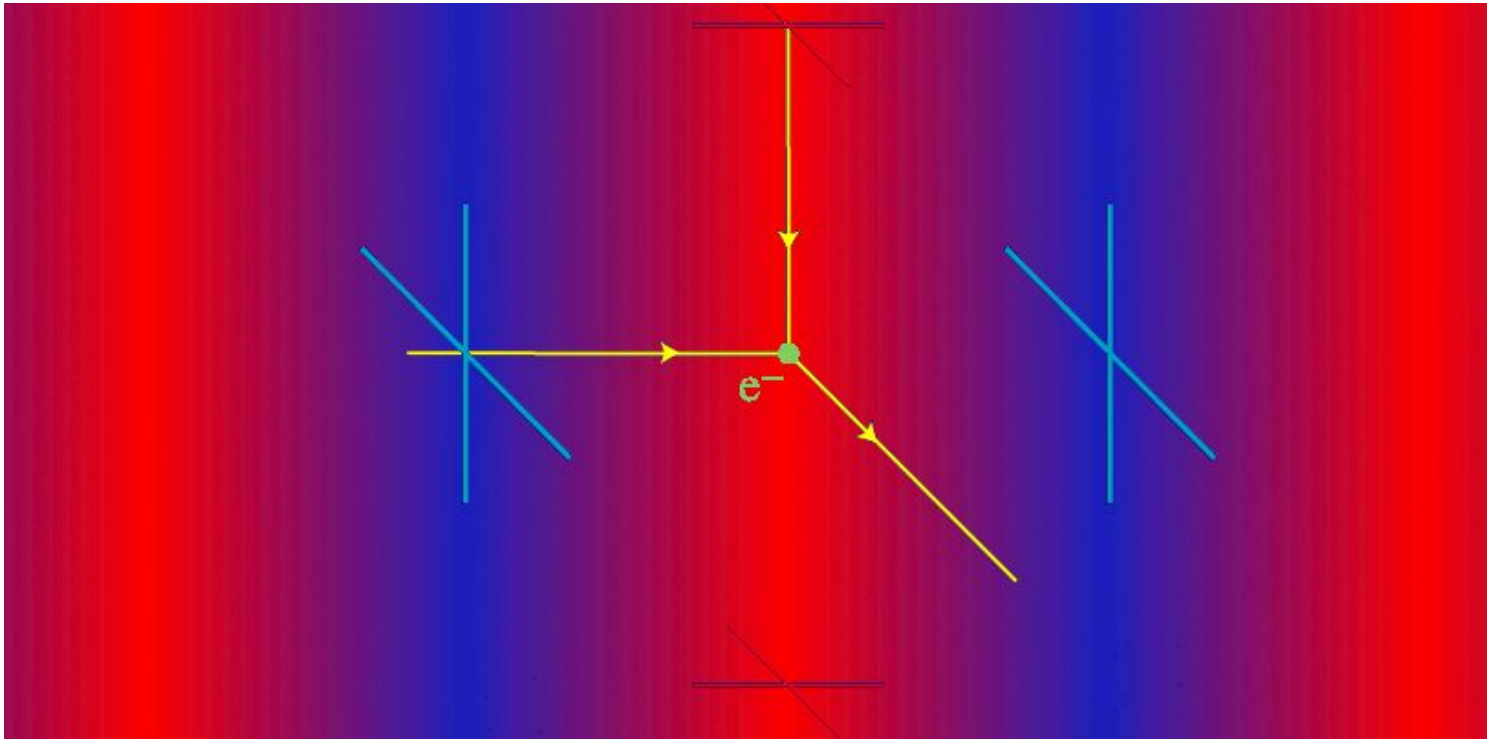

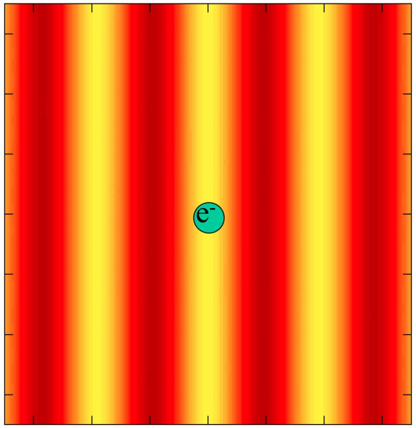

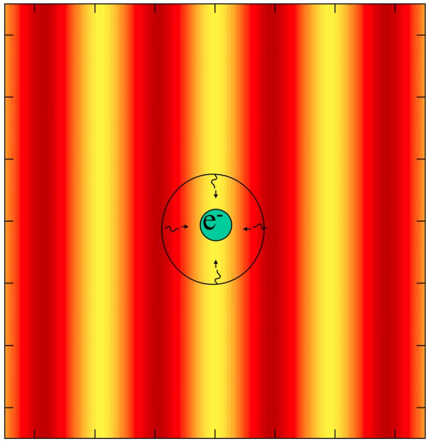

History of the Universe

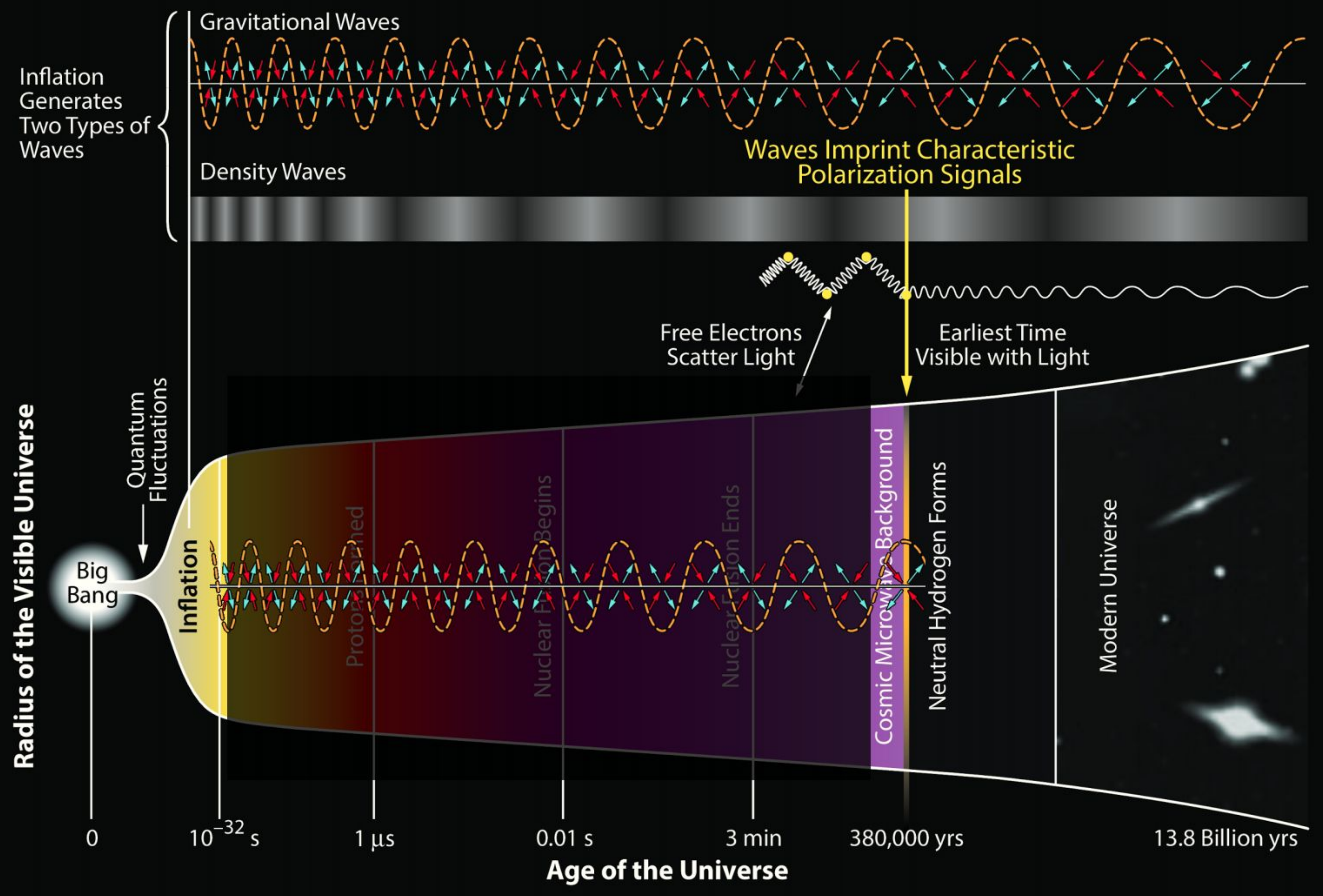

Polarization

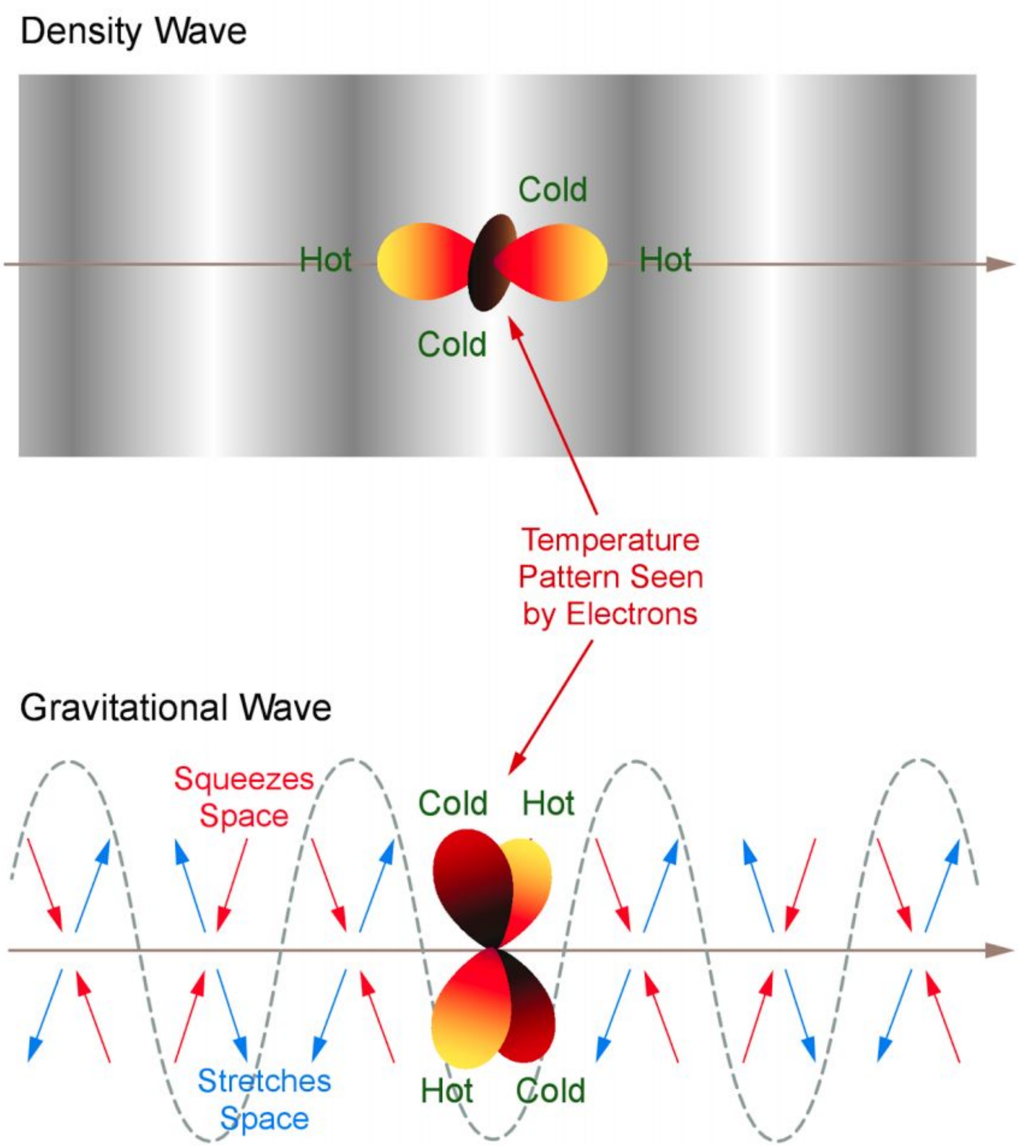

E-Mode Polarization Pattern

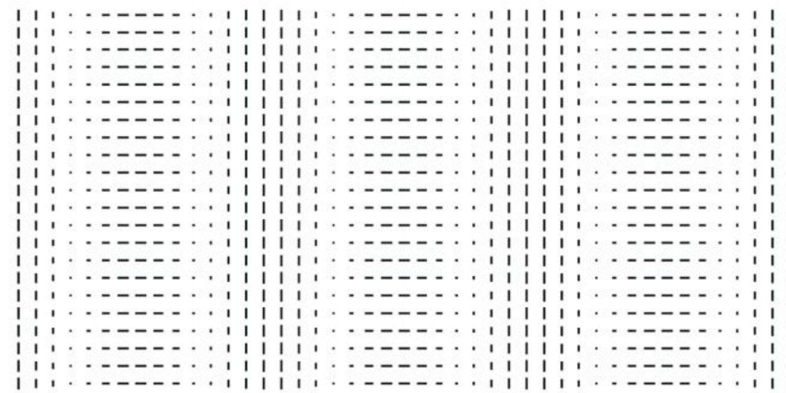

B-Mode Polarization Pattern

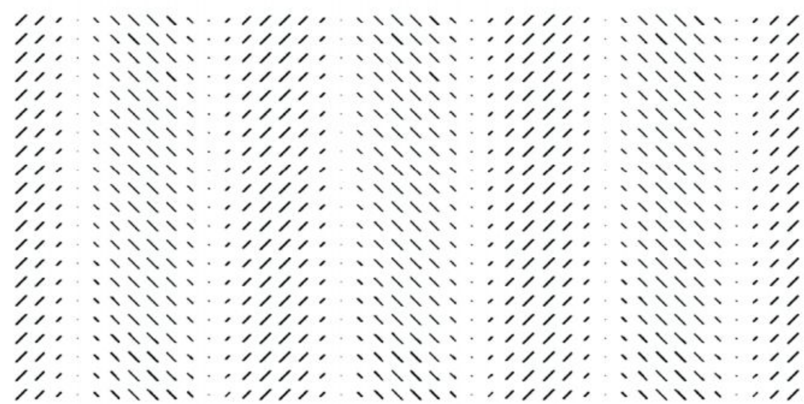

Polnarev, A. G. 1985, Sov. Ast., 29, 607

E and B mode

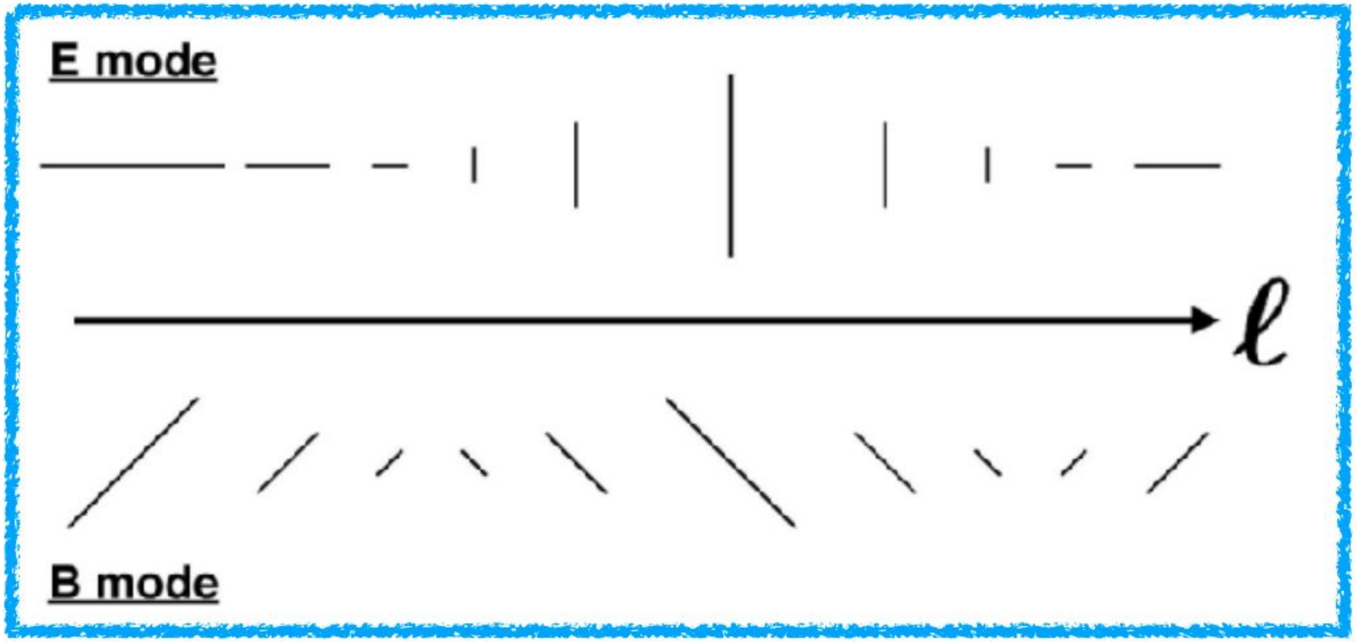

- **E mode**: Polarisation directions parallel or perpendicular to the wavevector
- **B mode**: Polarisation directions 45 degree tilted with respect to the wavevector

Parity

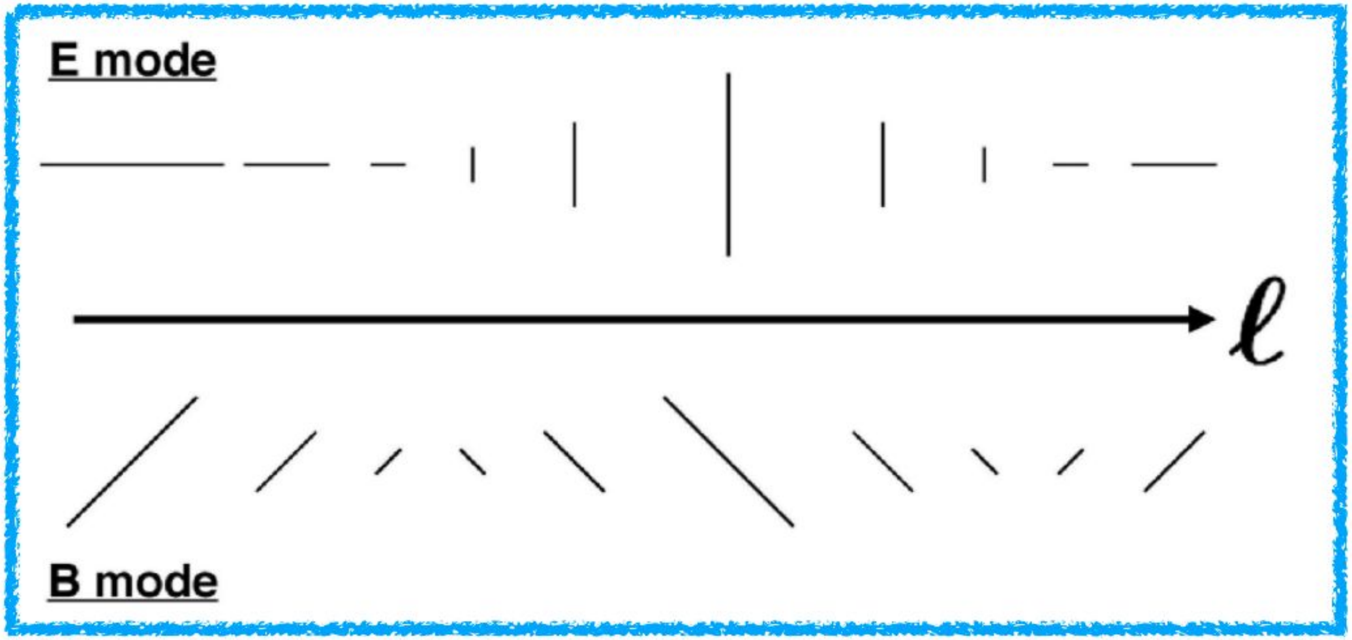

- **E mode**: Parity even
- **B mode**: Parity odd

Parity

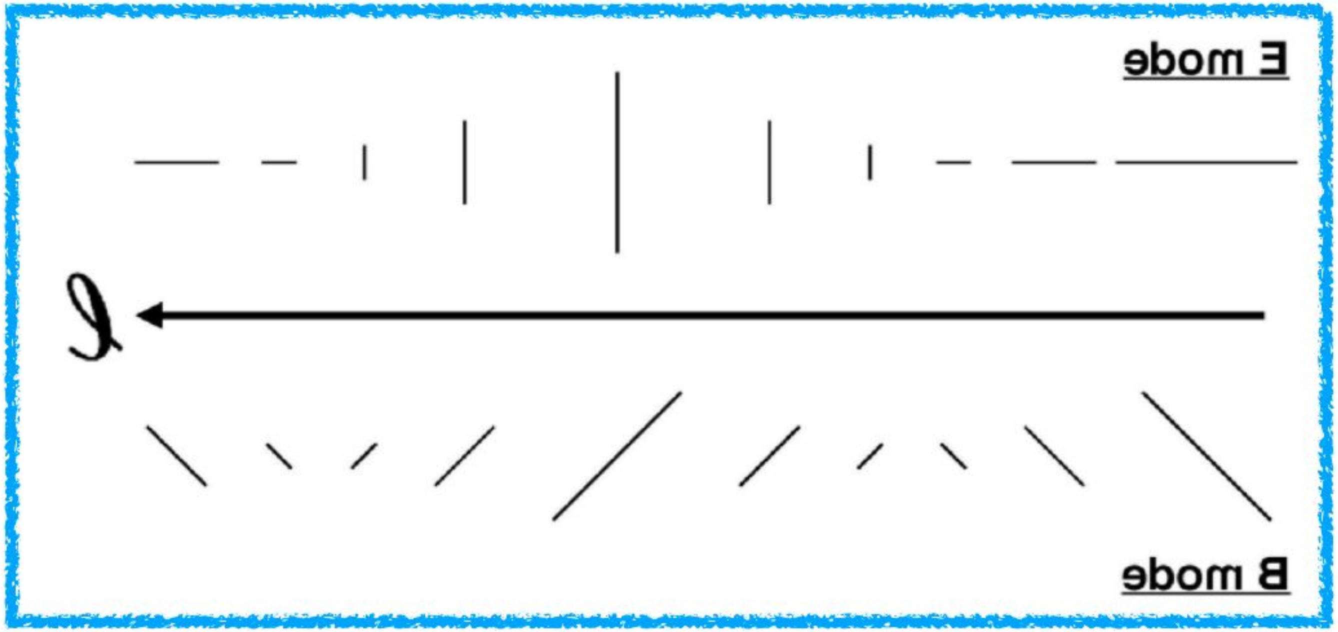

- **E mode**: Parity even
- **B mode**: Parity odd

Power Spectra

$$\langle E_{\boldsymbol{\ell}} E^*_{\boldsymbol{\ell}'} \rangle = (2\pi)^2 \delta_D^{(2)}(\boldsymbol{\ell} - \boldsymbol{\ell}') C_\ell^{EE}$$

$$\langle B_{\boldsymbol{\ell}} B^*_{\boldsymbol{\ell}'} \rangle = (2\pi)^2 \delta_D^{(2)}(\boldsymbol{\ell} - \boldsymbol{\ell}') C_\ell^{BB}$$

$$\langle T_{\boldsymbol{\ell}} E^*_{\boldsymbol{\ell}'} \rangle = \langle T^*_{\boldsymbol{\ell}} E_{\boldsymbol{\ell}'} \rangle = (2\pi)^2 \delta_D^{(2)}(\boldsymbol{\ell} - \boldsymbol{\ell}') C_\ell^{TE}$$

- However, <EB> and <TB> vanish for parity-preserving fluctuations because <EB> and <TB> change sign under parity flip

CMB Sky → Cosmology

Compute

Expand in Spherical Harmonics

a_{lm}

Gaussianity

WMAP CMB Sky

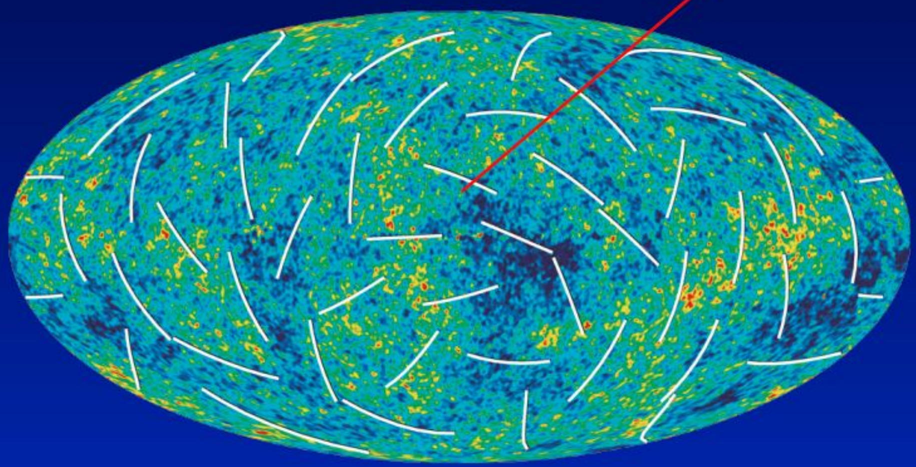

Power spectra

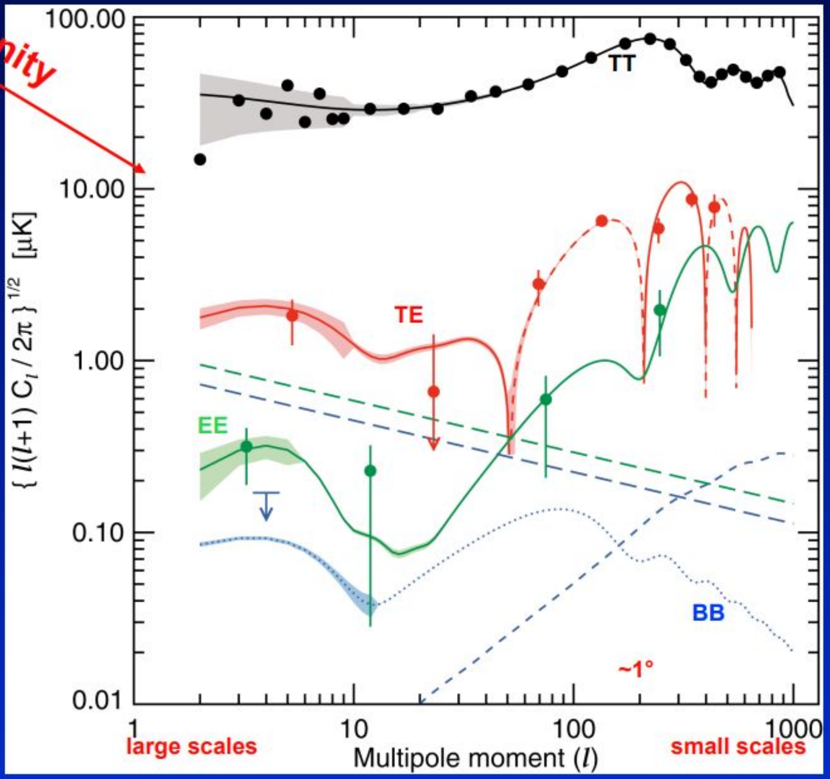

Measuring the CMB

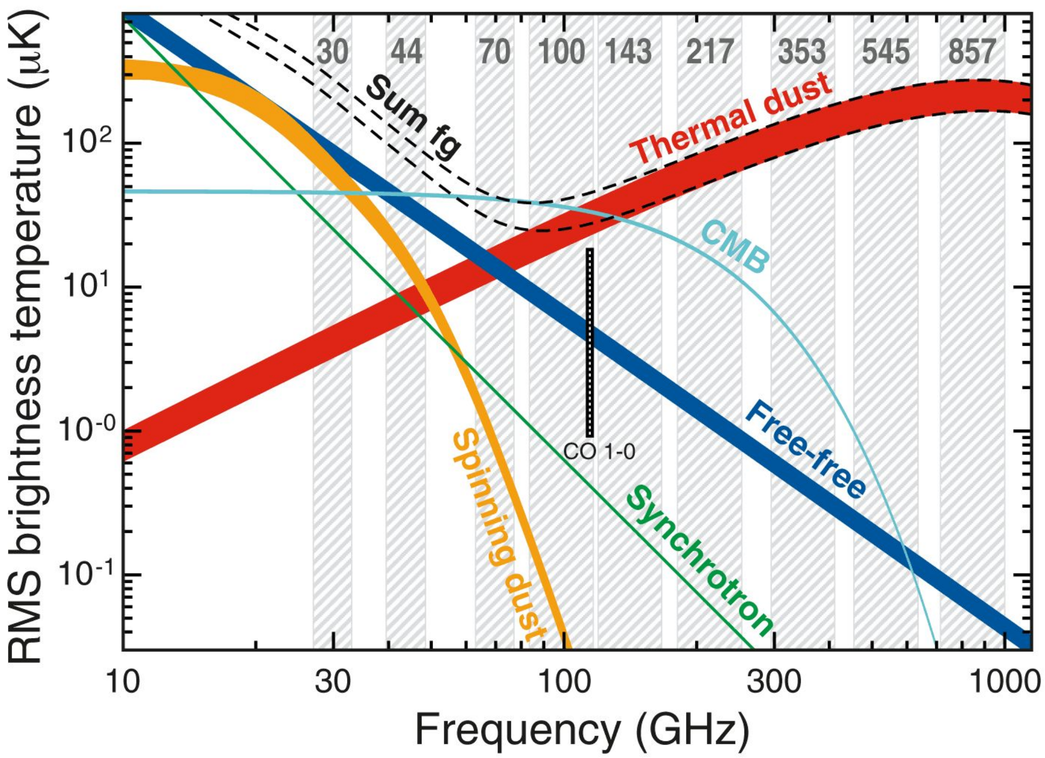

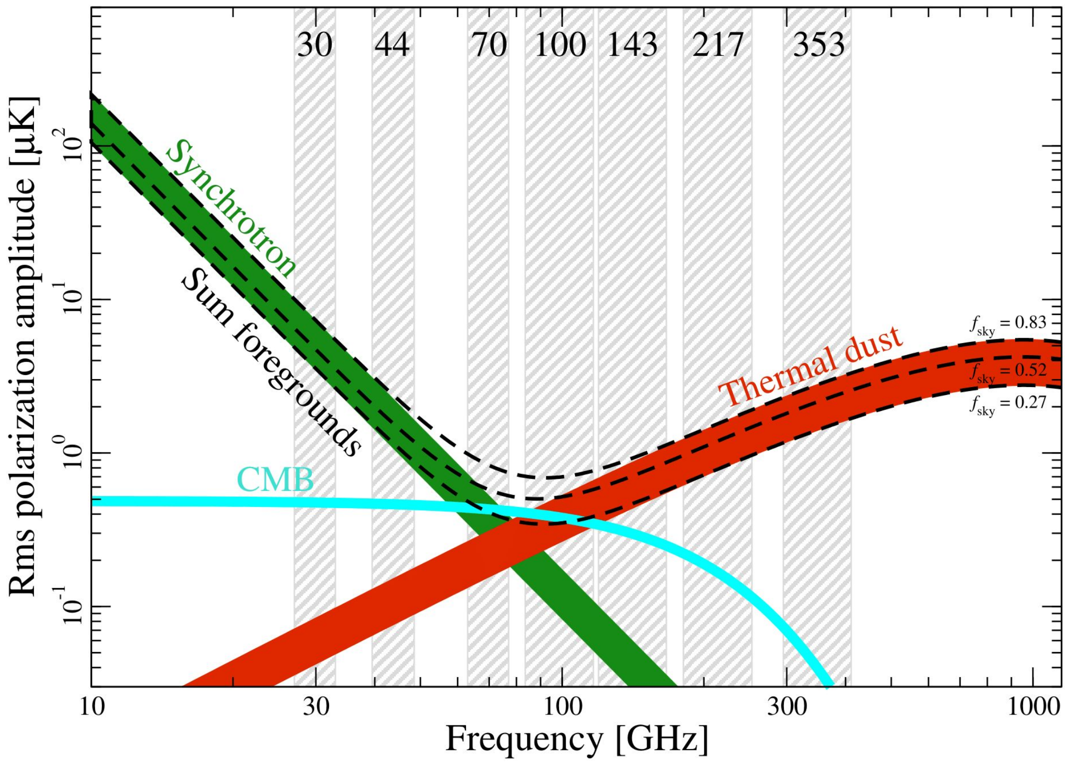

Measuring the CMB

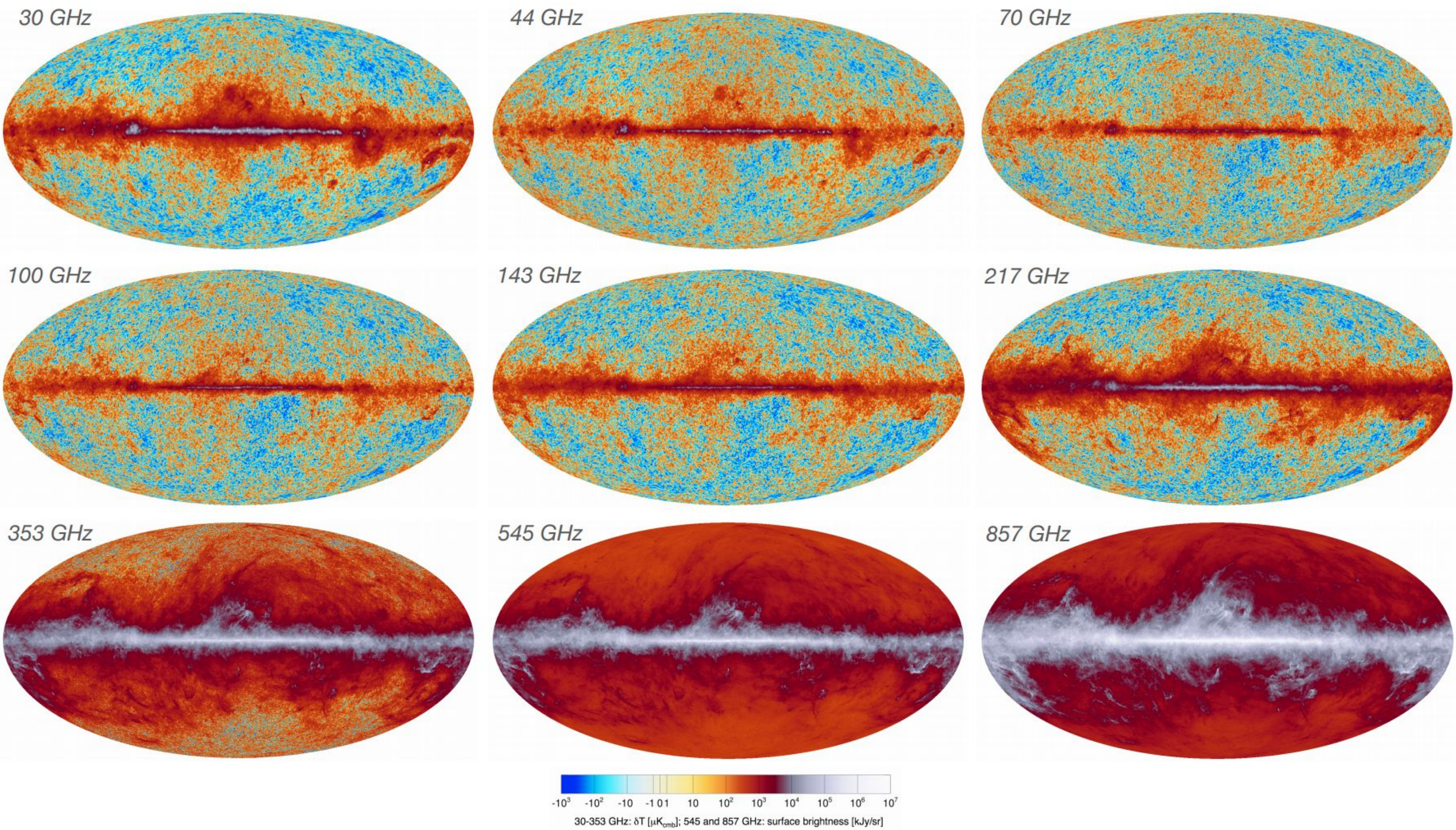

Measuring the CMB

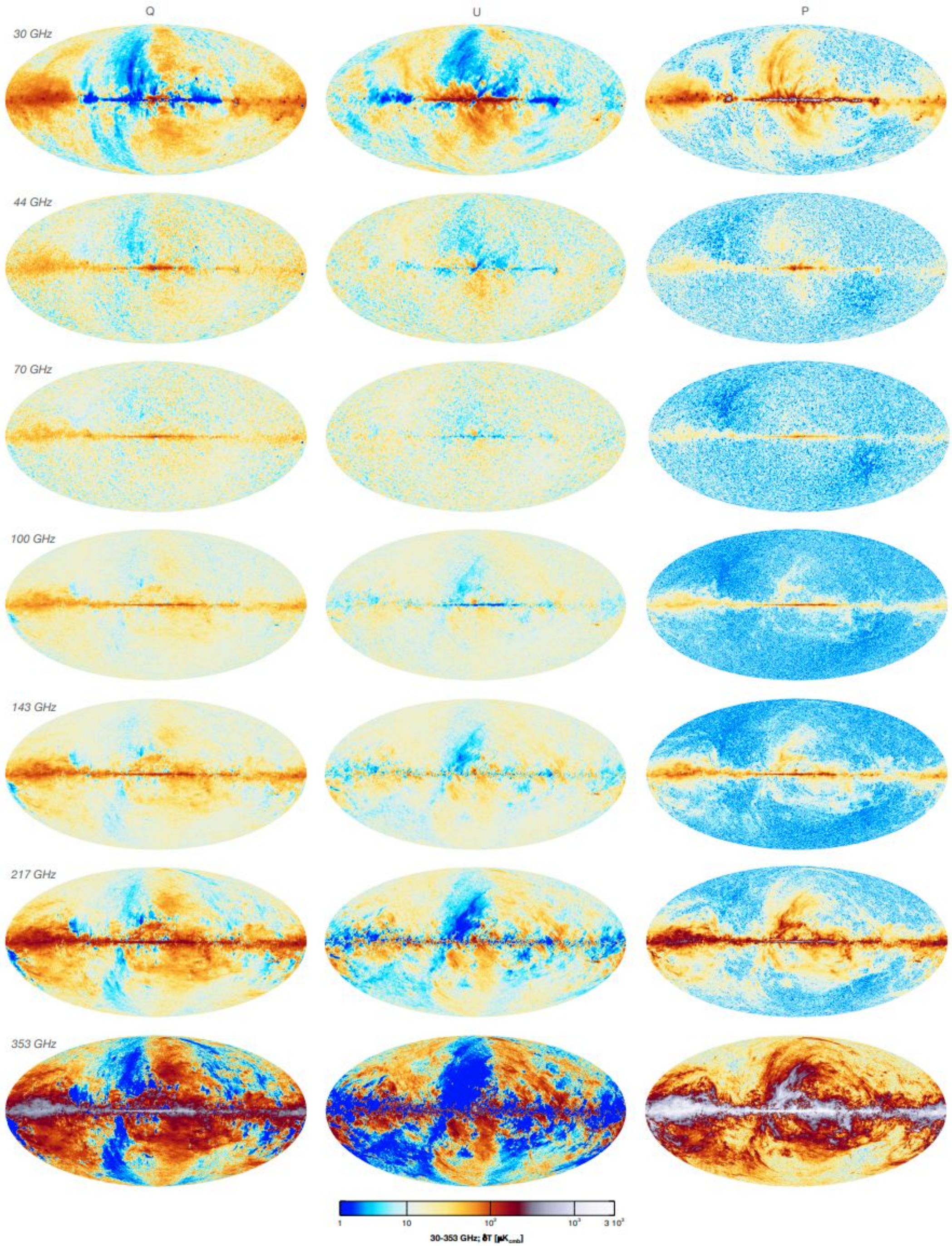

The 2018 Planck maps in polarization (Stokes Q, U, and polarized amplitude P)

- Q and U produced by E and B modes are given by

$$Q(\boldsymbol{\theta}) = \int \frac{d^2\ell}{(2\pi)^2}(E_{\boldsymbol{\ell}}\cos 2\phi_\ell - B_{\boldsymbol{\ell}}\sin 2\phi_\ell)\exp(i\boldsymbol{\ell}\cdot\boldsymbol{\theta})$$

$$U(\boldsymbol{\theta}) = \int \frac{d^2\ell}{(2\pi)^2}(E_{\boldsymbol{\ell}}\sin 2\phi_\ell + B_{\boldsymbol{\ell}}\cos 2\phi_\ell)\exp(i\boldsymbol{\ell}\cdot\boldsymbol{\theta})$$

Cosmic Microwave Background

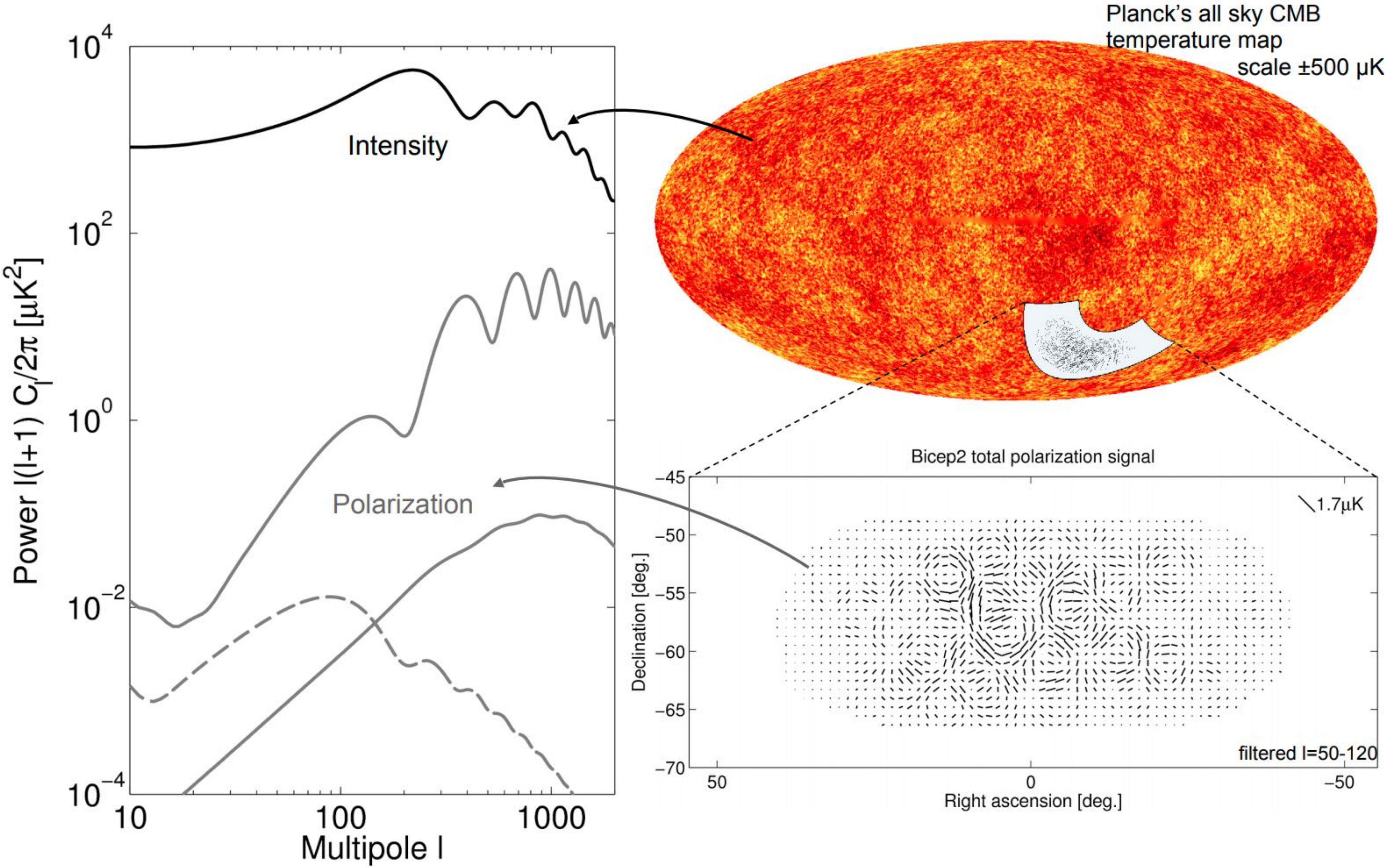

The Bicep2 Collaboration

CMB Polarization

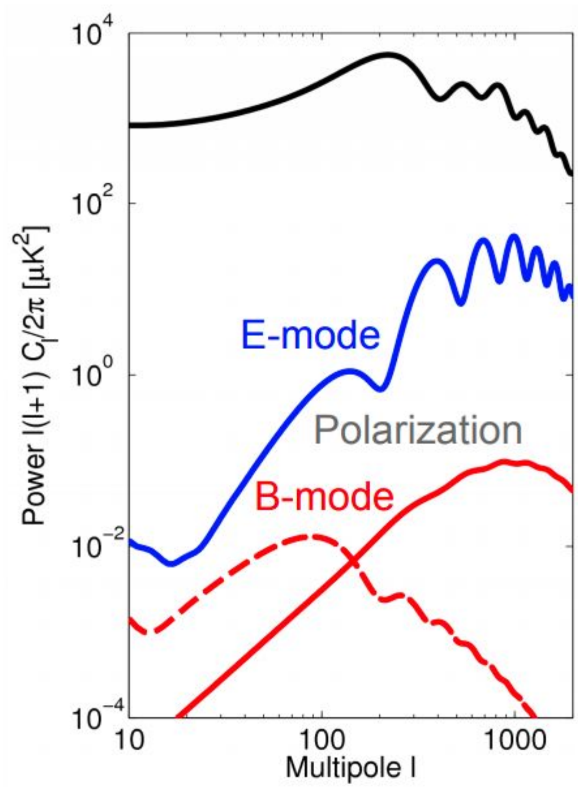

Need 2D basis to describe polarization map...

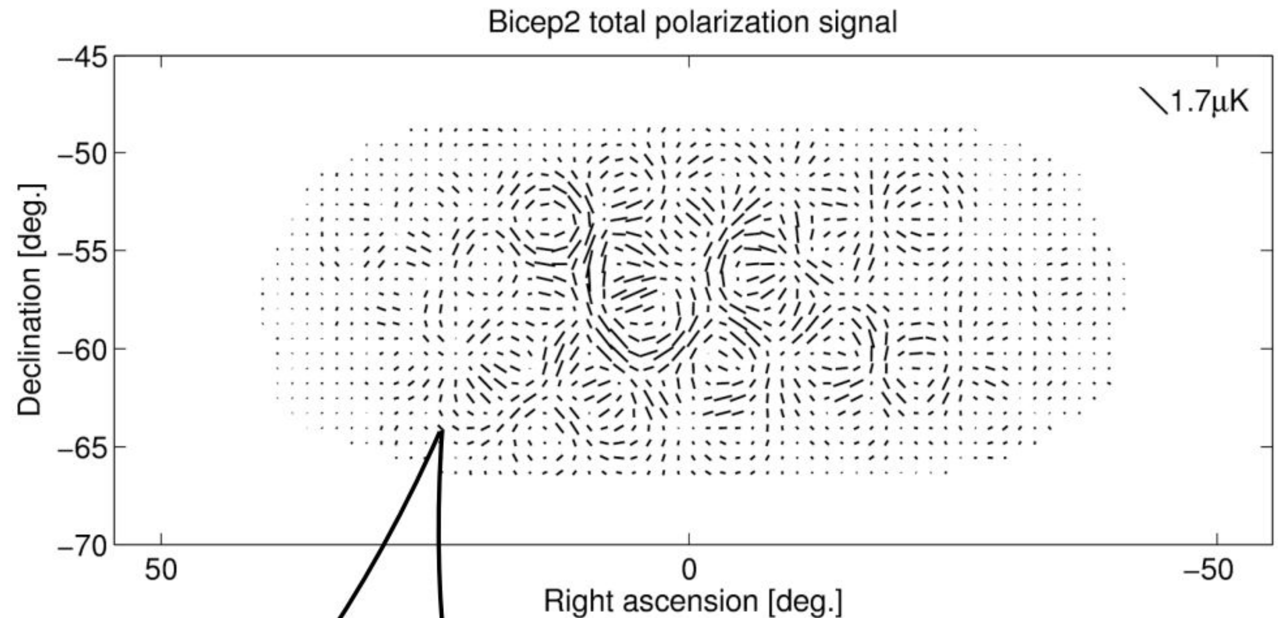

...clever choice for cosmology: E&B-modes

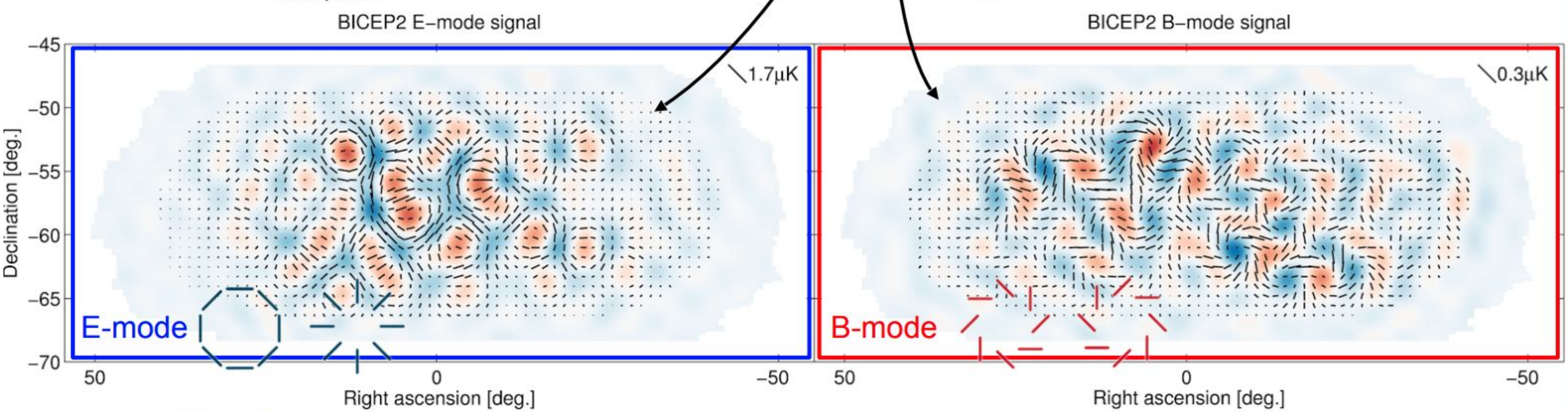

The Bicep2 Collaboration

CMB Polarization

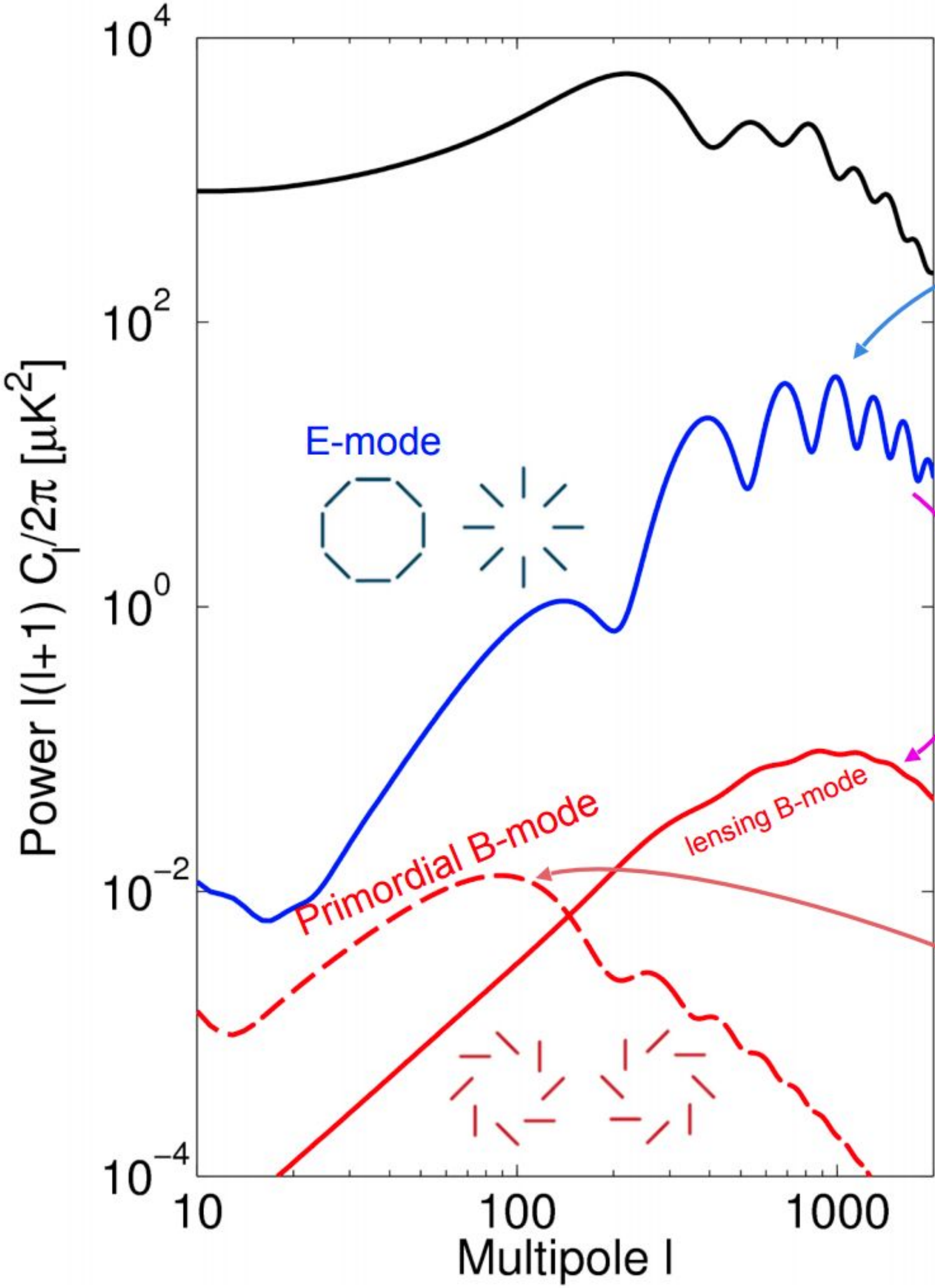

In standard ΛCDM only E-modes are present at last scattering

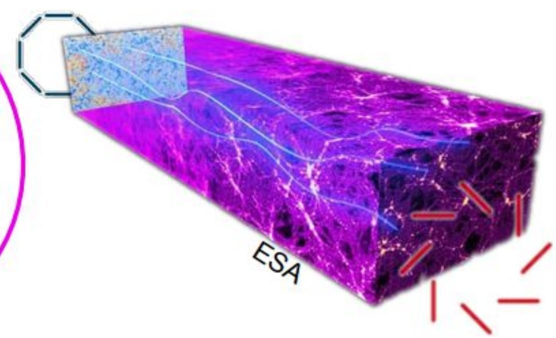

During propagation some of the E-modes are confused into B-modes by lensing

Inflationary gravitational waves are unique source of B-modes
→ peaking at l≈100 : degree scales

The Bicep2 Collaboration

CMB Polarization

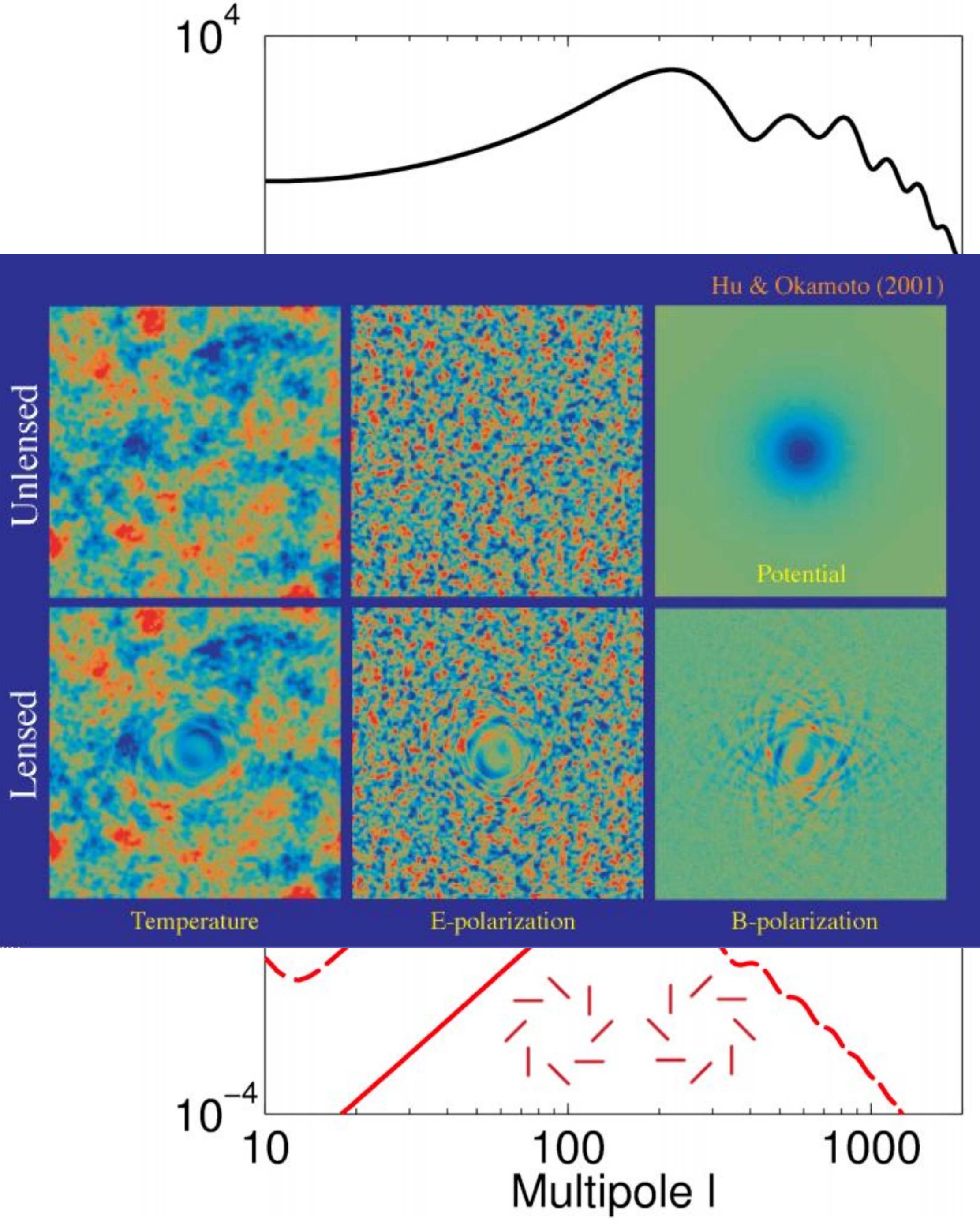

In standard ΛCDM only E-modes are present at last scattering

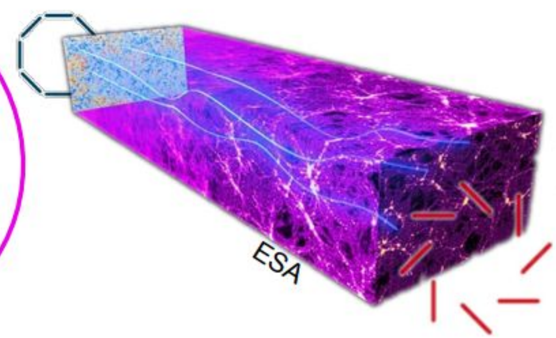

During propagation some of the E-modes are confused into B-modes by lensing

Inflationary gravitational waves are unique source of B-modes
→ peaking at l≈100 : degree scales

The Bicep2 Collaboration

CMB Polarization

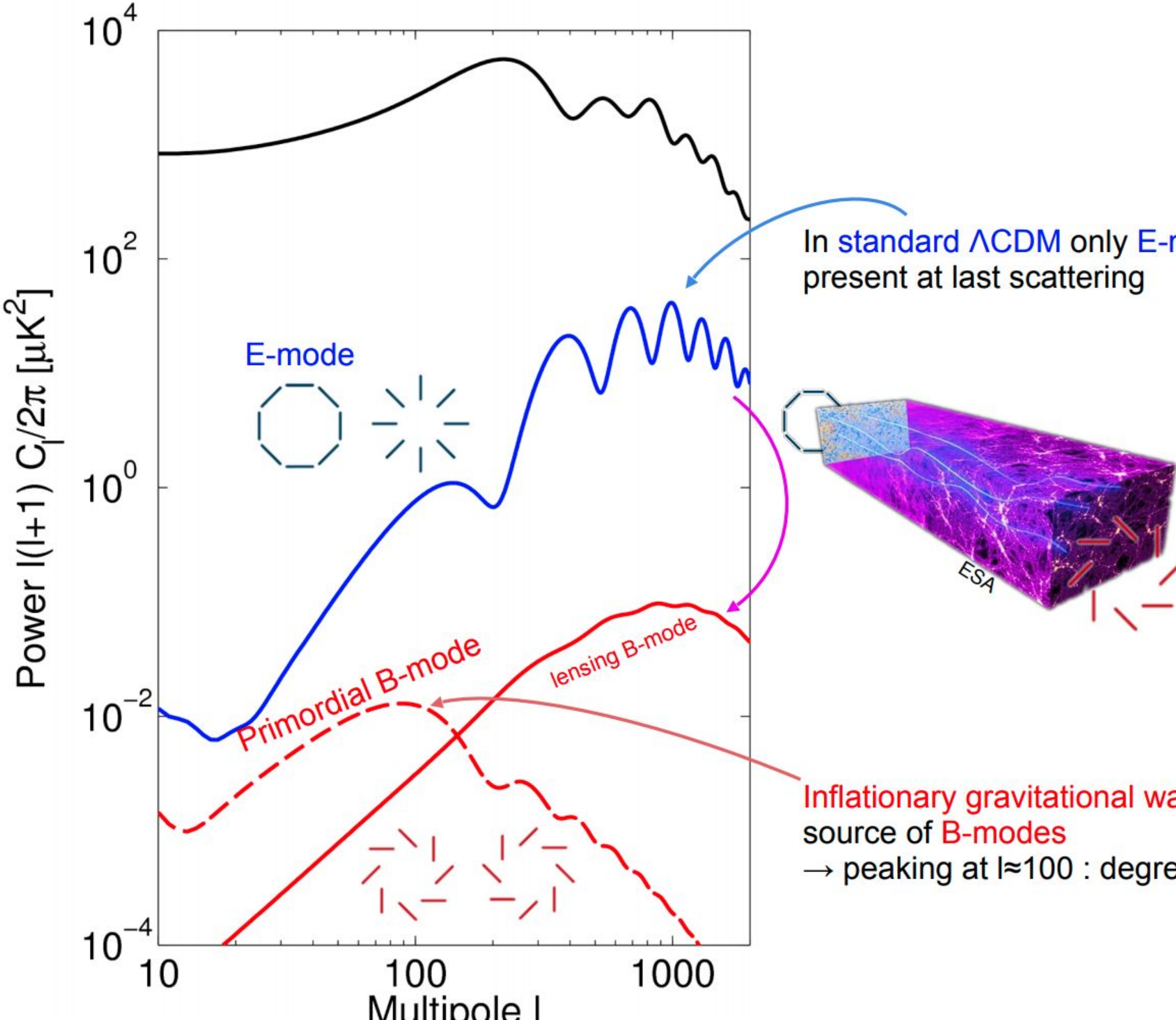

In standard ΛCDM only E-modes are present at last scattering

During propagation some of the E-modes are confused into B-modes by lensing

Inflationary gravitational waves are unique source of B-modes
→ peaking at l≈100 : degree scales

The Bicep2 Collaboration

CMB Polarization

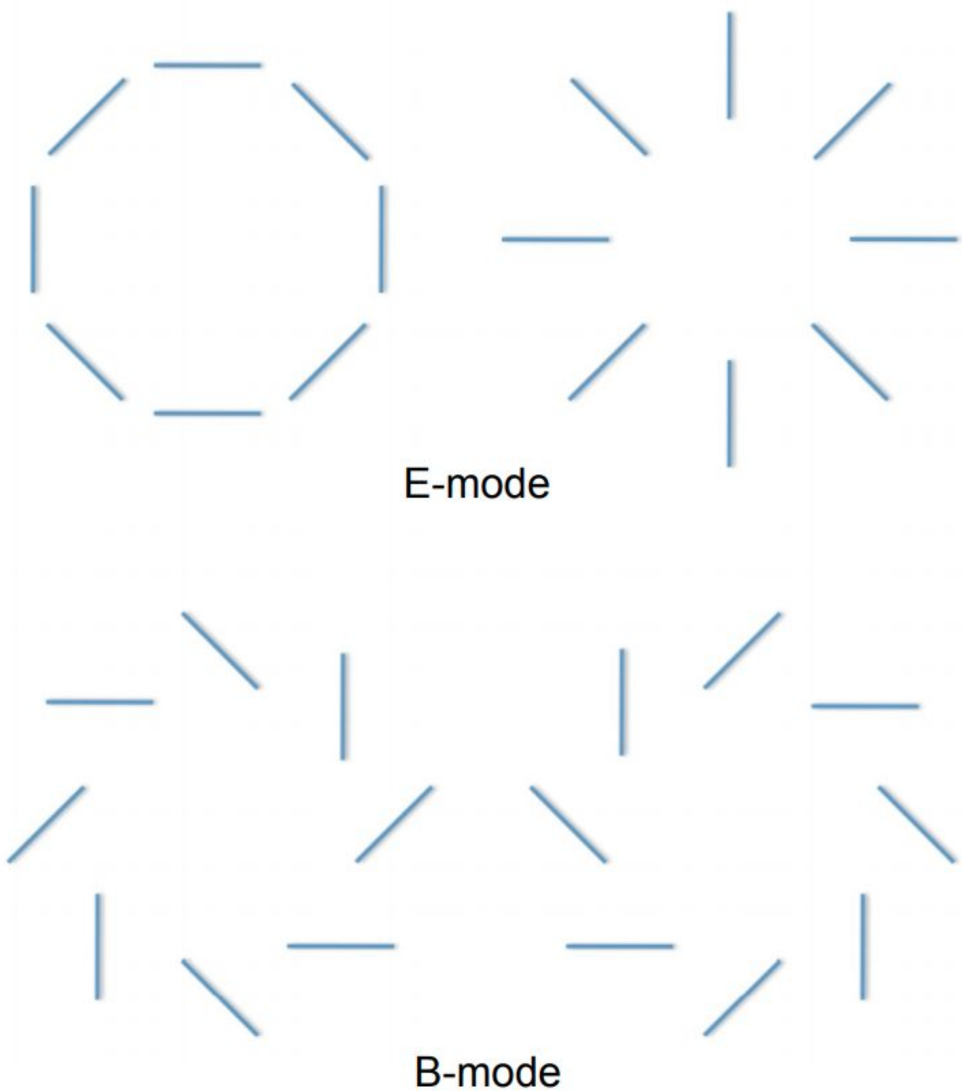

The plasma physics of the early universe causes the CMB to become slightly polarized.

Polarization can be described as the sum of E-modes and B-modes.

Only inflationary gravitational waves can induce significant B-mode polarization on degree angular scales.

A measurement of degree-scale B-modes would be direct evidence for the gravitational wave background, free of the parameter degeneracies and cosmic variance inherent to temperature measurements.

B modes until 2014

Search for B-modes

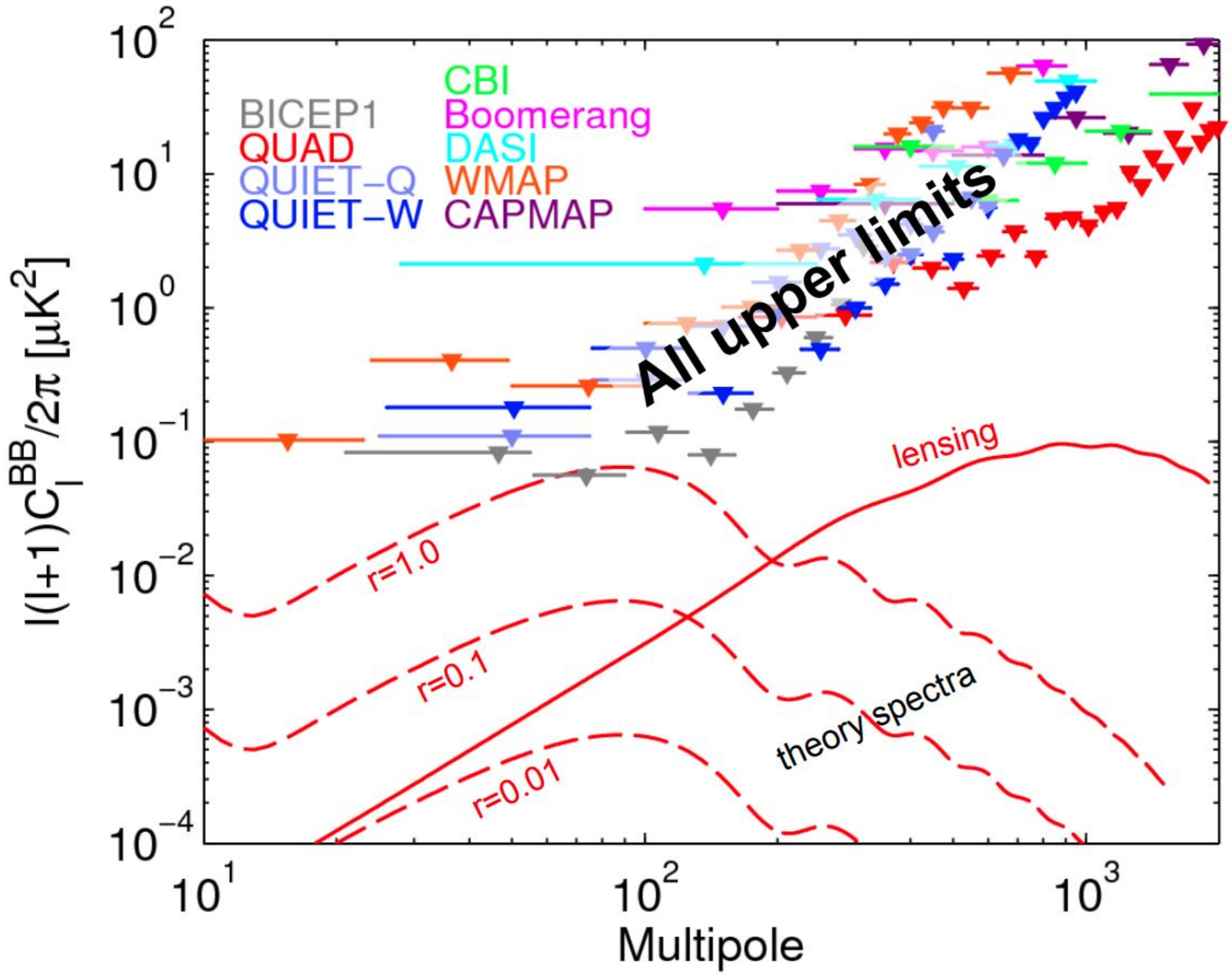

In simple inflationary gravitational wave models the

tensor-to-scalar ratio r

is the only parameter to the B-mode spectrum.

Up to now: just upper limits from searches for B-modes in the CMB polarization

Best limit on r from BICEP1:

r < 0.7 (95% CL)

At high multipoles lensing B-mode dominant.

Brian Keating for the Bicep2 Collaboration

B modes

Search for B-modes

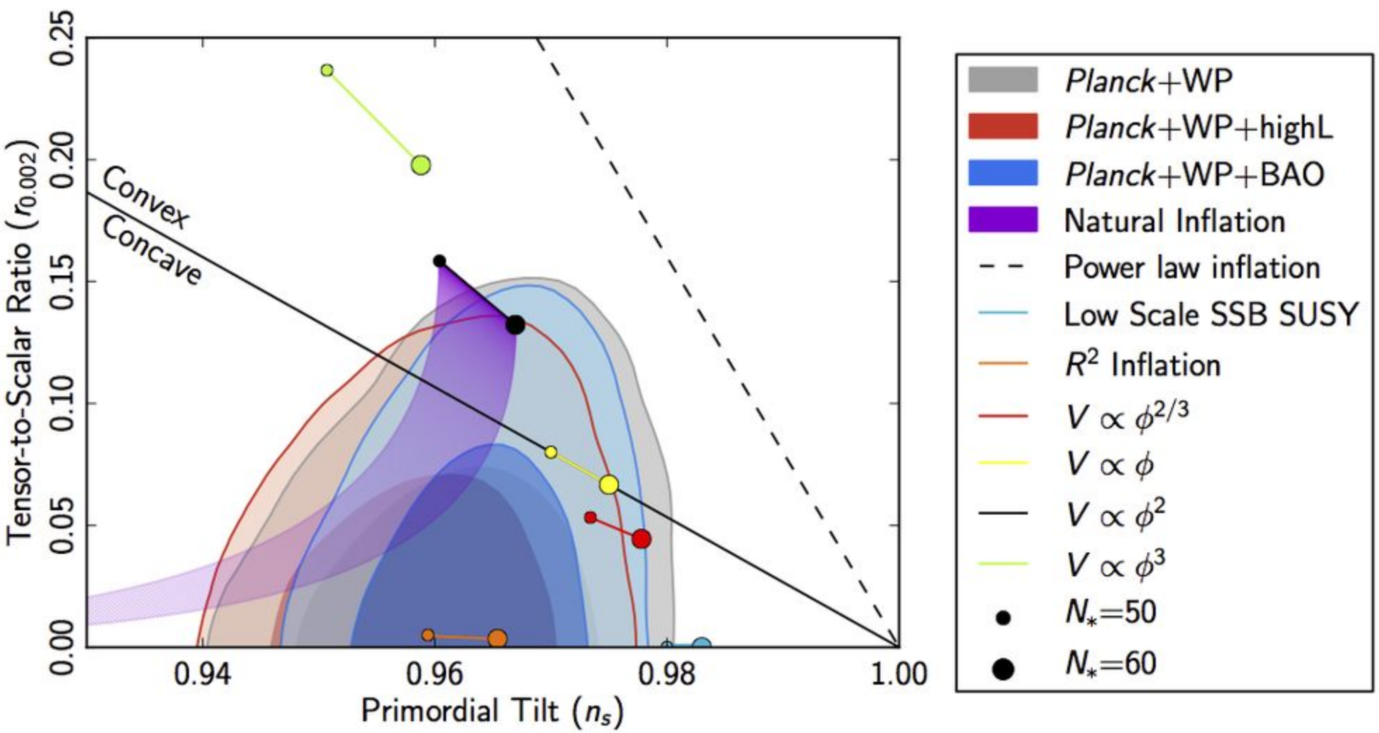

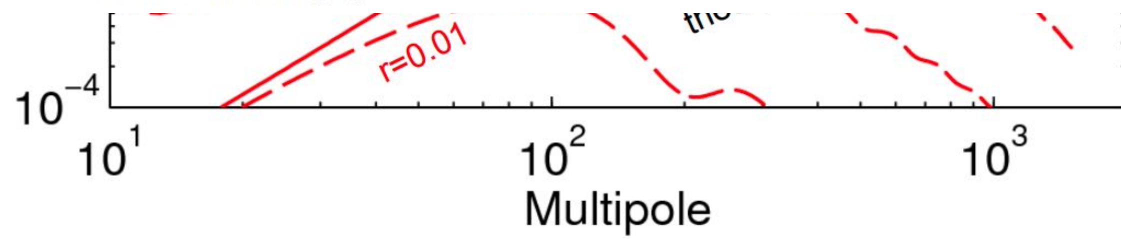

Brian Keating for the Bicep2 Collaboration

In simple inflationary gravitational wave models the

tensor-to-scalar ratio r

is the only parameter to the B-mode spectrum.

Up to now: just upper limits from searches for B-modes in the CMB polarization

Best limit on r from BICEP1:

r < 0.7 (95% CL)

At high multipoles lensing B-mode dominant.

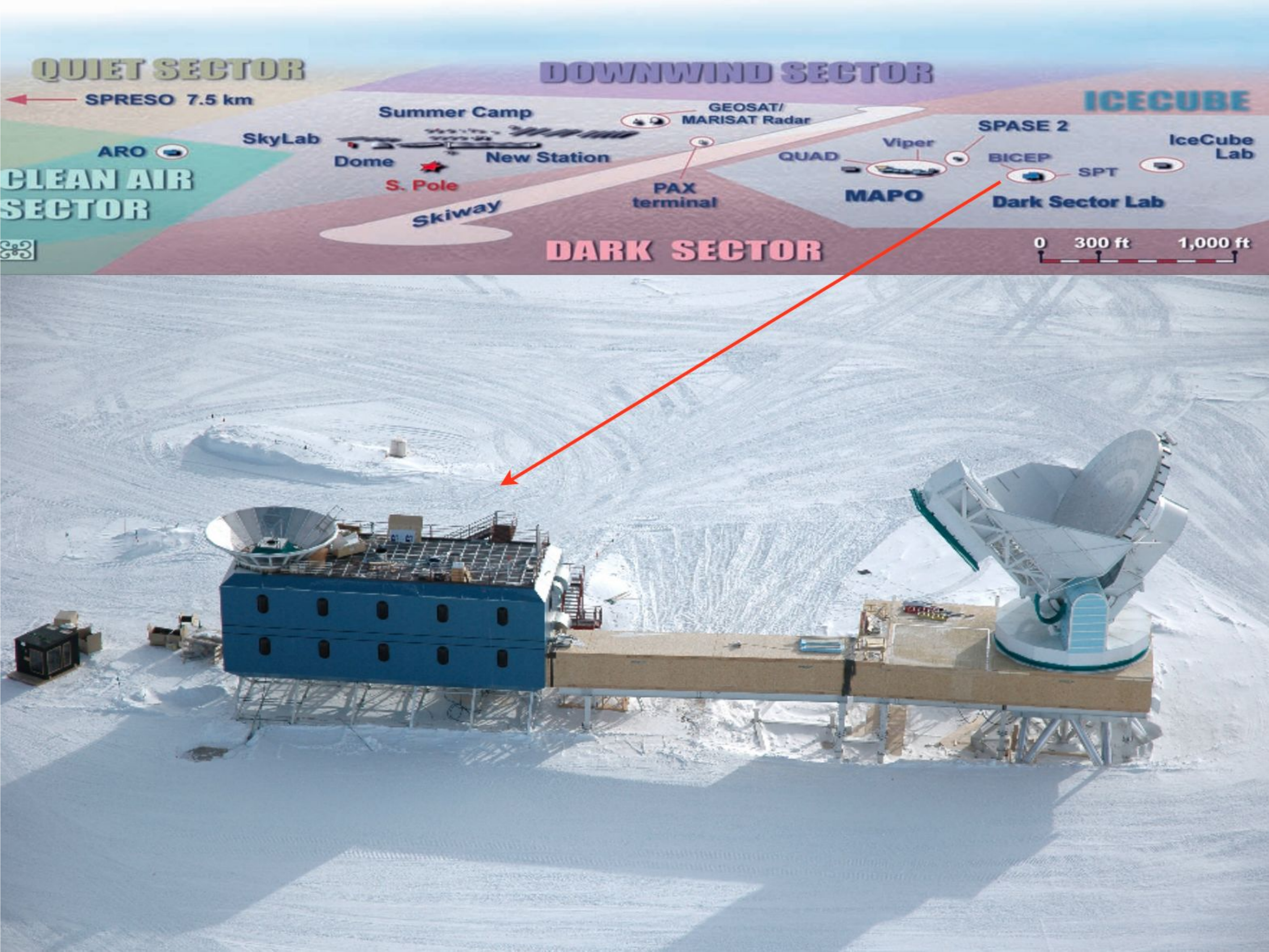
QUIET SECTOR
SPRESO 7.5 km
DOWNWIND SECTOR
ICECUBE
Summer Camp
GEOSAT/
MARISAT Radar
SkyLab
ARO
CLEAN AIR
SECTOR
Dome
New Station
S. Pole
Skiway
PAX
terminal
SPASE 2
Viper
QUAD
MAPO
BICEP
SPT
Dark Sector Lab
IceCube
Lab
DARK SECTOR
0
300 ft
1,000 ft

Observational Strategy

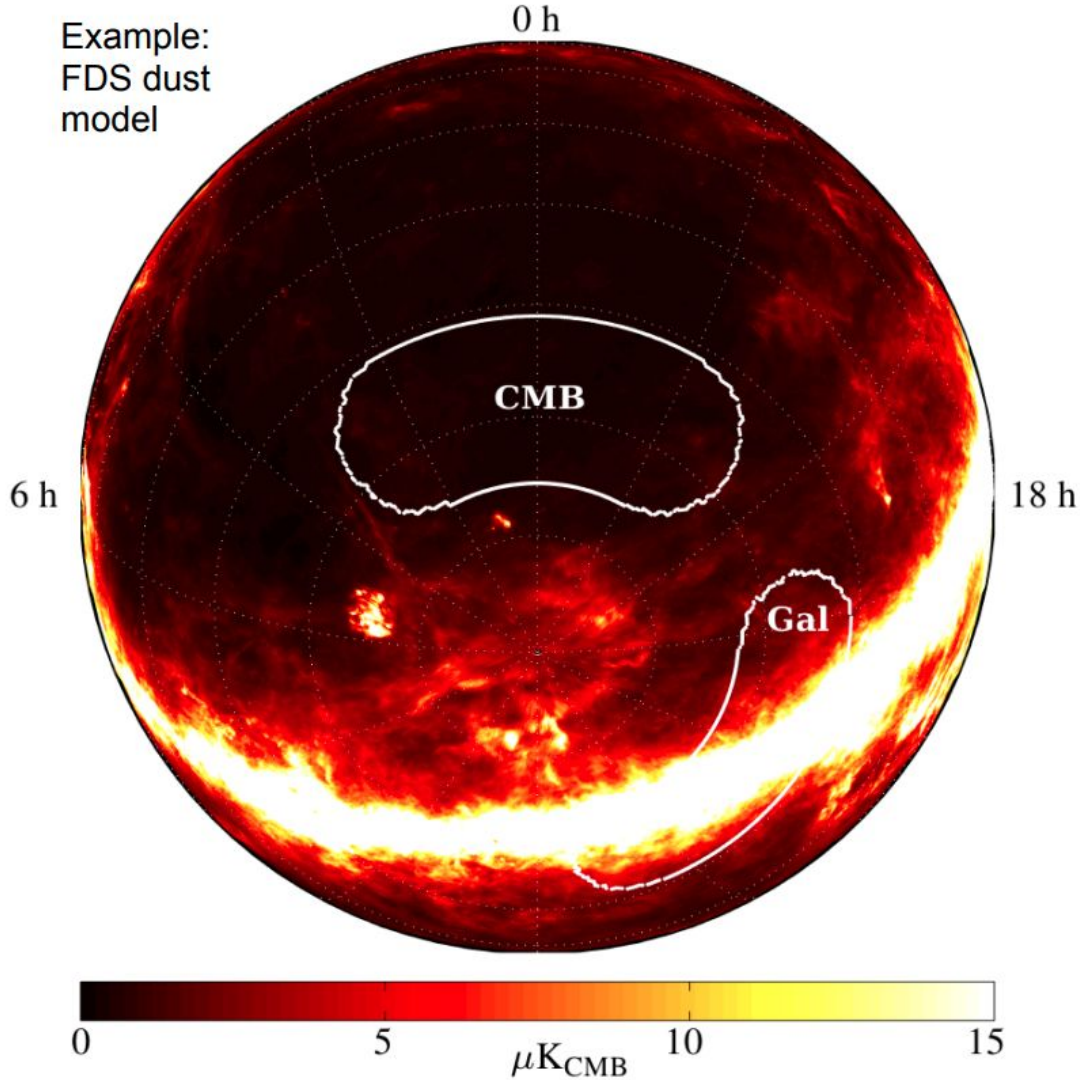

Target the "Southern Hole" - a region of the sky exceptionally free of dust and synchrotron foregrounds.

Detectors tuned to 150 GHz, near the peak of the CMB's 2.7 K blackbody spectrum.

At 150 GHz the combined dust and synchrotron spectrum is predicted to be at a minimum in the Southern Hole.

Expected foreground contamination of the B-mode power: r ≤ ~0.01.

BICEP2 E- and B-mode Maps

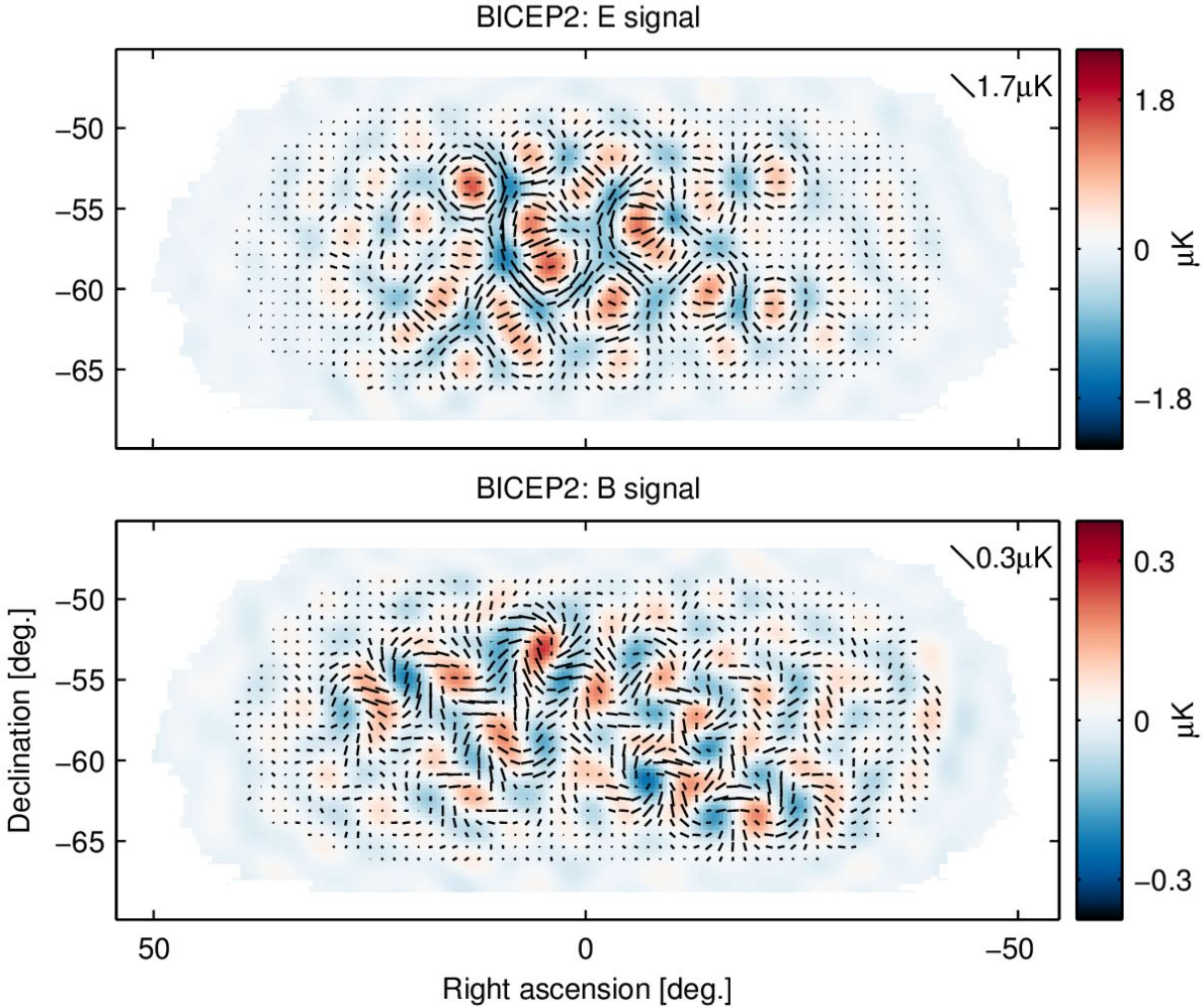

BICEP2 B-mode Power Spectrum

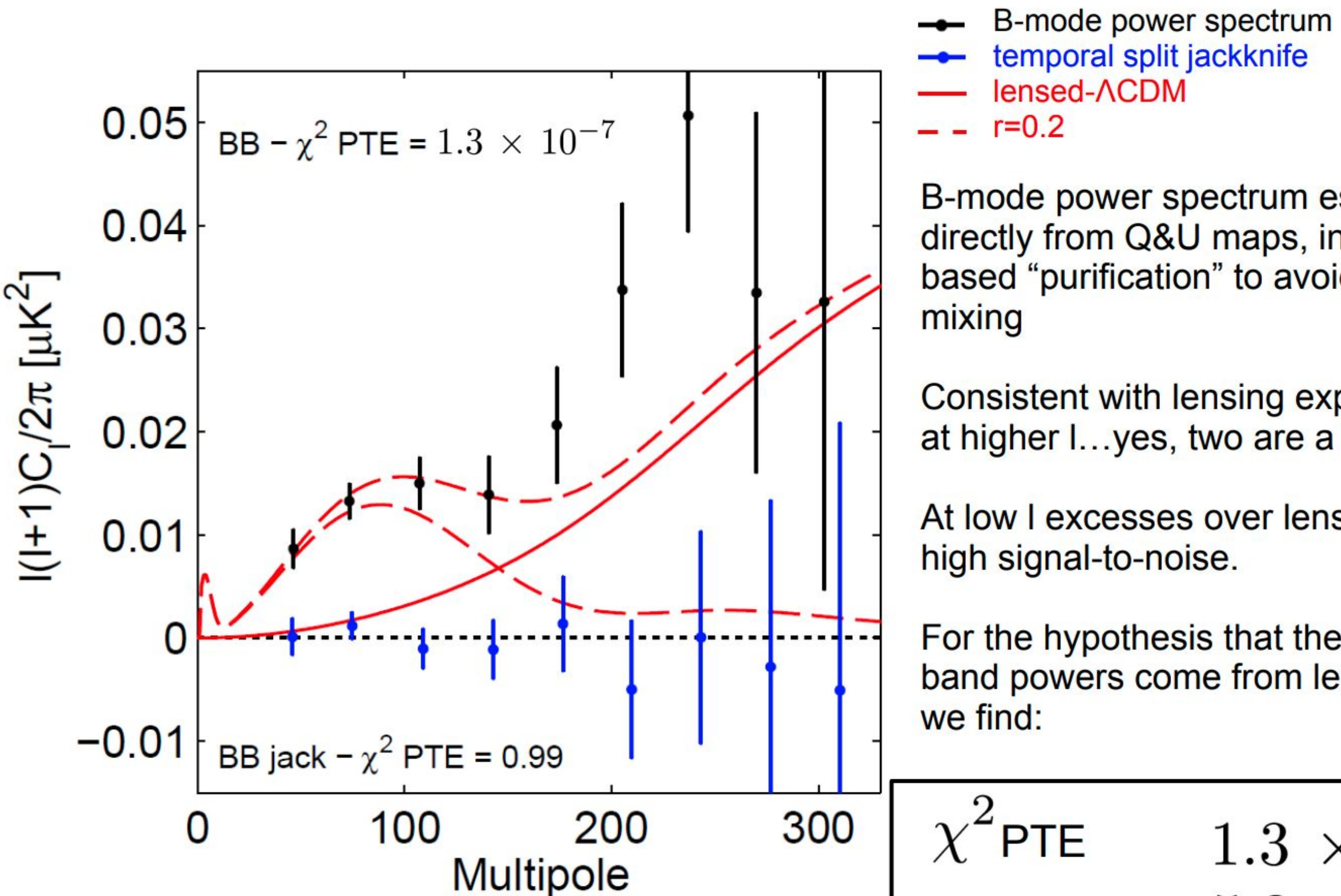

B-mode power spectrum estimated directly from Q&U maps, including map based "purification" to avoid E→B mixing

Consistent with lensing expectation at higher l…yes, two are a bit high…

At low l excesses over lensed-ΛCDM at high signal-to-noise.

For the hypothesis that the measured band powers come from lensed-ΛCDM we find:

χ^2 PTE	1.3×10^{-7}
significance	$5.3\,\sigma$

Constraint on Tensor-to-scalar Ratio r

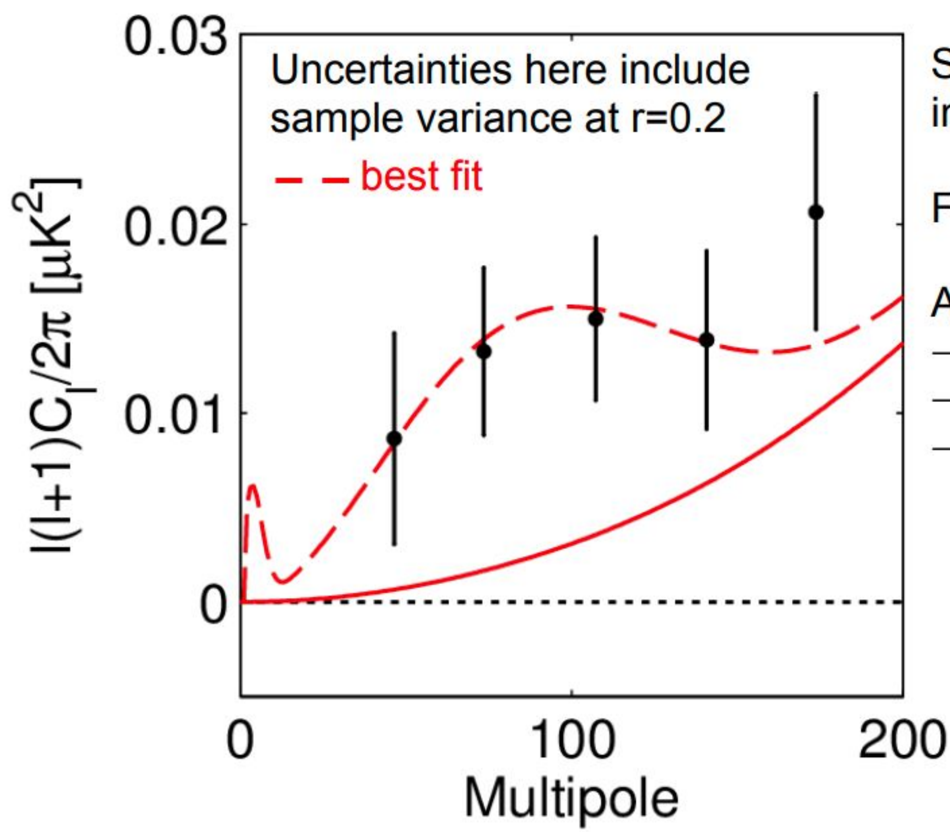

Substantial excess power in the region where the inflationary gravitational wave signal is expected to peak

Find the most likely value of the tensor-to-scalar ratio r

Apply "direct likelihood" method, uses:

→ lensed-ΛCDM + noise simulations

→ weighted version of the 5 bandpowers

→ B-mode sims scaled to various levels of r (n_T=0)

Within this simplistic model we find:

r = 0.2 with uncertainties dominated by sample variance

PTE of fit to data: 0.9

→ model is perfectly acceptable fit to the data

r = 0 ruled out at 7.0σ

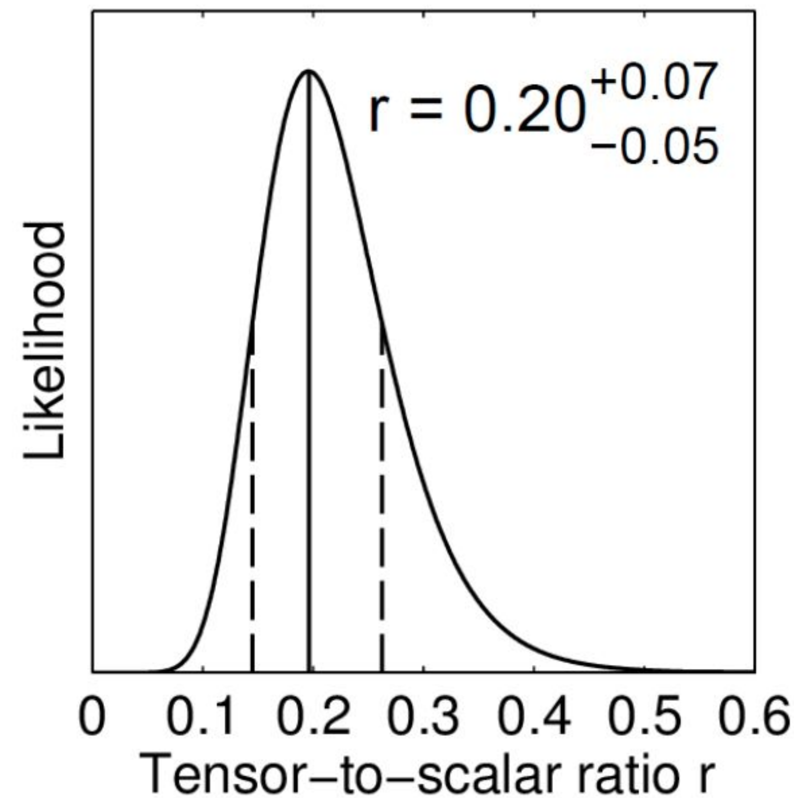

Polarized Dust Foreground Projections

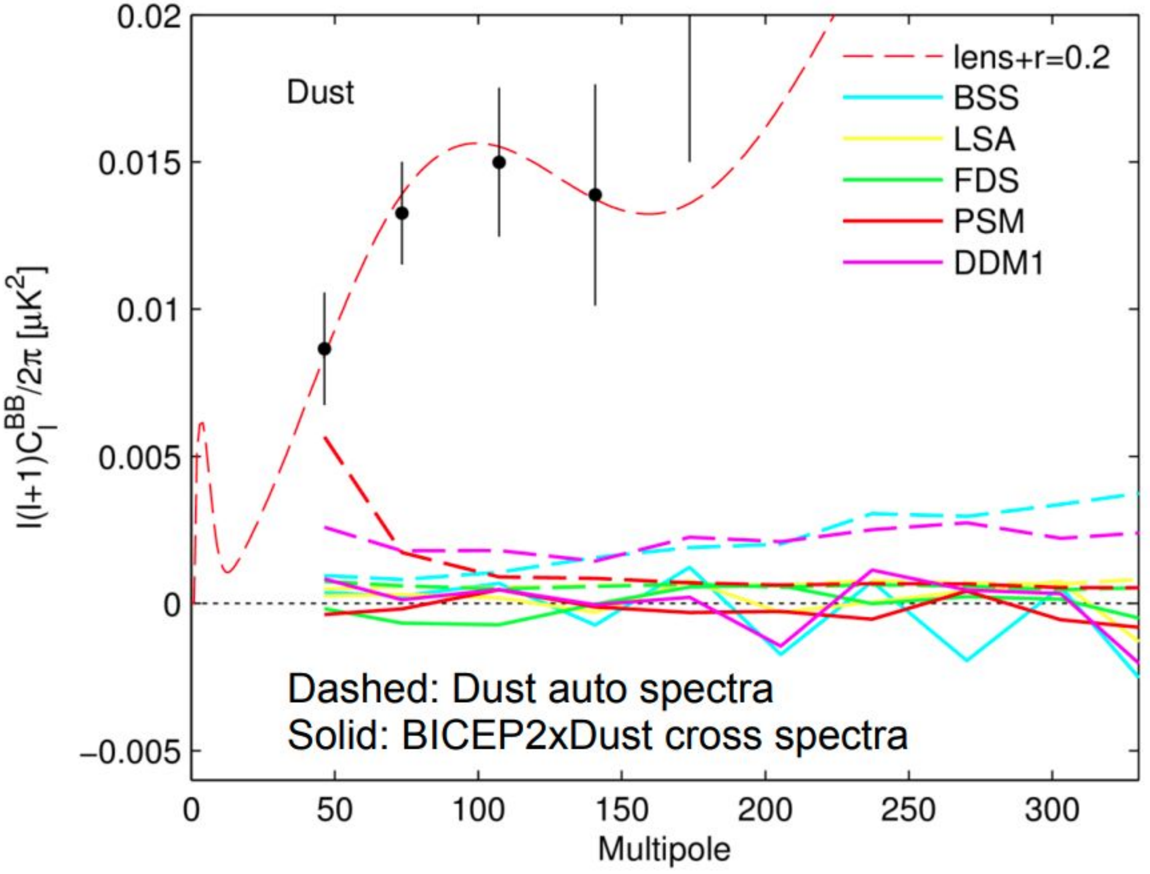

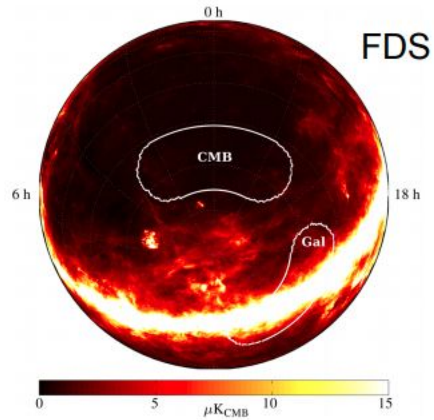

The BICEP2 region is chosen to have lowest foreground emission based on available pre-Planck models.

Use models of polarized dust emission to estimate foregrounds. **(default parameter values)**

Dust model auto spectra are well below observed signal level.

Cross spectra are lower, though this could indicate limitations of models.

Polarized Dust Foreground Measurements

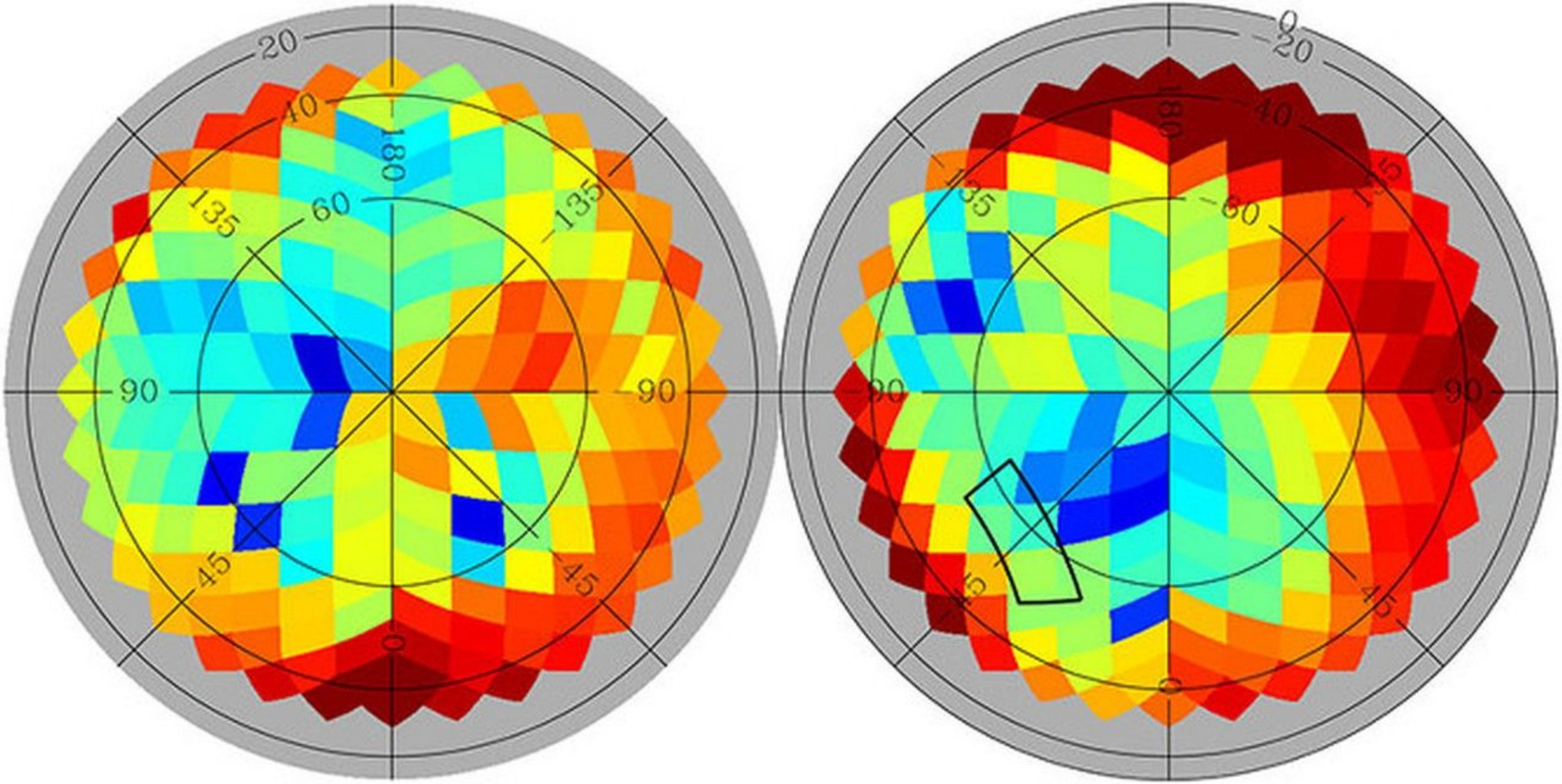

Map of the dust B-mode polarization, as estimated from the Planck data, in units of the signal expected from primordial gravitational waves. The green color corresponds to a Galactic signal comparable to the signal detected by the BICEP2 experiment over the sky patch marked with a black contour. Blue and red colours identify regions of fainter and brighter dust polarization.

The BICEP2 telescope looked at the area surrounded by the black box at right, which shows higher levels of dust than previously assumed. (Planck Collaboration)

Dust to dust

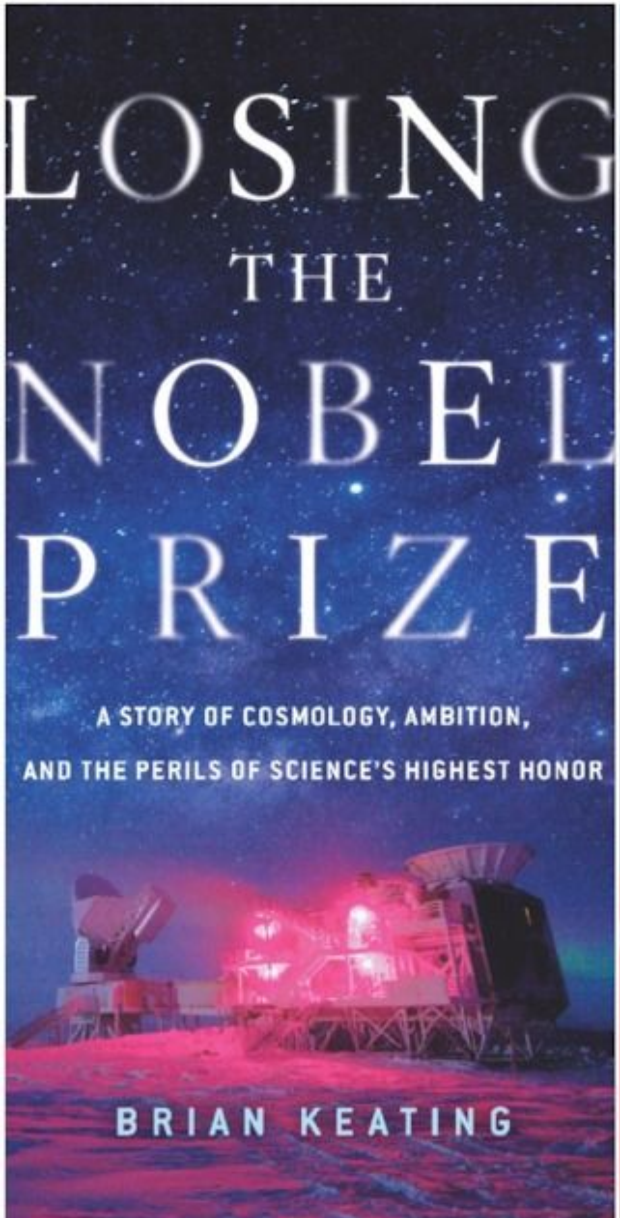
LOSING
THE
NOBEL
PRIZE
A STORY OF COSMOLOGY, AMBITION,
AND THE PERILS OF SCIENCE'S HIGHEST HONOR
BRIAN KEATING

B-modes Power Spectrum

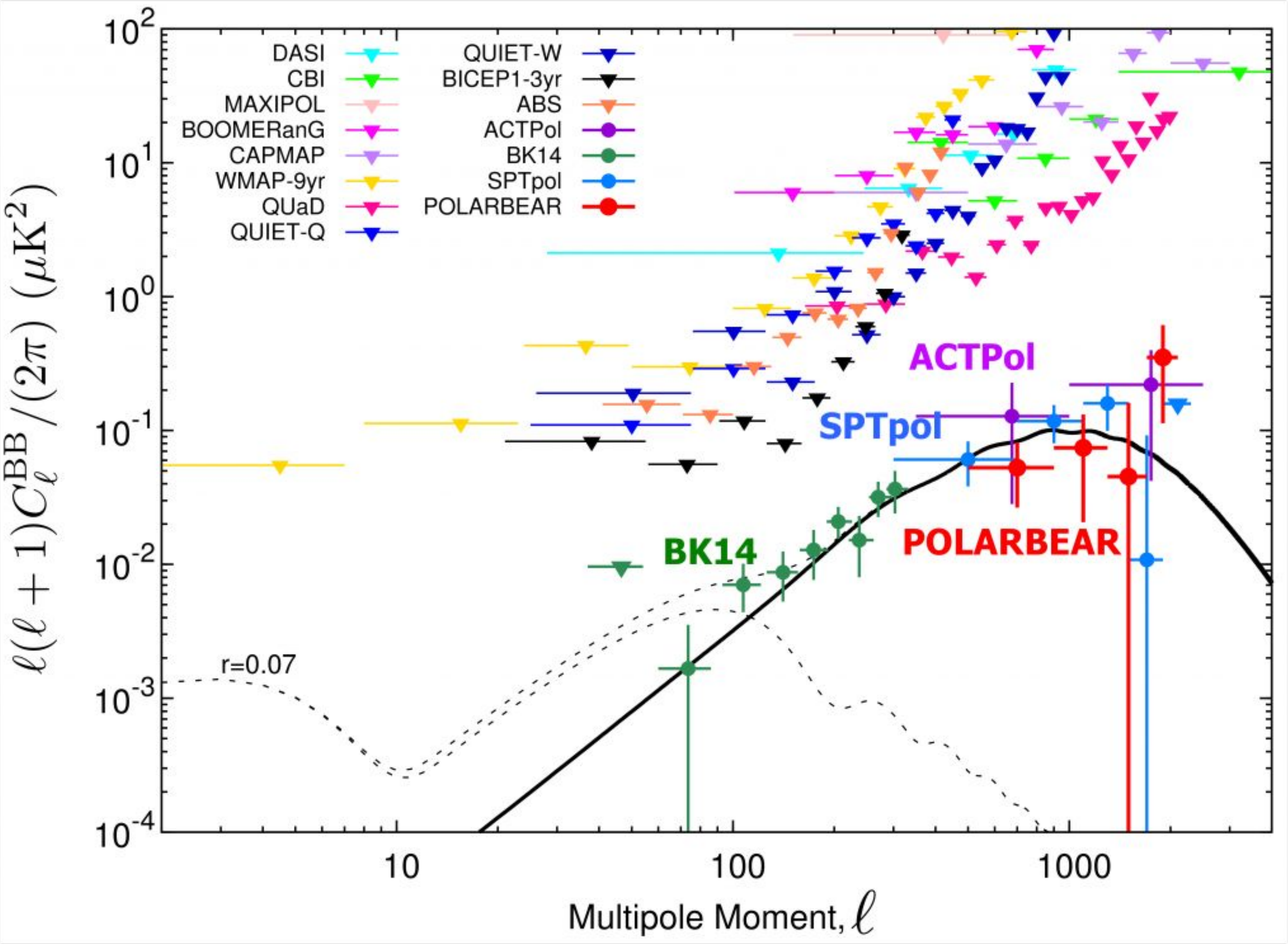

What comes next?

The Simons Array

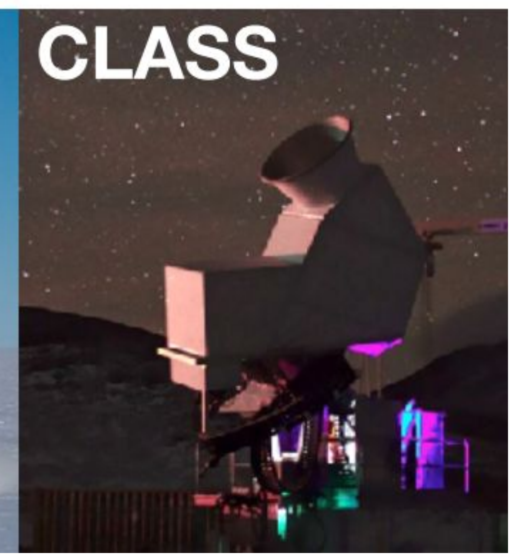

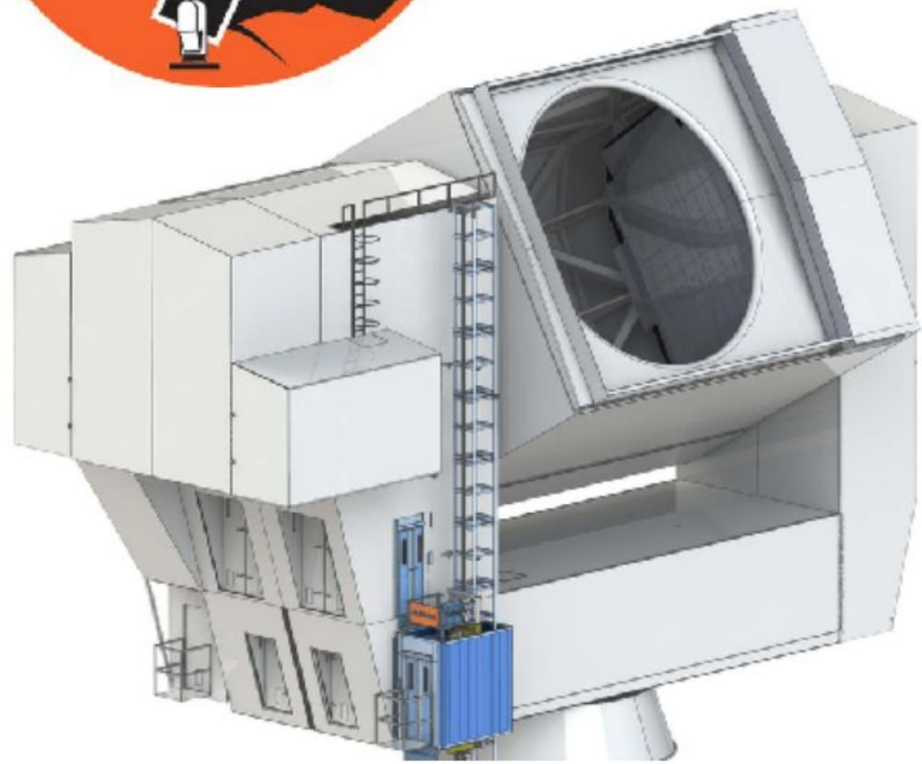

The Simons Array

SIMONS OBSERVATORY

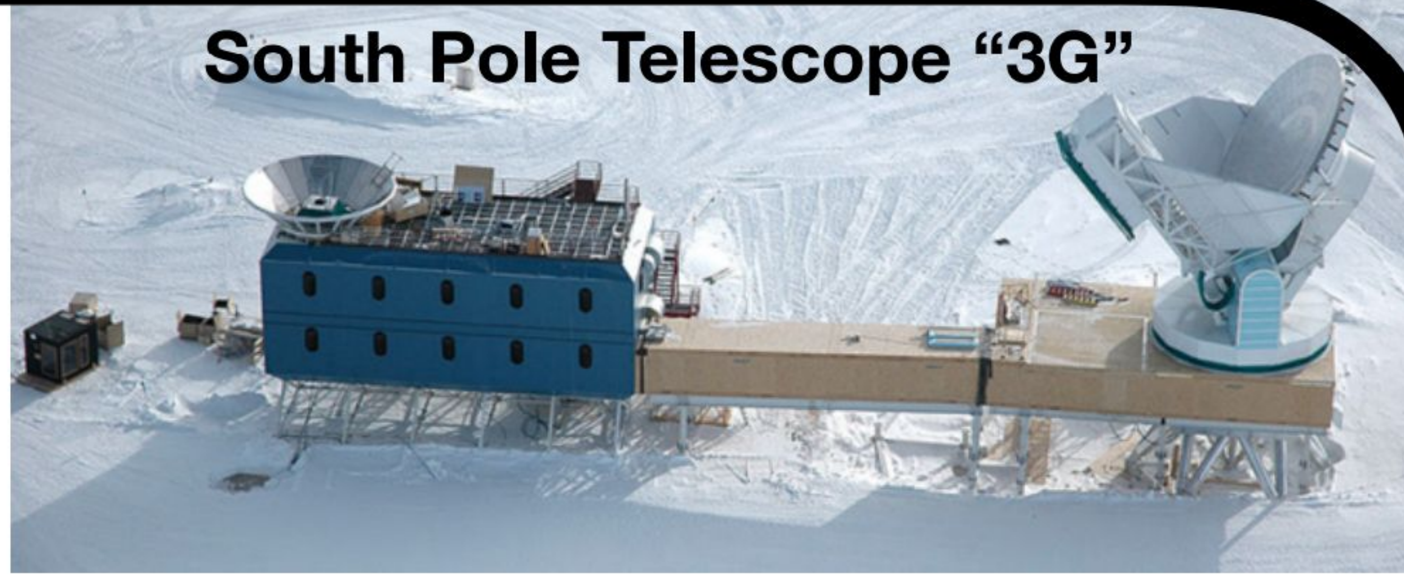

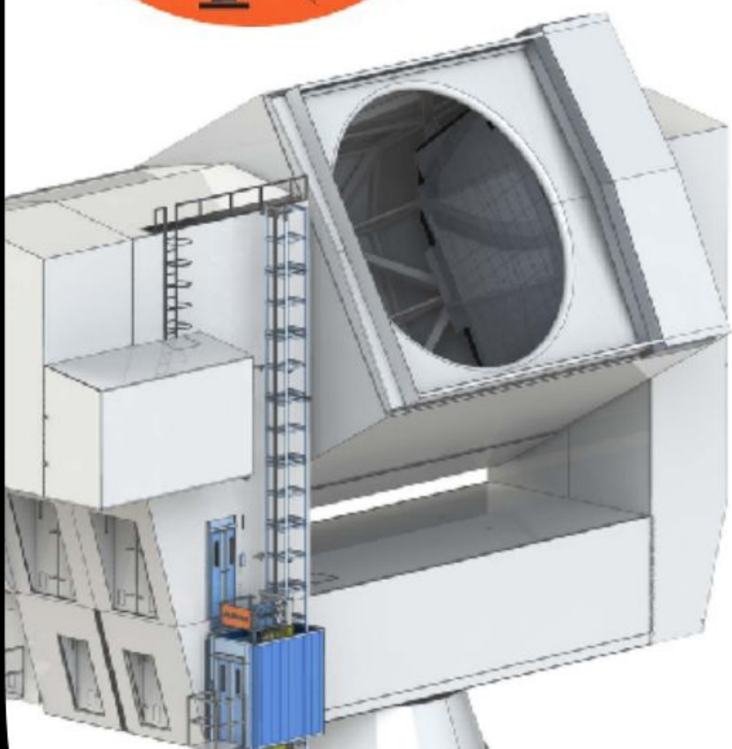

CMB-S4(?)

JAXA

+ participations from USA, Canada, Europe

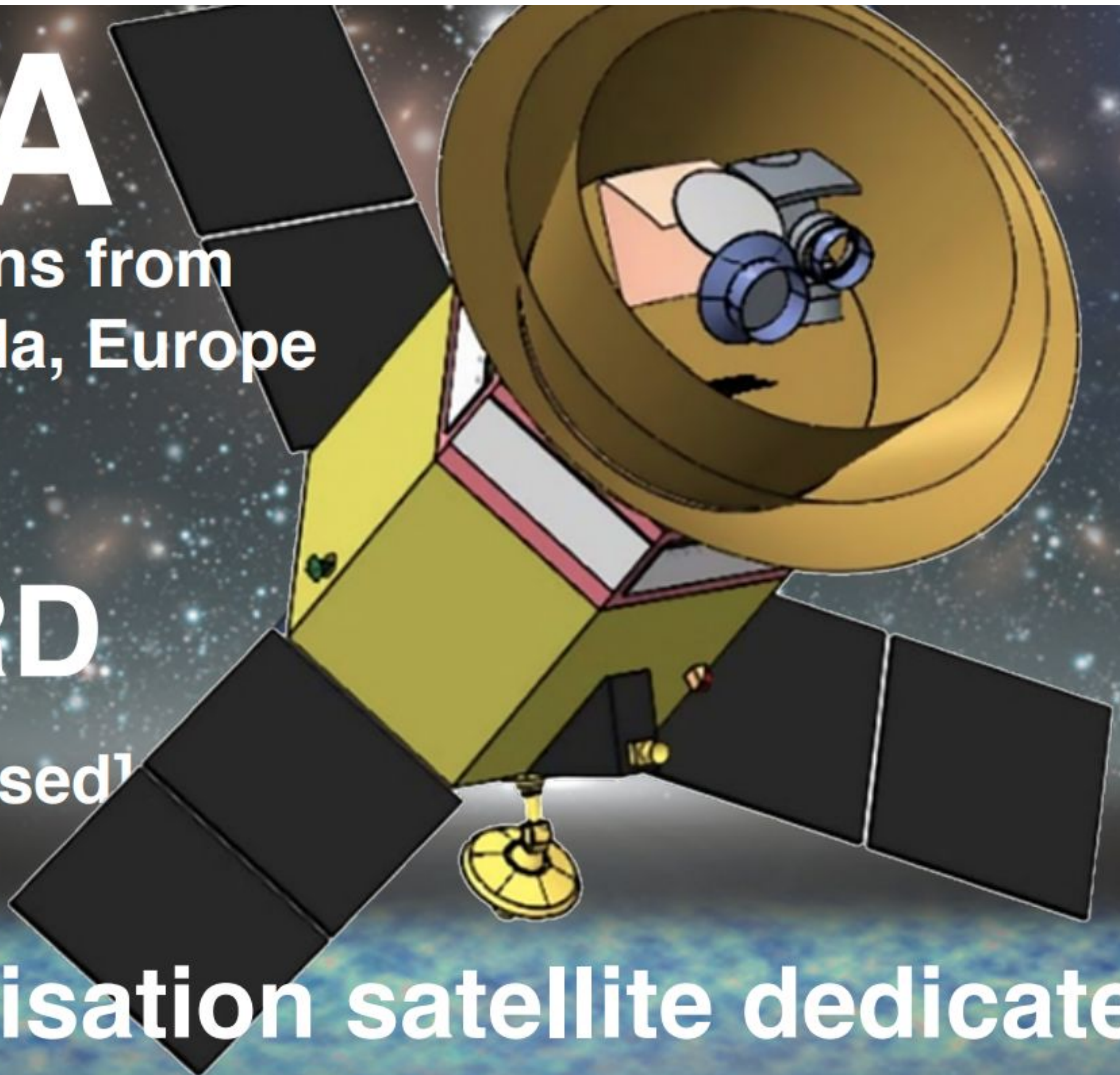

LiteBIRD

2027– [proposed]

Polarisation satellite dedicated to measure CMB polarisation from primordial GW, with a few thousand TES bolometers in space

JAXA

+ participations from
USA, Canada, Europe

LiteBIRD

2027– **Selected!**

May 21: JAXA has chosen LiteBIRD as the strategic large-class mission.

We will go to L2!

CMB Secondary Anisotropies

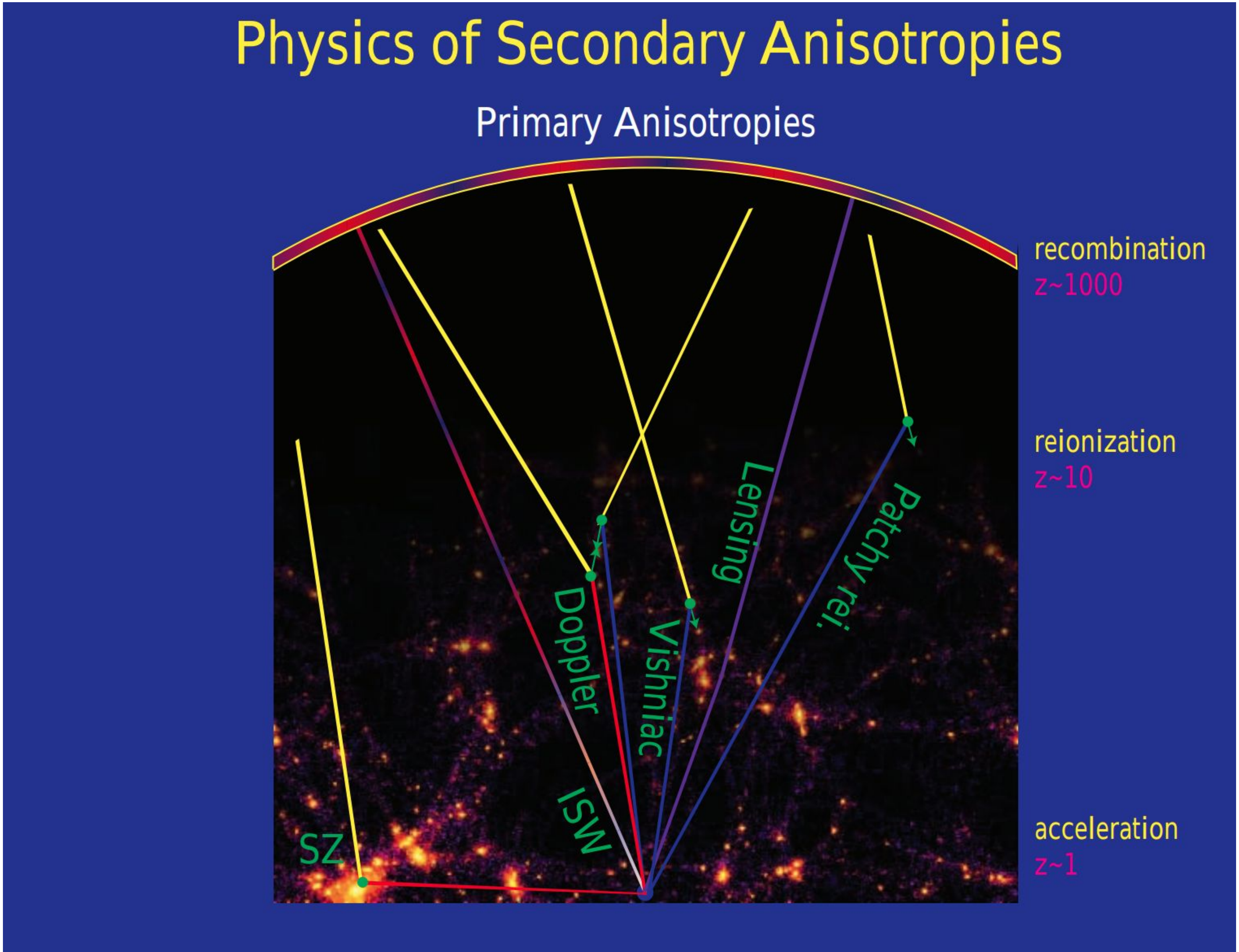

Epoch of Reionization

Epoch of reionization

Big Bang

Universe expanding and cooling

Present day

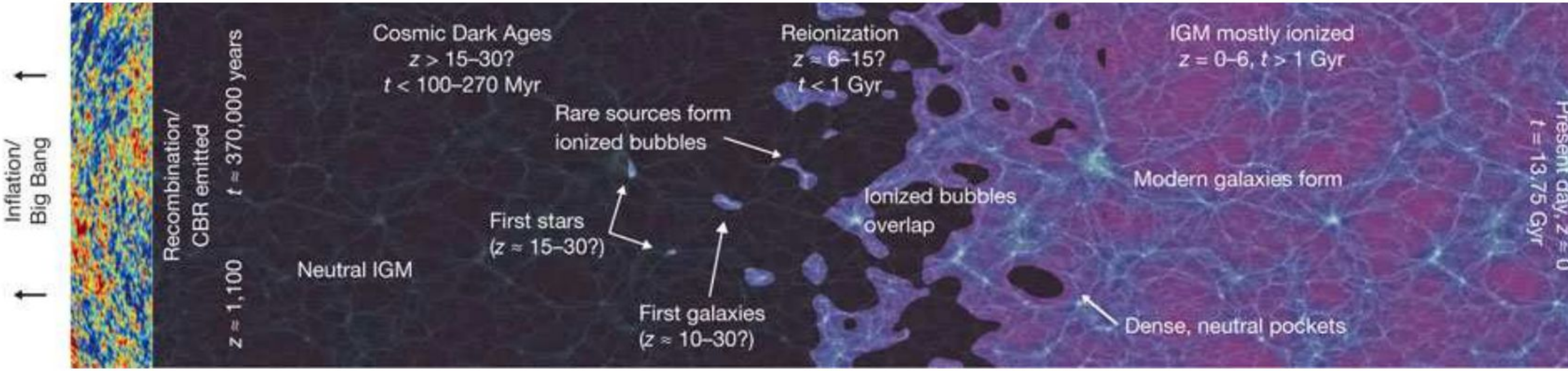

Figure courtesy: `http://www.nature.com/nature/journal/v468/n7320/fig_tab/nature09527_F1.html`

Epoch of reionization

Big Bang

Universe expanding and cooling

Present day

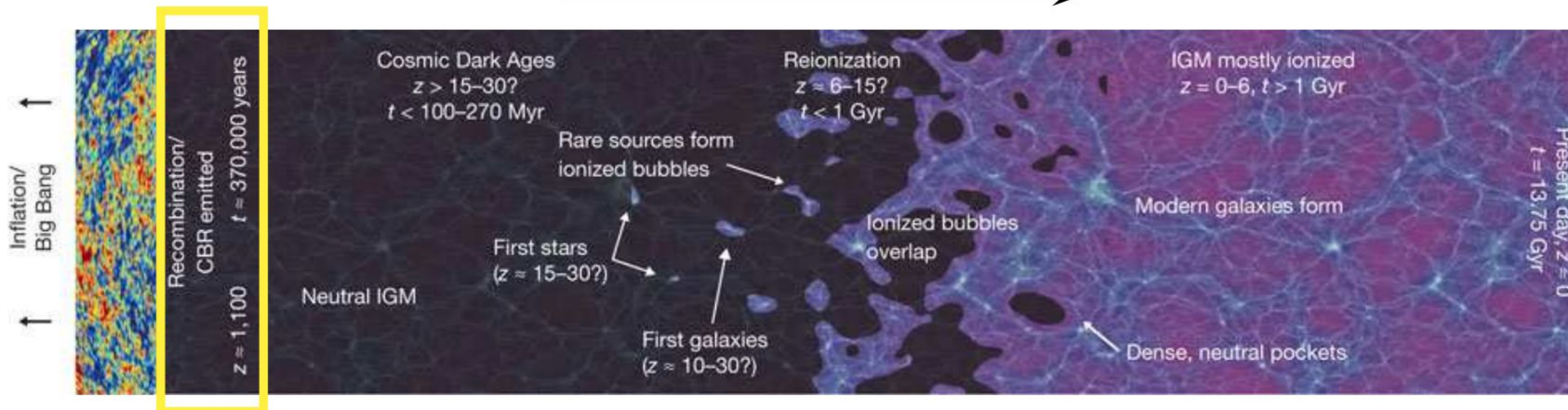

Last scattering epoch

First hydrogen atoms form

Figure courtesy: http://www.nature.com/nature/journal/v468/n7320/fig_tab/nature09527_F1.html

Epoch of reionization

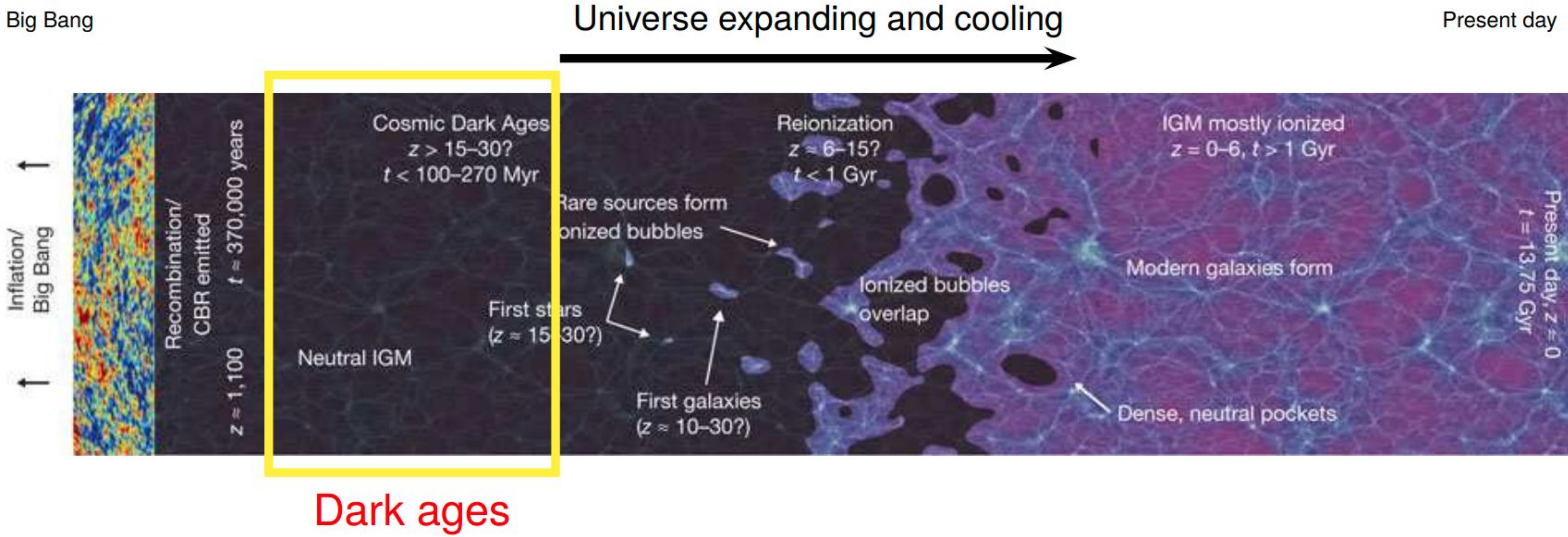

Figure courtesy: http://www.nature.com/nature/journal/v468/n7320/fig_tab/nature09527_F1.html

Epoch of reionization

Big Bang | **Universe expanding and cooling** → | Present day

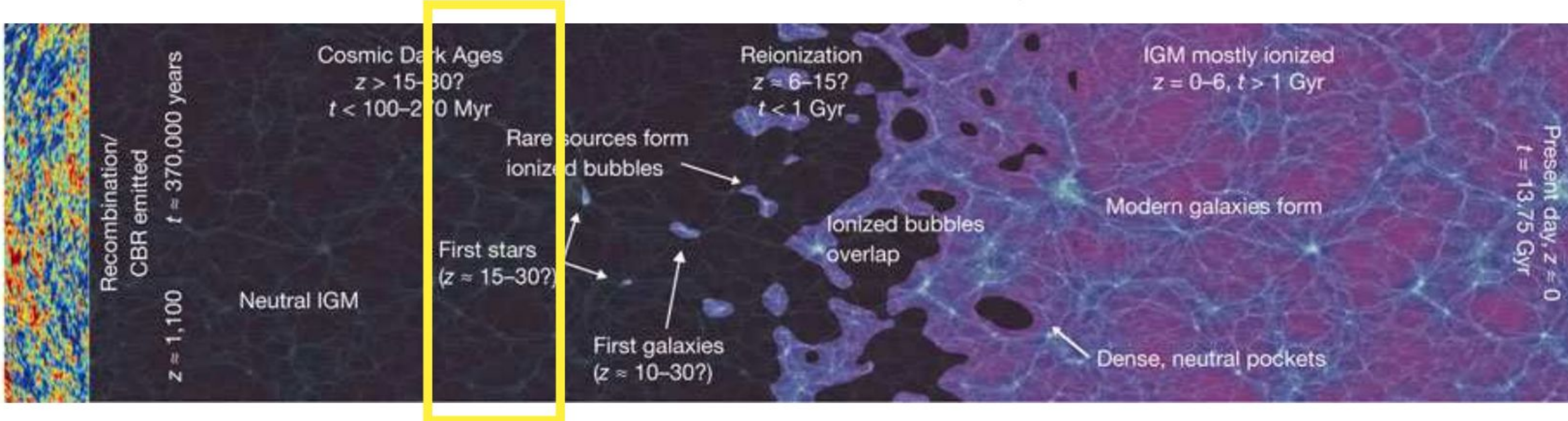

First stars form

Figure courtesy: http://www.nature.com/nature/journal/v468/n7320/fig_tab/nature09527_F1.html

Epoch of reionization

Big Bang

Universe expanding and cooling

Present day

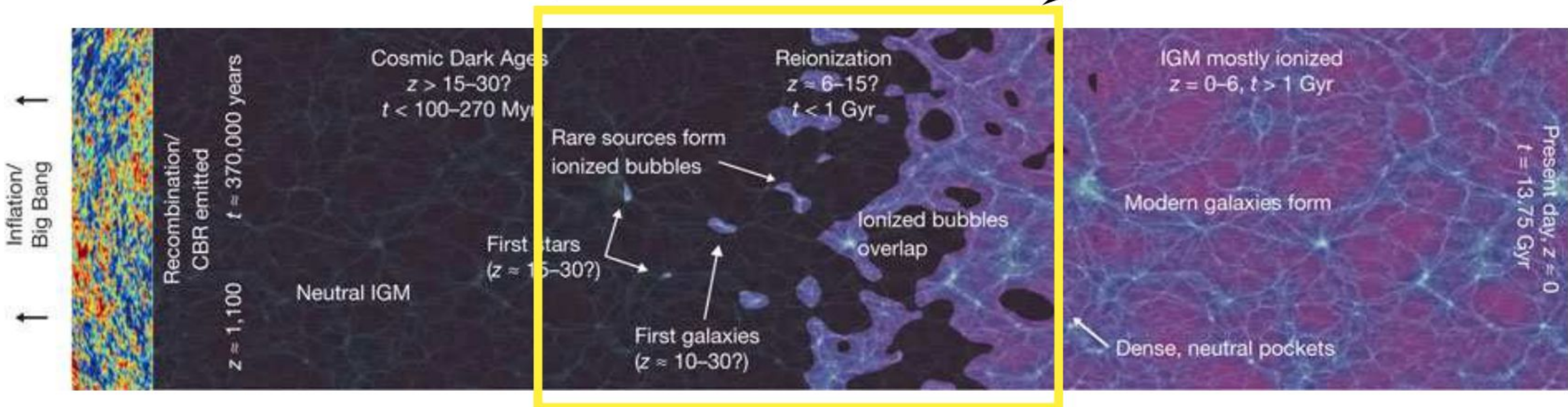

Reionization

Figure courtesy: `http://www.nature.com/nature/journal/v468/n7320/fig_tab/nature09527_F1.html`

Epoch of reionization

Big Bang

Universe expanding and cooling

Present day

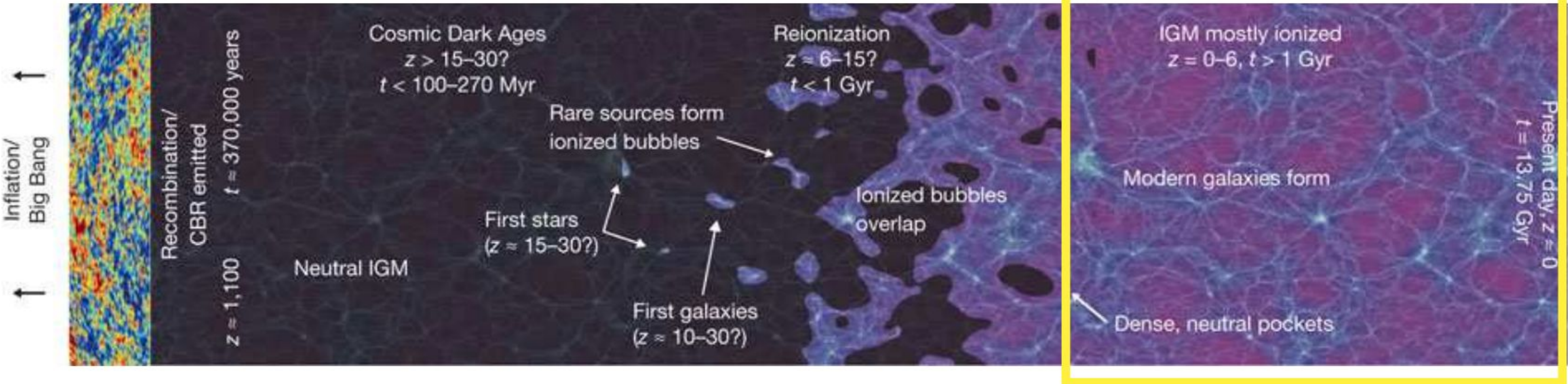

Post-reionization

Figure courtesy: http://www.nature.com/nature/journal/v468/n7320/fig_tab/nature09527_F1.html

Epoch of reionization

Big Bang | Universe expanding and cooling | Present day

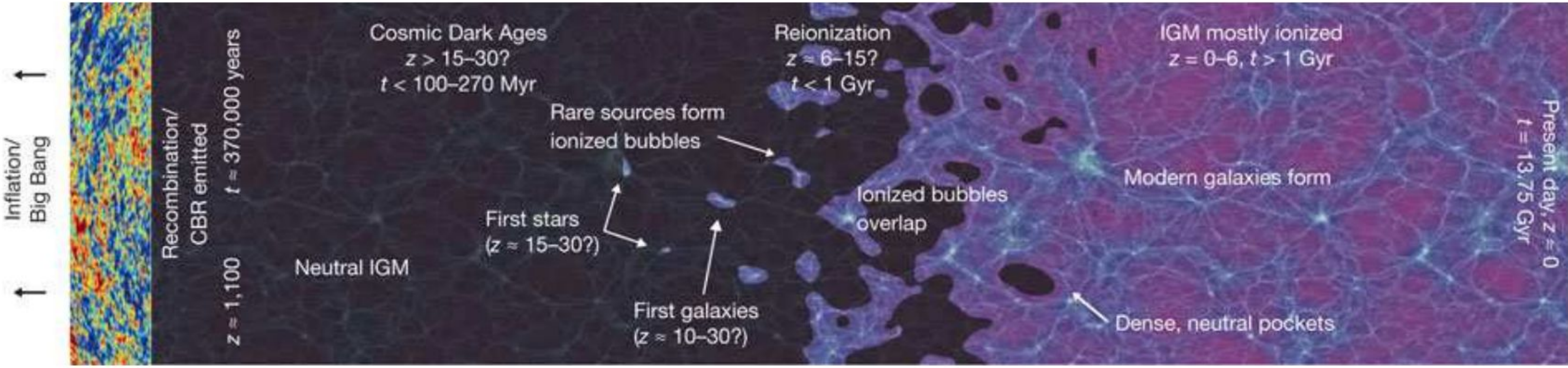

Dark ages

Strong probe of cosmology

Reionization

1. First stars
2. Cosmology

Post-reionization

1. Galaxy formation
2. Cosmology

Evidence for reionization of the Inter-Galactic Medium

- CMB
- Lyman alpha Forest

CMB angular Power Spectrum

- CMB photons scatter off free electrons.
- Th ... rvations is the ... attering off fre

$$\tau_{\rm el} = \sigma_T c \int_{t_{\rm LSS}}^{t_0} {\rm d}t\, n_e\, (1+z)^3$$

Provided by reionization

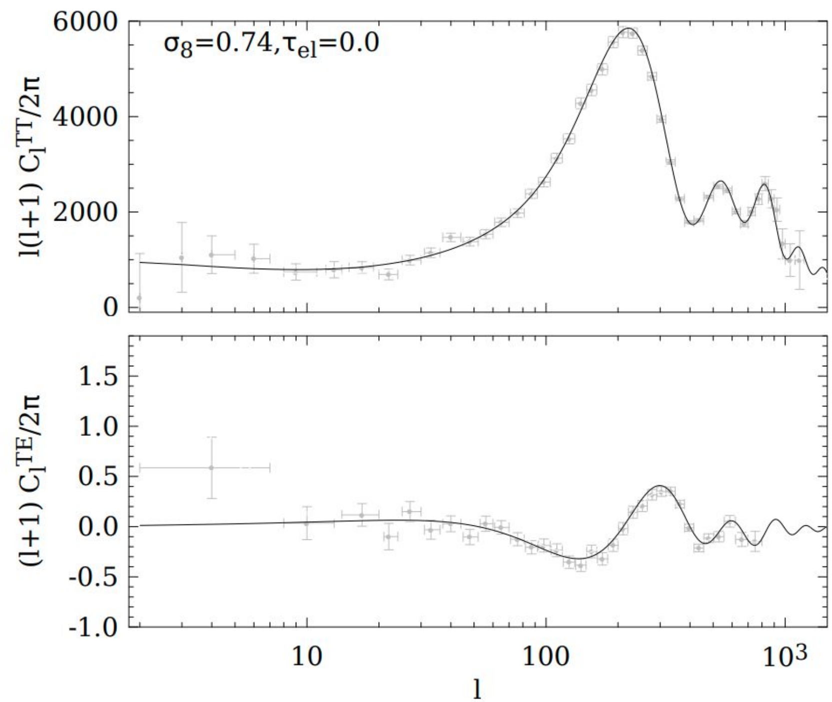

CMB angular Power Spectrum

- CMB photons scatter off free electrons.
- Th … rvations is the … attering off fre…

$$\tau_{\rm el} = \sigma_T c \int_{t_{\rm LSS}}^{t_0} {\rm d}t \, n_e \, (1+z)^3$$

Provided by reionization

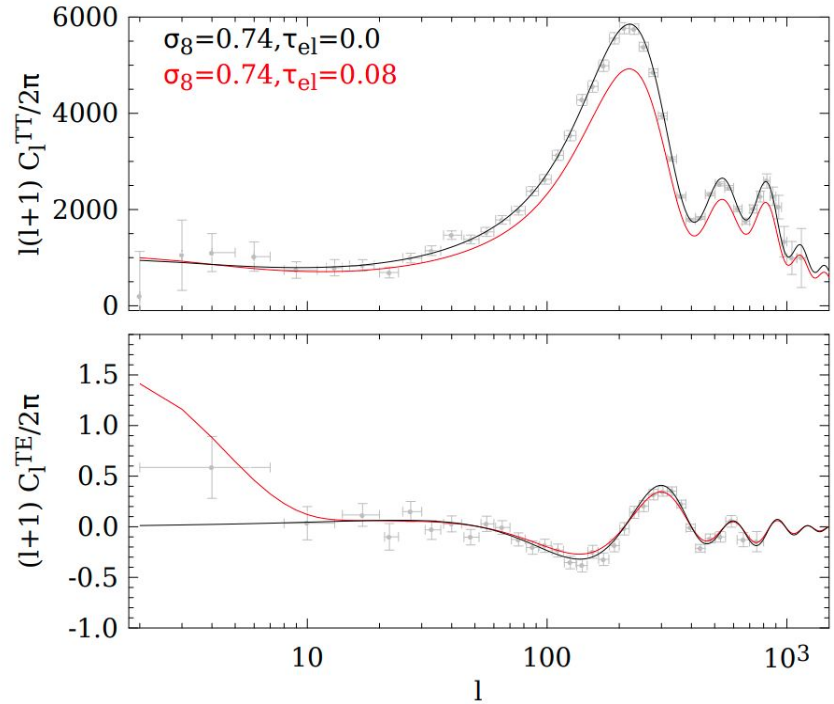

CMB angular Power Spectrum

- CMB photons scatter off free electrons.
- Th … rvations is the … attering off fre …

$$\tau_{\rm el} = \sigma_T c \int_{t_{\rm LSS}}^{t_0} {\rm d}t\, n_e\, (1+z)^3$$

Provided by reionization

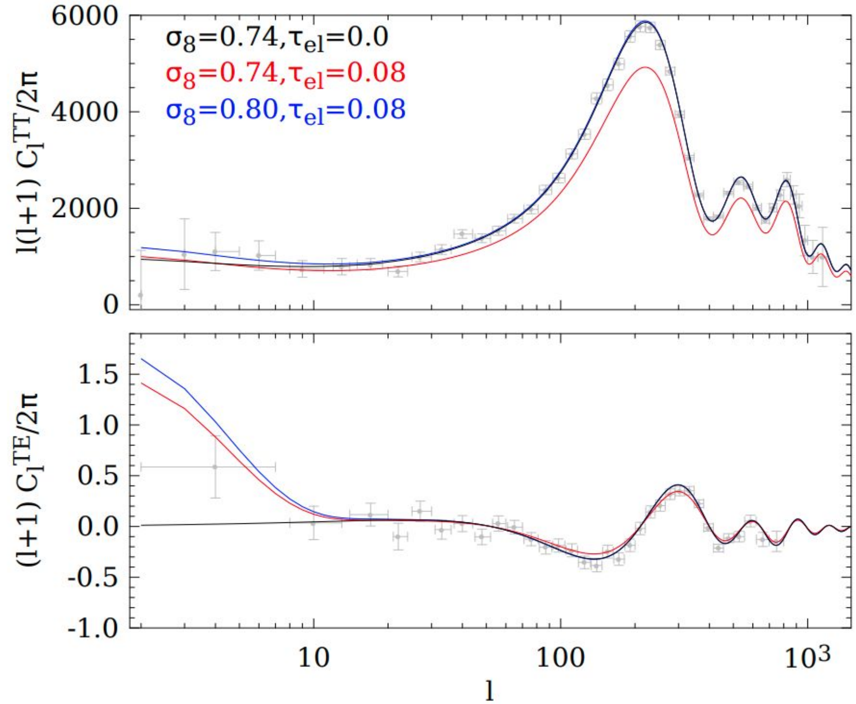

CMB angular Power Spectrum

- Current constraints on reionization come from polarization signal at large angular scales
- (weak signal, can be confused with polarized foregrounds, e.g., WMAP, Planck)
- dampening of anisotropies at (almost) all angular scales

$$\tau_{\rm el} = \sigma_T \, c \, n_H \int_0^{z_{\rm re}} {\rm d}z \left| \frac{{\rm d}t}{{\rm d}z} \right| (1+z)^3$$

- (effect is degenerate with amplitude of density power spectrum)
- Planck and high resolution ground based experiments can break the degeneracy through lensing of the CMB

Thomson scattering $\tau_{\rm el}$ from CMBR

NCRA

$$\tau_{\rm el} = \sigma_T c \int_0^{z[t]} {\rm d}t\, n_e\, (1+z)^3$$

Planck Collaboration (2016)

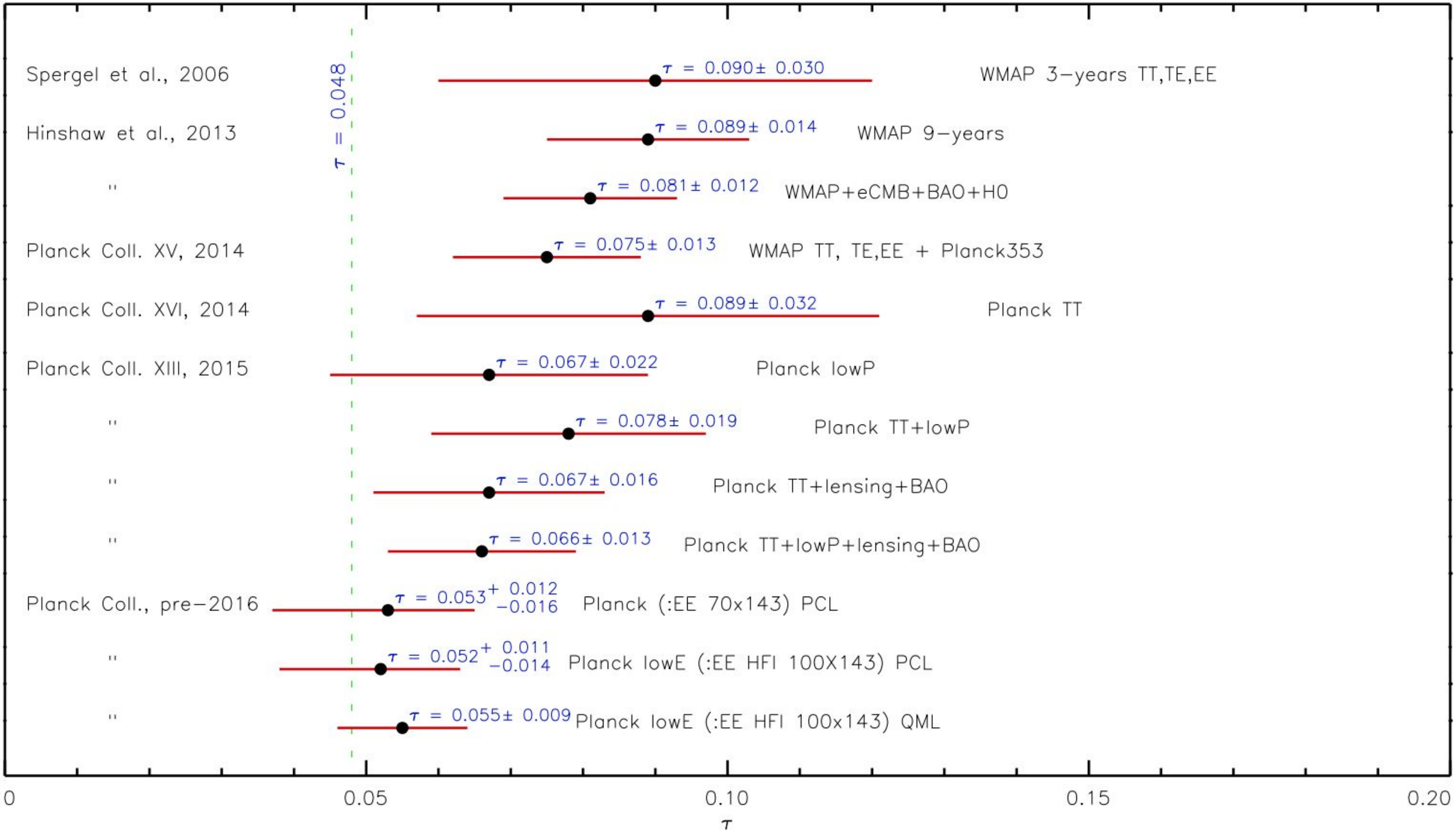

Evidence for reionization: Lyman-α forest

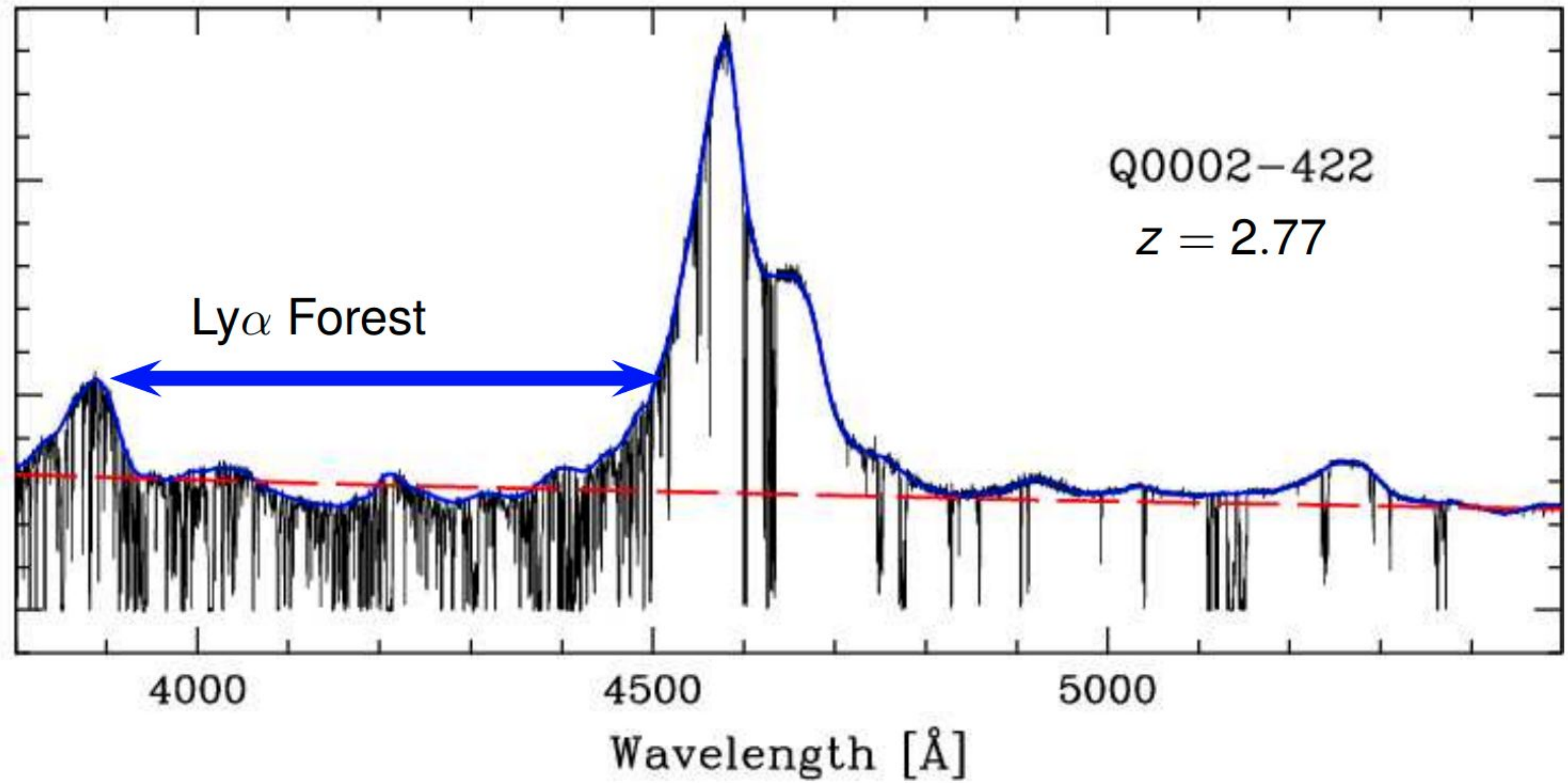

The absorption lines blueward of the emission line arise from Lyα transition ($n = 1$ to $n = 2$) of neutral hydrogen (HI) present between the quasar and us.

Absorption lines

- The IGM is detected through the absorption features it produces in the spectrum of a background bright source of light (typically a QSO).

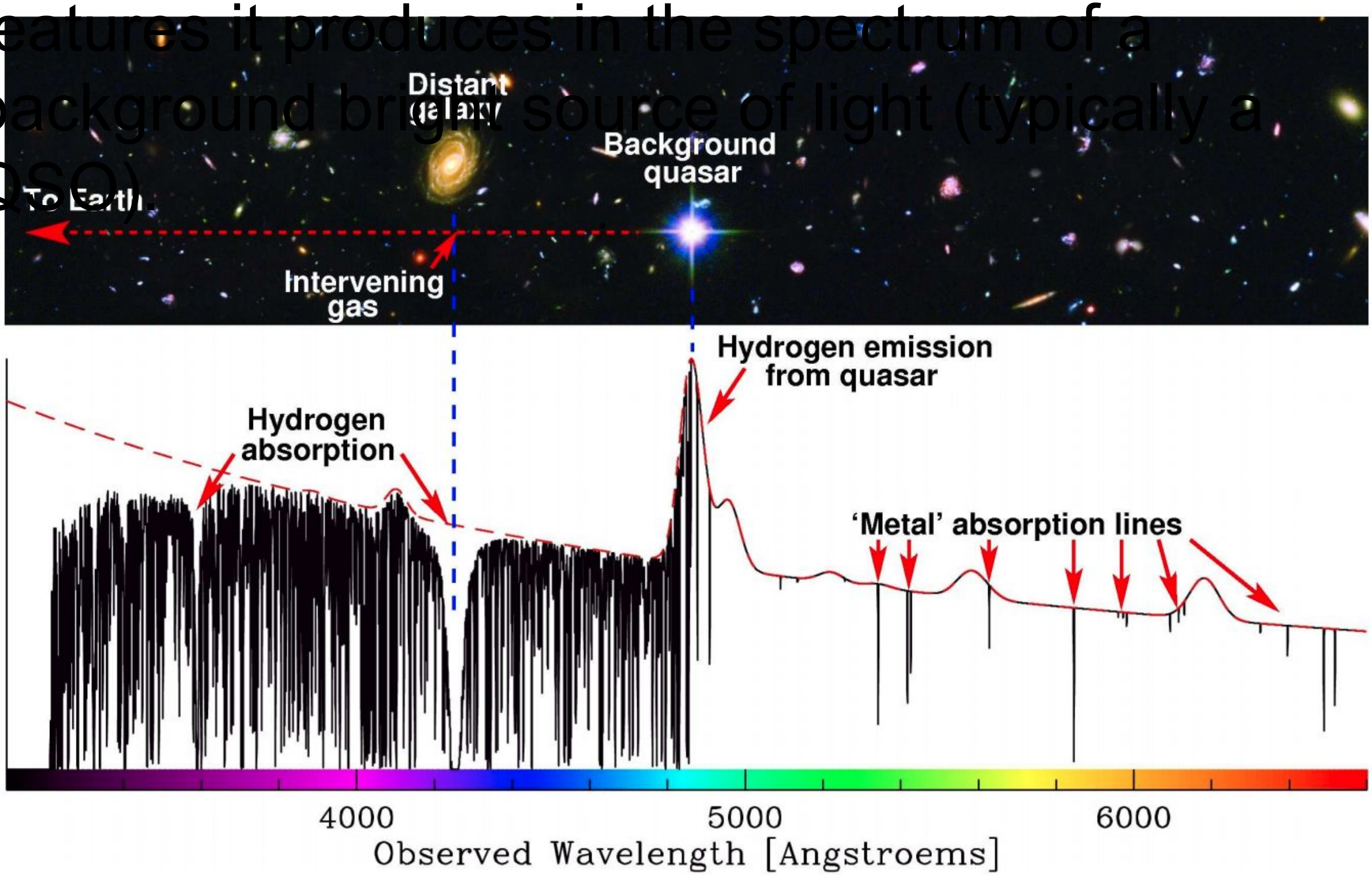

http://www.eso.org/~jliske/qsoal/

Absorption lines

- Consider radiation (photons) emitted at the QSO (at $z = z_Q$) rest frame frequency $\nu_Q > \nu_{fi}$. As the universe expands, the frequency will decrease and will reach ν_{fi} at a redshift z given by

$$\frac{\nu_Q}{1+z_Q} = \frac{\nu_{fi}}{1+z} \implies \lambda_Q(1+z_Q) = \lambda_{fi}(1+z)$$

- Example: Consider a QSO at $z_Q = 3$. Consider a photon emitted at wavelength $\lambda_Q = 1187$ Å, then it would reach the Lyα wavelength 1216 Å at $z \approx 1187 \times 4/1216 - 1 \approx 2.9$. If there is neutral hydrogen at that position, it will produce an absorption signature.
- We will observe the feature at $\lambda = \lambda_Q(1+z_Q) \approx 4742$ Å. Thus any absorption arising at a redshift z will show up at $\lambda = \lambda_{fi}(1+z)$.

Absorption signatures

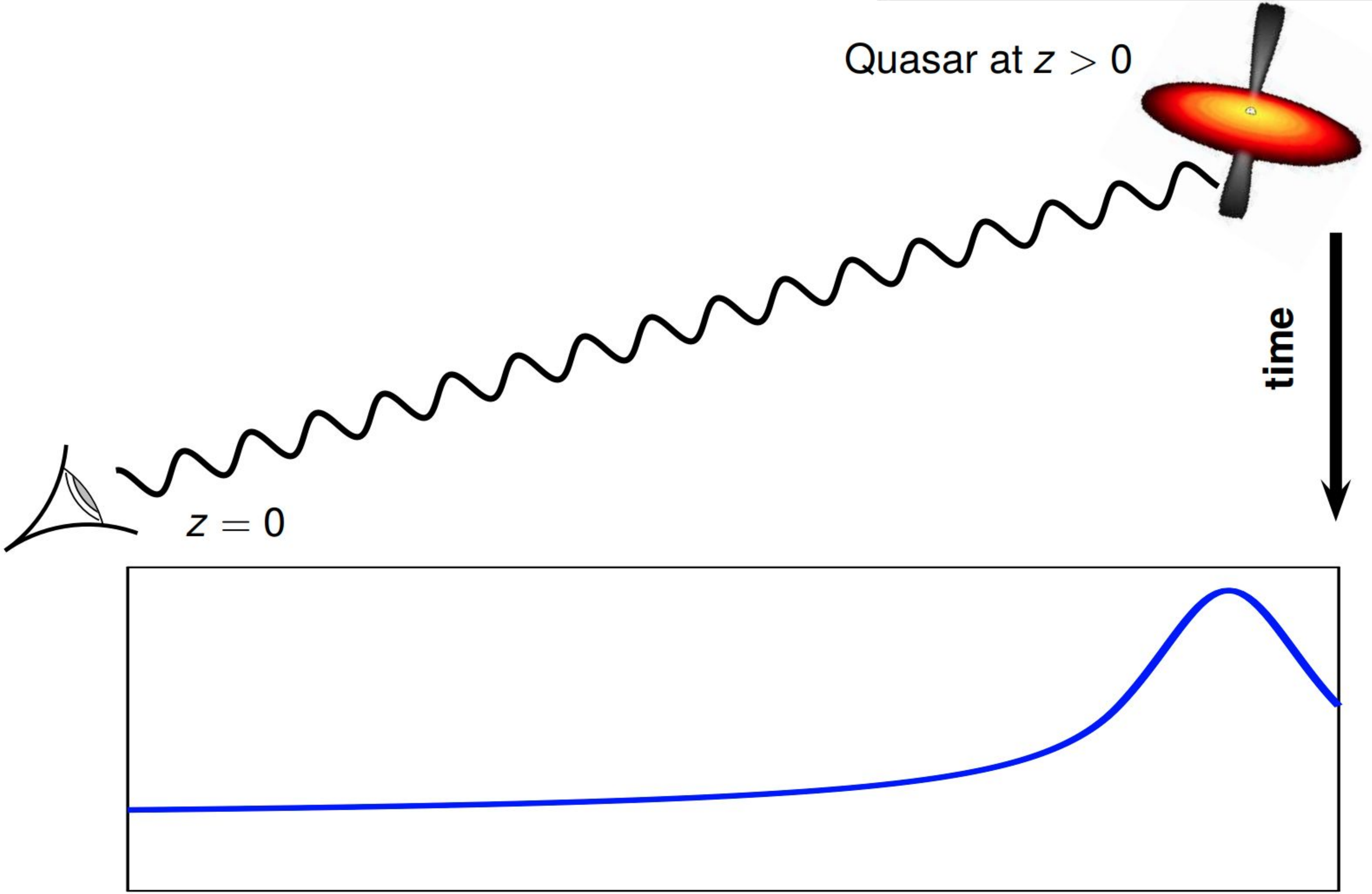

Absorption signatures

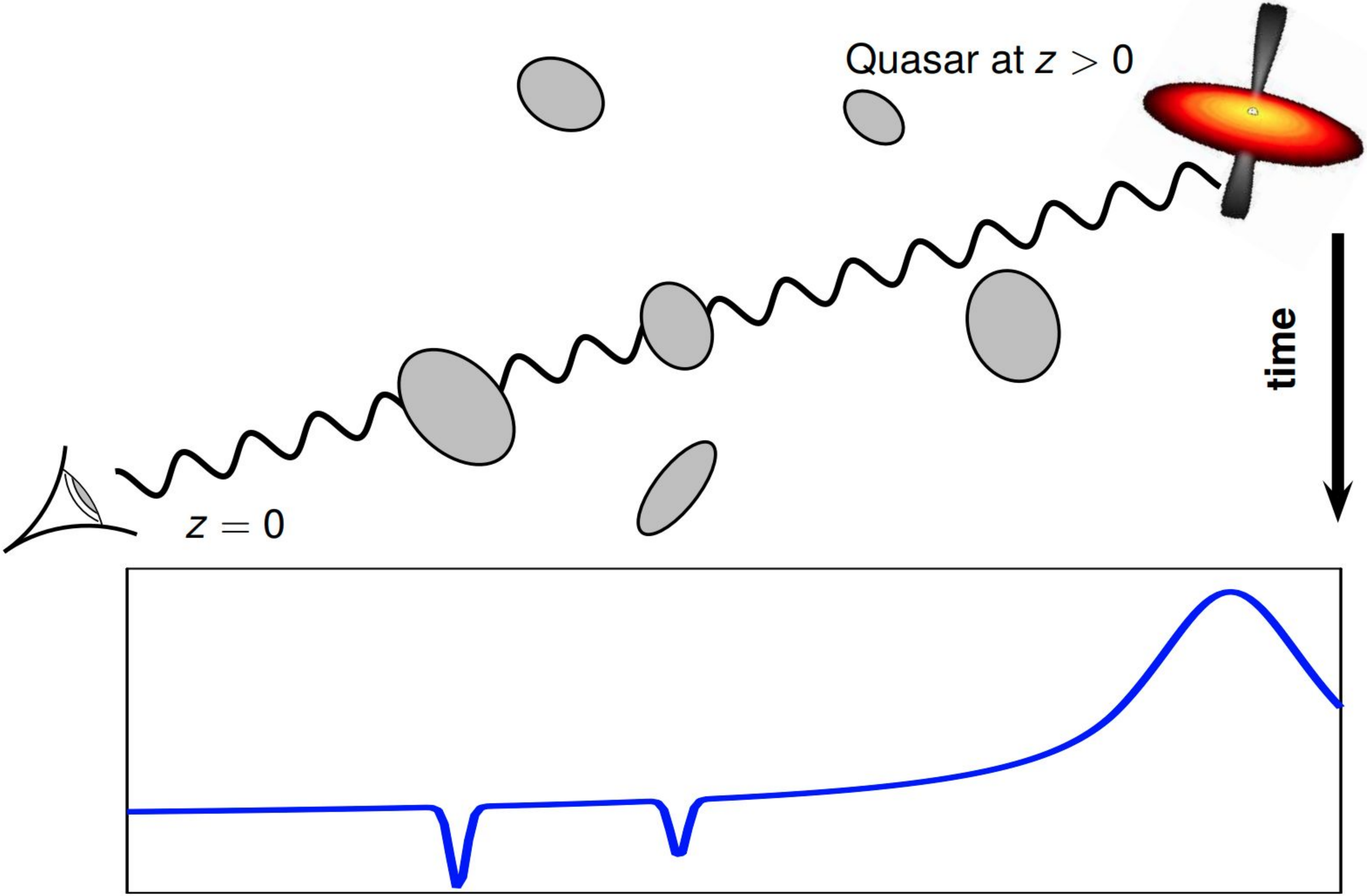

Absorption spectra

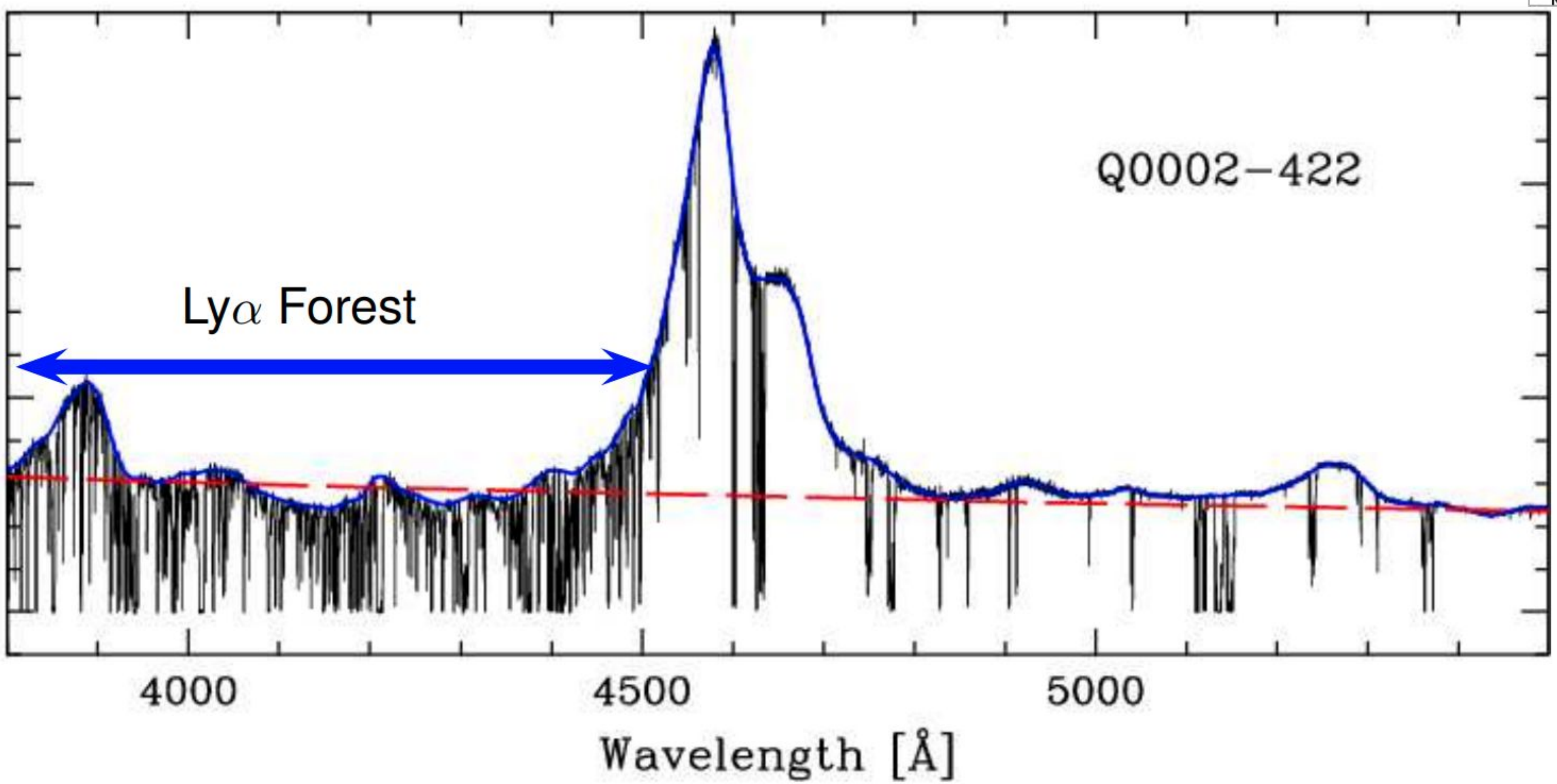

- The absorption lines blueward of the emission line arise from Lyα transition of neutral hydrogen (HI) present between the QSO and us.
- The unabsorbed regions correspond to either ionized regions or no matter at all.

Gunn-Peterson effect

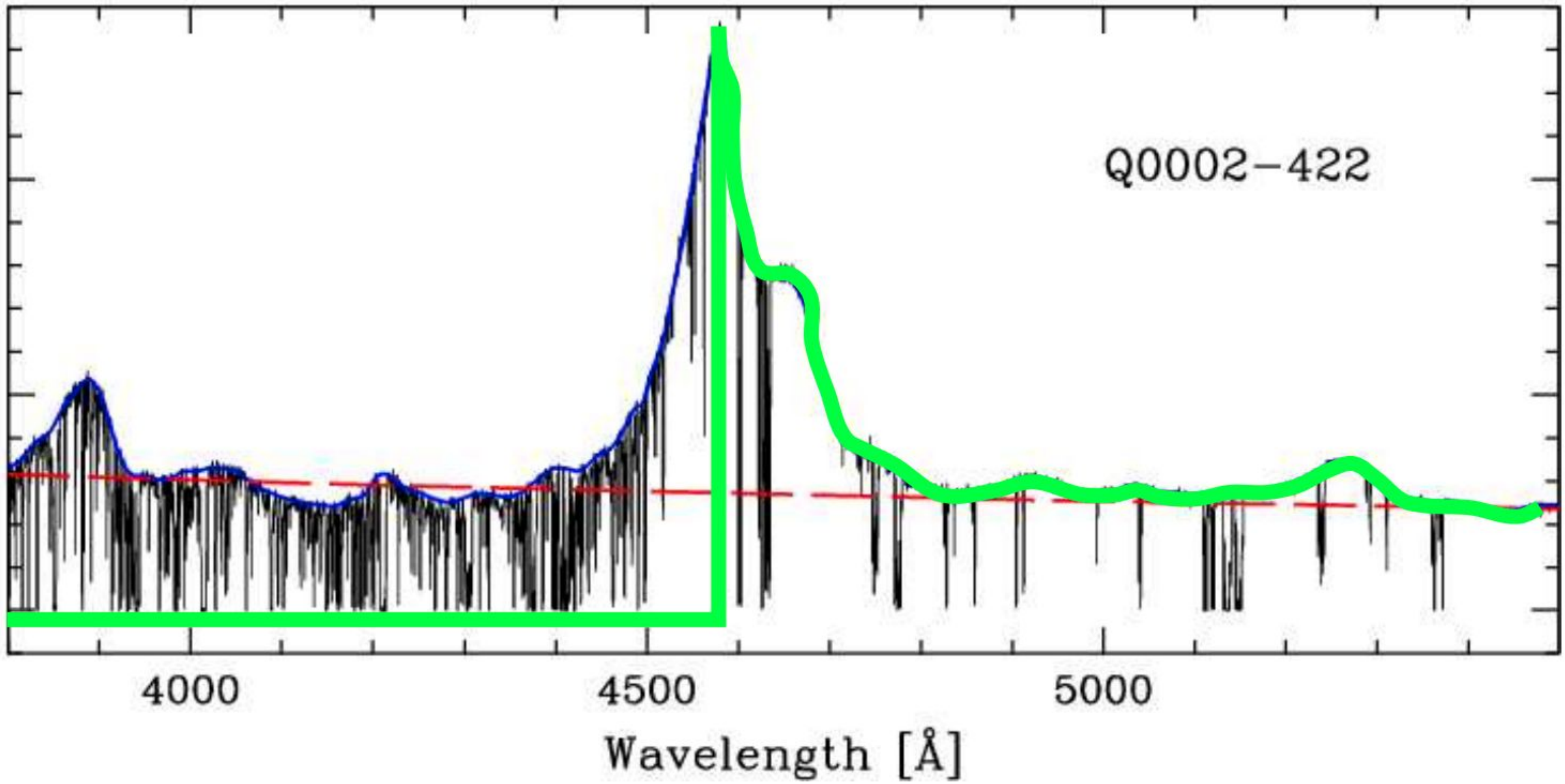

Observed flux $\sim$ Unabsorbed flux $\times\ \exp\left(-10^5\, x_{\rm HI}\right)$, where $x_{\rm HI} = \rho_{\rm HI}/\rho_H$.

The fact that there is non-zero flux implies that $x_{\rm HI} \simeq 10^{-5}$

Non-zero flux observed till $z \sim 5.5$

QSO absorption lines at $z \sim 6$

$z \approx 0$

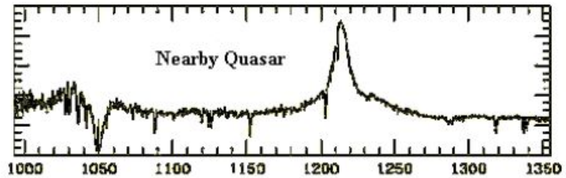

$z \approx 3$

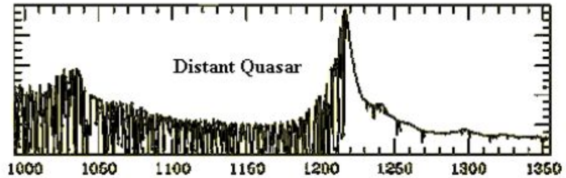

$x_{\mathrm{HI}} \lesssim 10^{-5}$

$z = 5.80$

$z = 5.82$

$z = 5.99$

$z = 6.28$

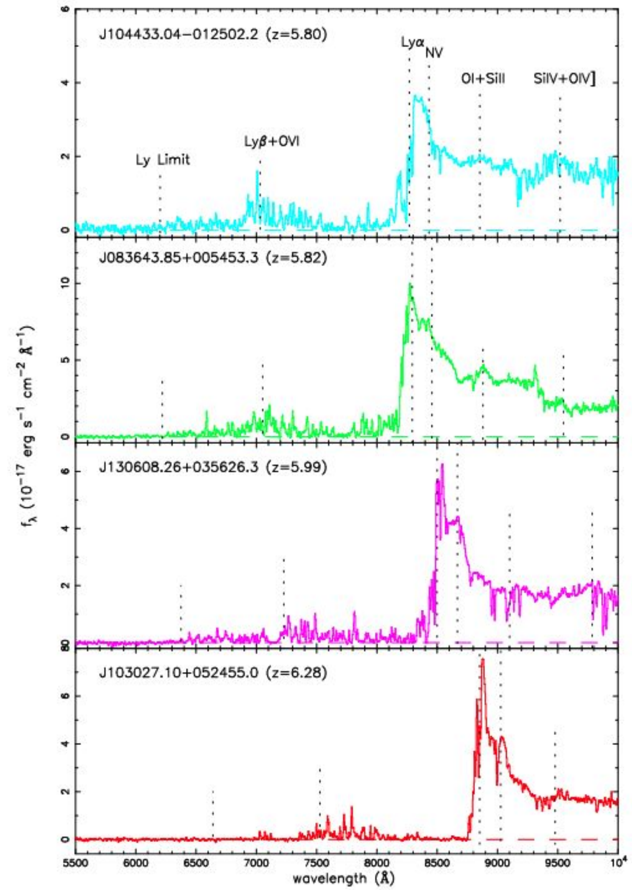

QSO absorption lines at $z \sim 6$

$z \approx 0$

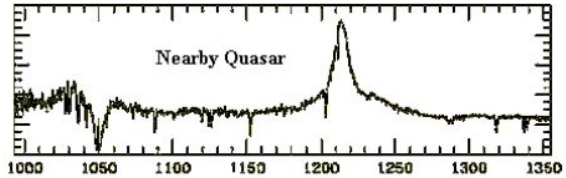

$z \approx 3$

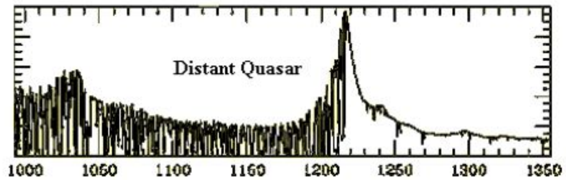

$x_{\rm HI} \lesssim 10^{-5}$

$z = 5.80$

$z = 5.82$

$z = 5.99$

$z = 6.28$

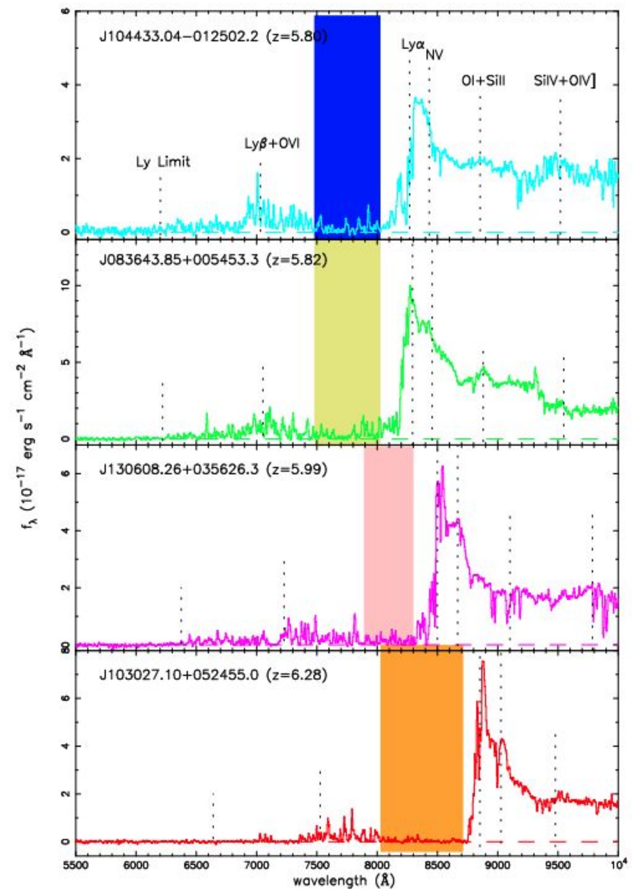

Does this absorption mean high neutrality?

QSO absorption lines at $z \sim 6$

- Gunn-Peterson optical depth:

$$\tau_{\rm GP} \approx \left(\frac{\bar{x}_{\rm HI}}{10^{-5}}\right)$$

- So, even a neutral fraction $x_{\rm HI} \approx 10^{-4}$ would produce **complete absorption**!
- Lyα transition "too strong", saturates too easily....

Around z~6 large dark gaps appear in the spectrum

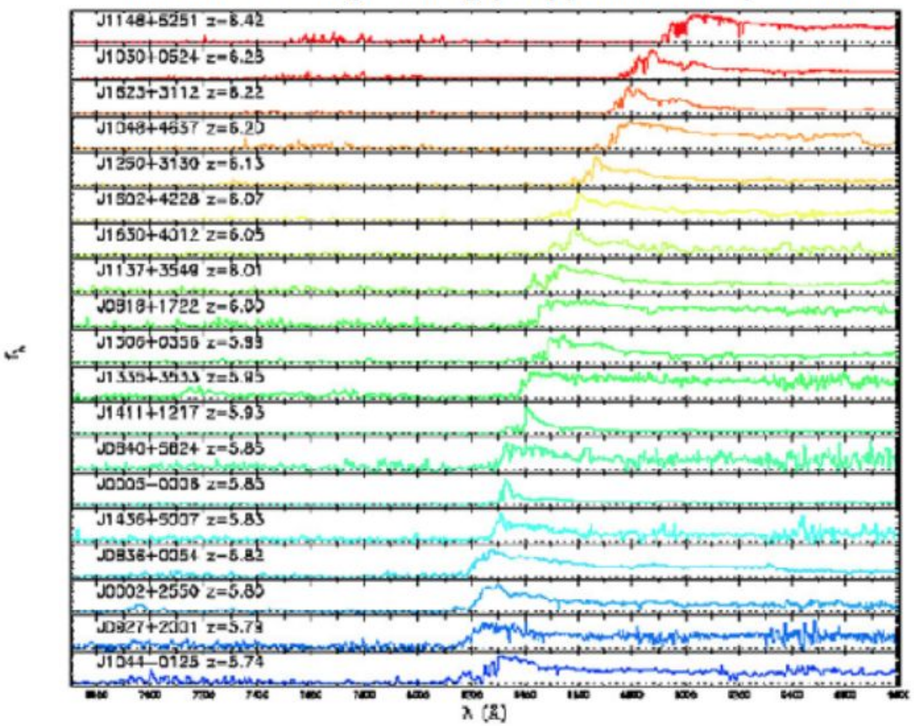

Fan et al. 2006

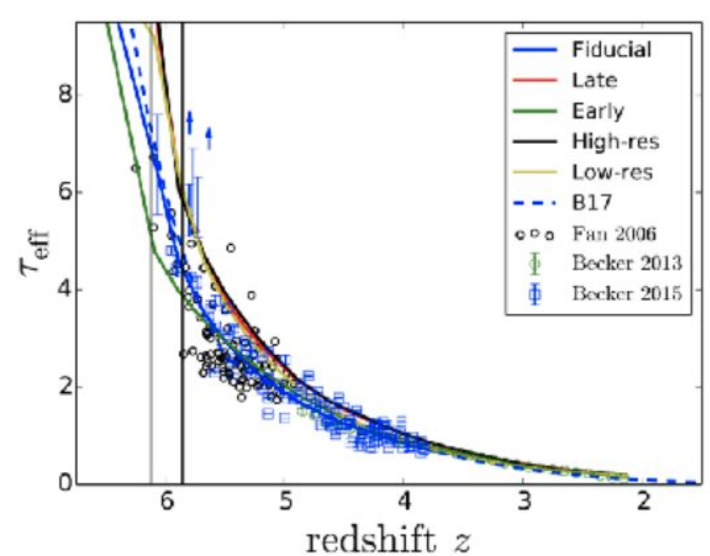

Barnett et al. 2017

Observations of low-z quasars show a clear Gunn-Peterson effects, suggesting that reionization ended around z~6 (rapid increase in optical depth at z>6).

Perspectives

- Epoch of reionization? When did the sources produce enough photons to ionize the Universe? z = 20 or z = 6?
- Nature of reionization? Sudden or Gradual? Homogeneous or Inhomogeneous?
- What are the sources responsible? Stars, quasars, Exotic Particles?
- Confusing statements while interpreting the data:
  - Quasar absorption spectra imply that “redshift of reionization” is z ~ 6?

Extremely active field of research in Trieste!!
(Fontanot, Cristiani, Dodorico, Feruglio,..)

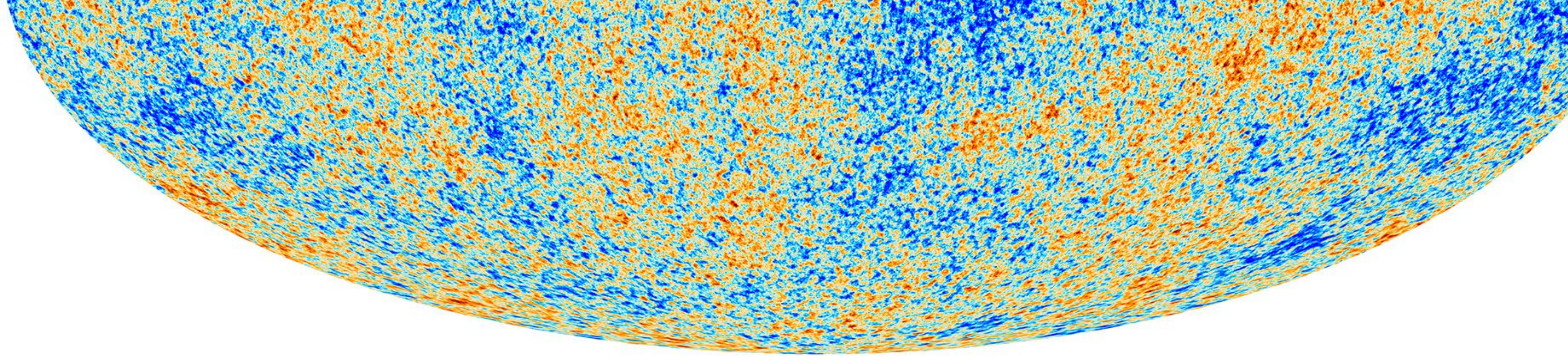

Adapted from L. Van Speybroeck

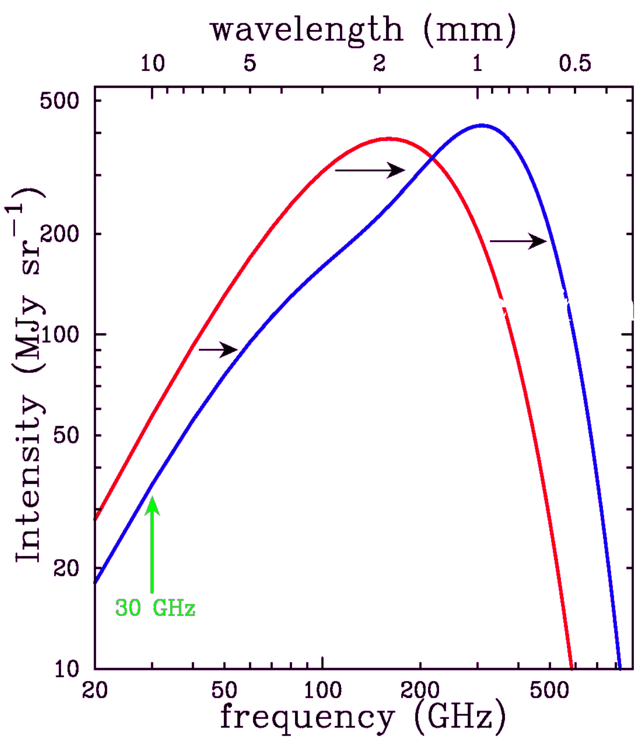

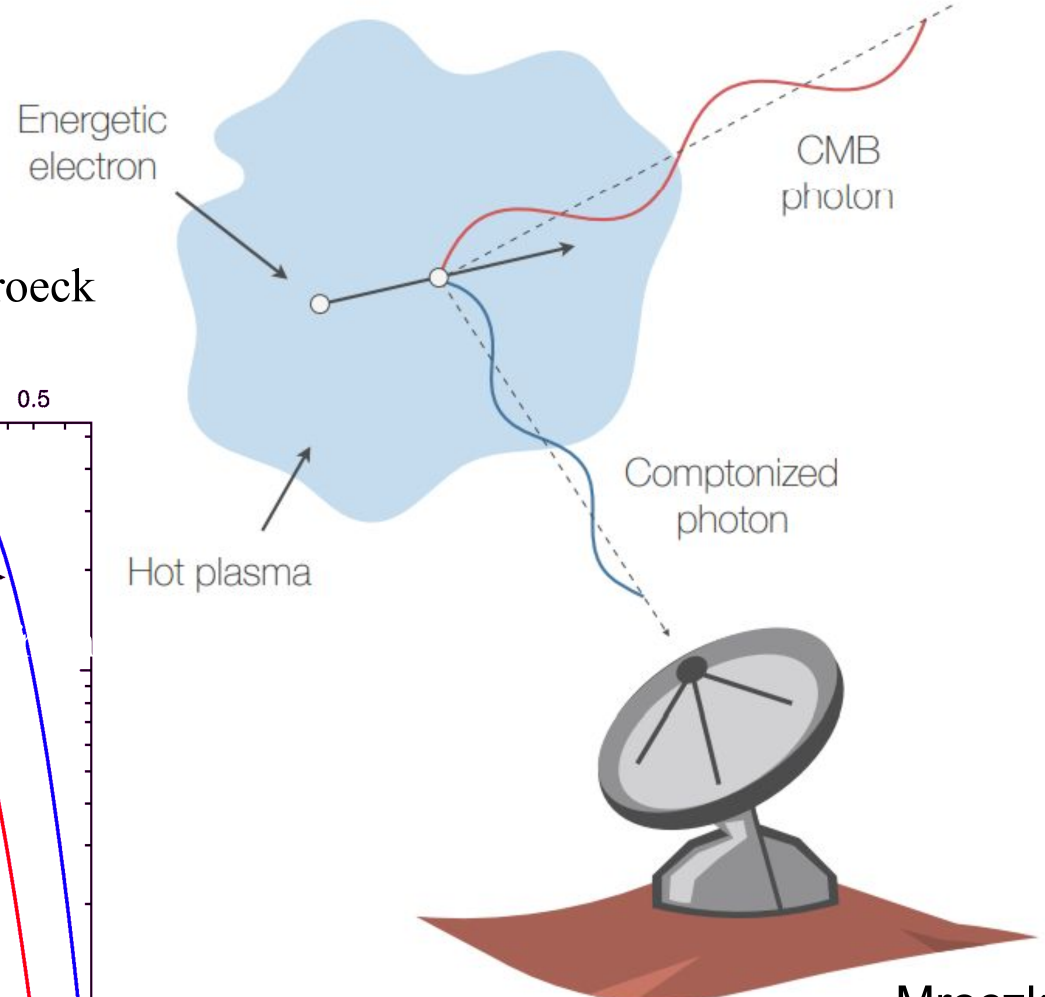

Mroczkowski et al. 2019

Observing the SZ effect

Spectral distortion

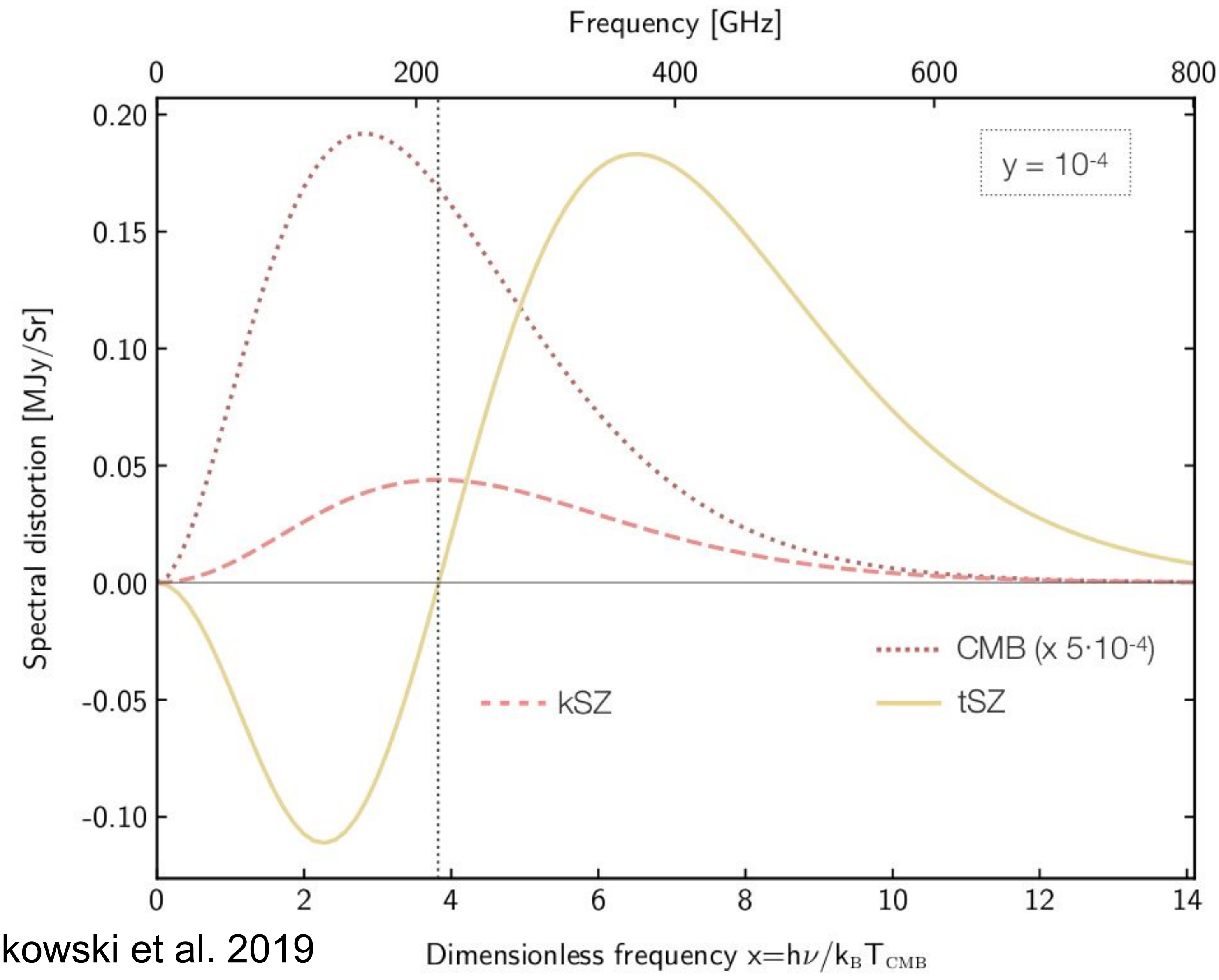

Mroczkowski et al. 2019

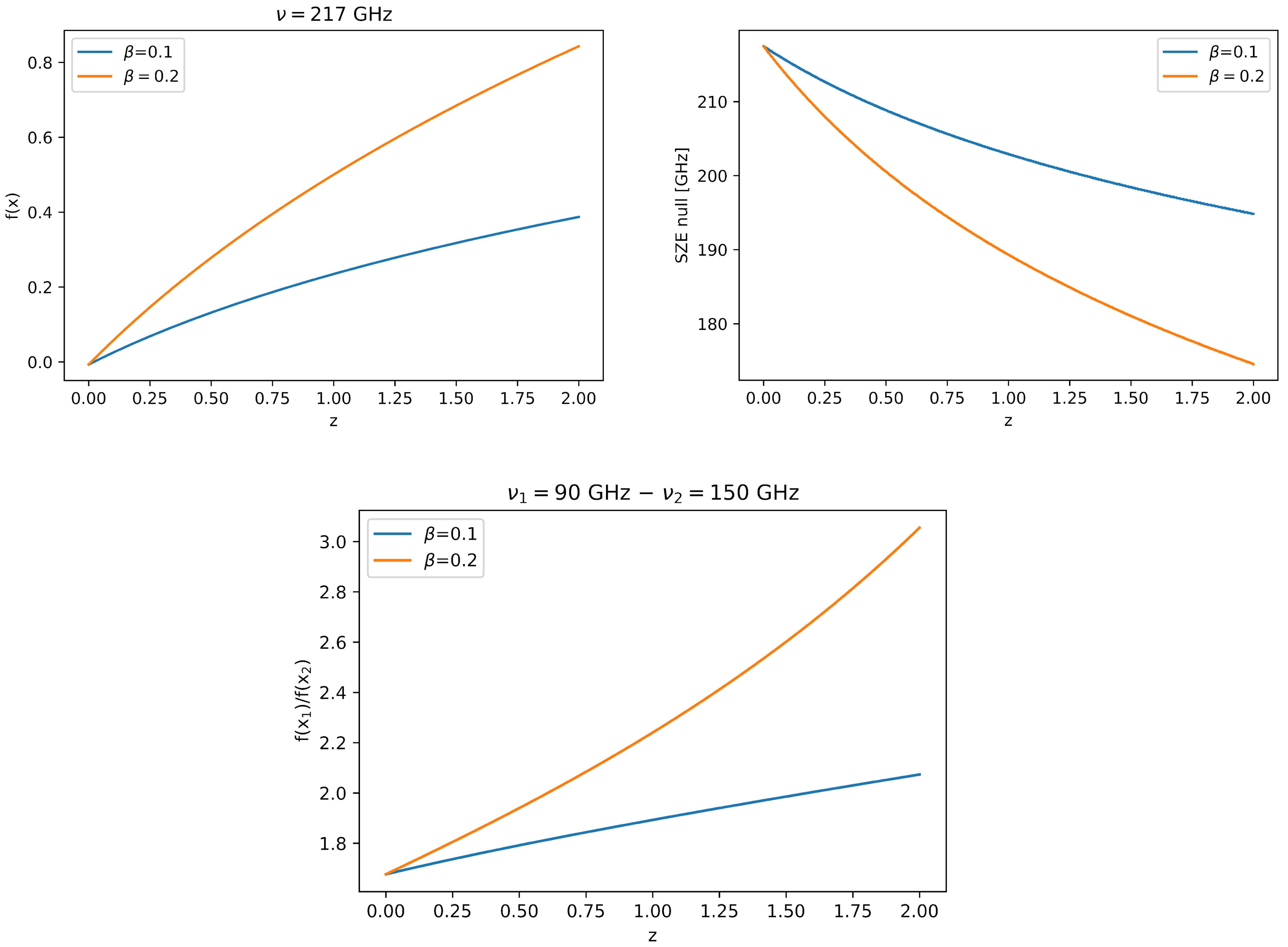

ν = 217 GHz
β=0.1
β = 0.2
f(x)
z
0.0
0.2
0.4
0.6
0.8
0.00
0.25
0.50
0.75
1.00
1.25
1.50
1.75
2.00
SZE null [GHz]
180
190
200
210
ν1 = 90 GHz − ν2 = 150 GHz
β=0.2
f(x1)/f(x2)
1.8
2.0
2.2
2.4
2.6
2.8
3.0

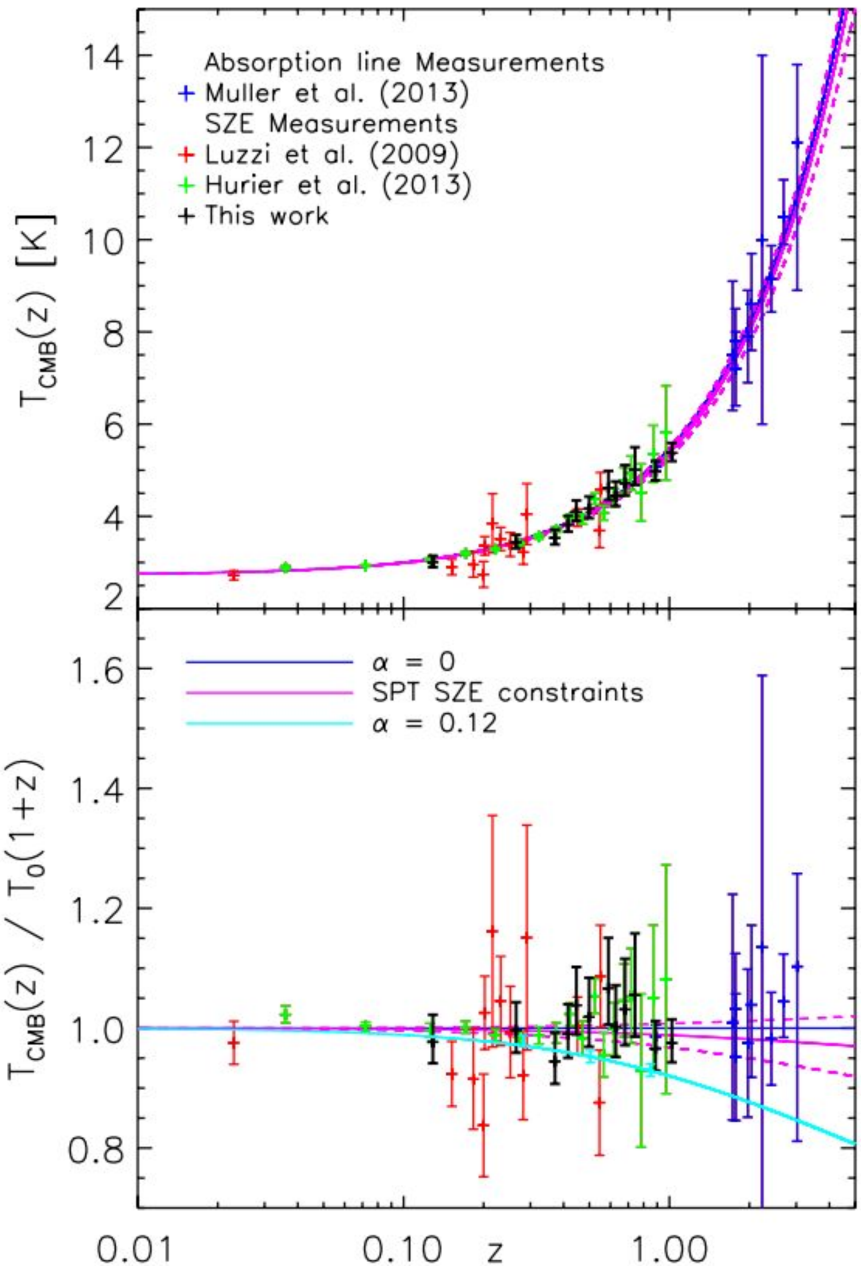

Saro et al. 2014

Method	Reference	z	N	$T_{\rm CMB}$ (K)	β	Label
SZ effect towards clusters	Saro et al. (2014) [18]	$0.055-1.350$	158	-	0.017 ± 0.030	[a]
		$0.3-1.350$		-	0.016 ± 0.031	[b]
	de Martino et al. (2015) [15]	< 0.3	481	-	-0.007 ± 0.013	[c]
	Luzzi et al. (2015) [16]	$0.011-0.972$	103	-	0.012 ± 0.016	[d]
		$0.011-0.972$	99	-	0.014 ± 0.016	[e]
		$0.3-0.972$	33	-	0.020 ± 0.017	[f]
	Luzzi et al. (2009) [14]	$0.023-0.546$	13	-	0.065 ± 0.080	[g]
		$0.200-0.546$	7	-	0.044 ± 0.087	[h]
		$0.3-0.546$	2	-	0.05 ± 0.14	[i]
	Hurier et al. (2014) [17]	$0-1$	813	-	0.009 ± 0.017	[j]
		$0.30-0.35$	81	3.562 ± 0.050	-0.006 ± 0.022	[k]
		$0.35-0.40$	50	3.717 ± 0.063		
		$0.40-0.45$	45	3.971 ± 0.071		
		$0.45-0.50$	26	3.943 ± 0.112		
		$0.50-0.55$	20	4.380 ± 0.119		
		$0.55-0.60$	18	4.075 ± 0.156		
		$0.60-0.65$	12	4.404 ± 0.194		
		$0.65-0.70$	6	4.779 ± 0.278		
		$0.70-0.75$	5	4.933 ± 0.371		
		$0.75-0.80$	2	4.515 ± 0.621		
		$0.85-0.90$	1	5.356 ± 0.617		
		$0.95-1.00$	1	5.813 ± 1.025		
QSO absorption lines	Muller et al. (2013) [19]	0.89	1	$5.0791^{+0.0993}_{-0.0994}$	0.005 ± 0.022	[l]
	Noterdeame et al. (2011) [20]	1.7293	1	$7.5^{+1.6}_{-1.2}$		
		1.7738	1	$7.8^{+0.7}_{-0.6}$		
		2.0377	1	$8.6^{+1.1}_{-1.0}$		
	Cui et al. (2005) [21]	1.77654	1	7.2 ± 0.8		
	Ge et al. (2001) [22]	1.9731	1	7.9 ± 1.0		
	Srianand et al. (2000) [23]	2.33771	1	$6-14$		
	Srianand (2008) [24]	2.4184	1	9.15 ± 0.72		
	Noterdaeme et al. (2010) [25]	2.6896	1	$10.5^{+0.8}_{-0.6}$		
	Molaro et al. (2002) [26]	3.025	1	$12.1^{+1.7}_{-3.2}$		

Avgoustidis et al. 2019

H_0 constraints from X-ray and SZE observations

- Very simple idea that traces back to the work Cavaliere et al. (1977 $E \propto \int n_e^2 dl$
- It is $A \propto \int n_e dl$ on a distance-measuring techniques that depend on a comparison of 2 observables:

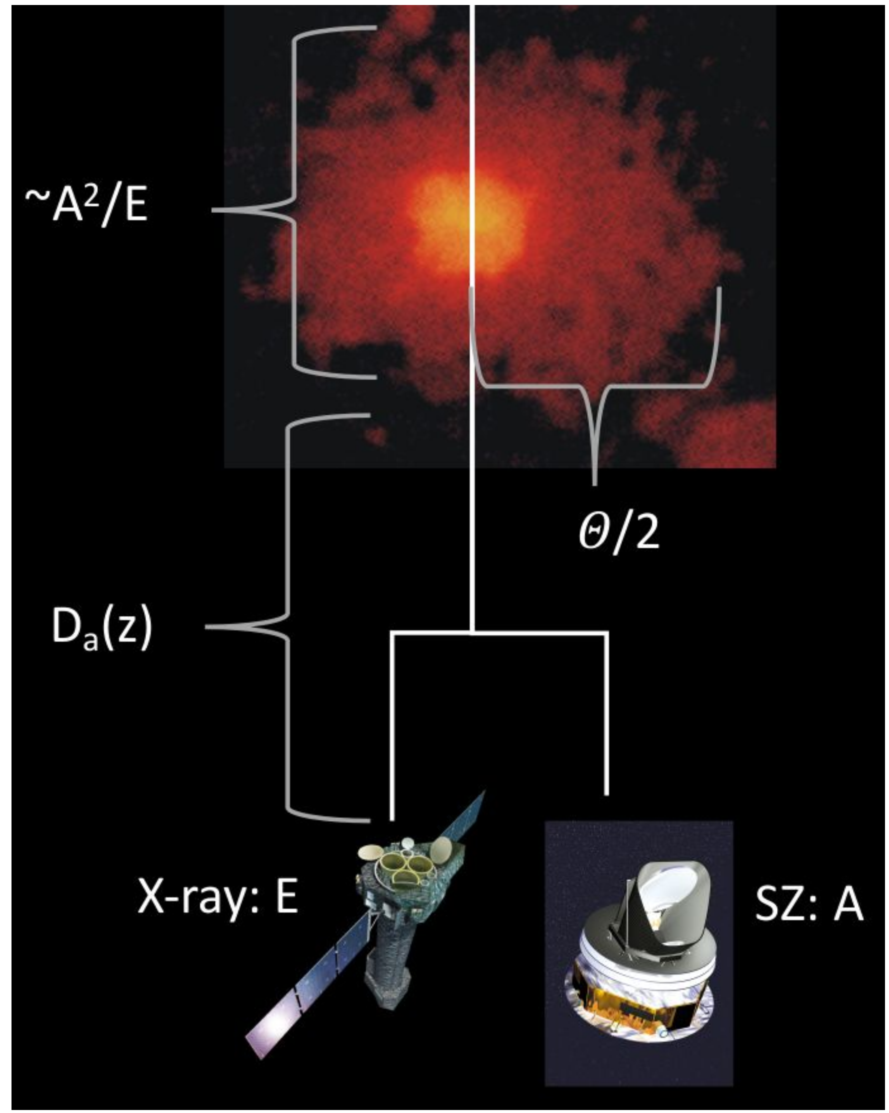

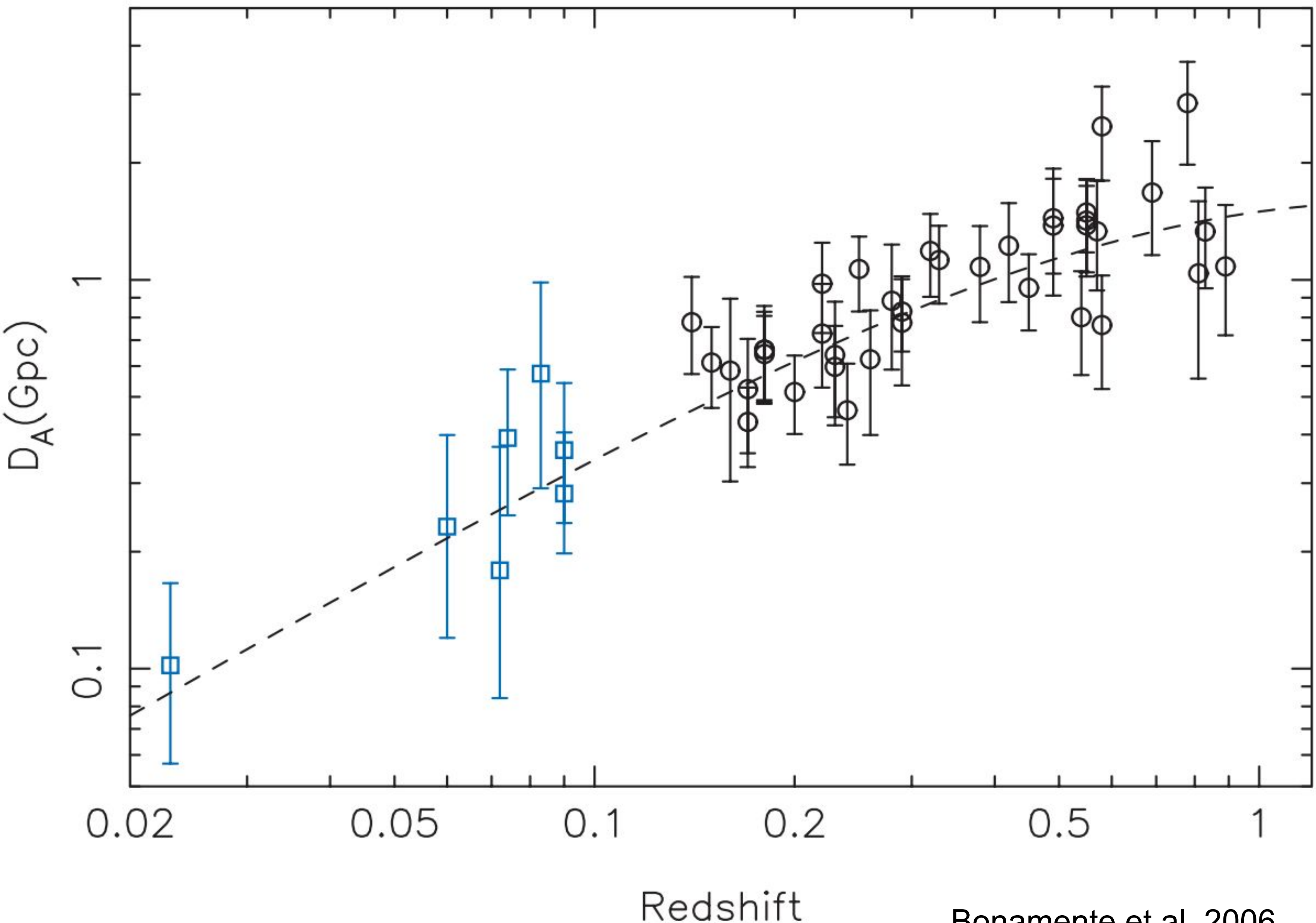

Bonamente et al. 2006

- Birkinshaw (1979)
- Reese et al. (2000)
- Patel et al. (2000)
- Mason et al. (2001)
- Reese et al. (2002)
- Sereno (2003)
- Udomprasert et al. (2004)
- Reese et al. (2004)

SZ measurements from RT, OVRO and BIMA, X-ray from ROSAT

Article	Number	redshift	Ω_m, Ω_Λ	value	SZ data source	X-ray data source
Reese et al. (2000)	2	0.55	0.3, 0.7	$63^{+12\,+21}_{-9\,-21}$	OVRO, BIMA	ROSAT
Patel et al. (2000)	1	0.322	0.3, 0.7	$52.2^{+11.4\,+18.5}_{-11.9\,-17.7}$	OVRO, BIMA, MMT[2]	ROSAT, ASCA[3]
Mason et al. (2001)	7	< 0.1	0.3, 0.7	$66^{+14\,+15}_{-11\,-15}$	OVRO	ROSAT
Grainge et al. (2002a)	1	0.143	1, 0	57^{+23}_{-16}	RT	ROSAT, ASCA
Reese et al. (2002)	18	0.14 – 0.78	0.3, 0.7	$60^{+4\,+13}_{-4\,-18}$	OVRO, BIMA	ROSAT
Saunders et al. (2003)	1	0.217	0.3, 0.7	85^{+20}_{-17}	RT	ROSAT, ASCA
Reese (2004)	26	0 – 0.78	0.3, 0.7	$61 \pm 3 \pm 18$	RT, OVRO, BIMA	ROSAT
Battistelli et al. (2003)	1	0.0231	0.27, 0.73	84 ± 26	OVRO, WMAP[4], MITO[5]	ROSAT
Udomprasert et al. (2004)	7	< 0.1	0.3, 0.7	$67^{+30\,+15}_{-18\,-6}$	CBI	ROSAT, ASCA, BeppoSAX[6]
Schmidt et al. (2004)	3	0.09 – 0.45	0.3, 0.7	69 ± 8	various	Chandra
Jones et al. (2005)	5	0.14 – 0.3	0.3, 0.7	$66^{+11\,+9}_{-10\,-8}$	RT	ROSAT, ASCA
Bonamente et al. (2006)	38	0.14 – 0.89	0.3, 0.7		OVRO, BIMA	Chandra
	double β-model with HSE			$76.9^{+3.9\,+10.0}_{-3.4\,-8.0}$		
	isothermal β-model			$73.7^{+4.6\,+9.5}_{-3.8\,-7.6}$		
	isothermal β-model with excised core			$77.6^{+4.8\,+10.1}_{-4.3\,-8.2}$		

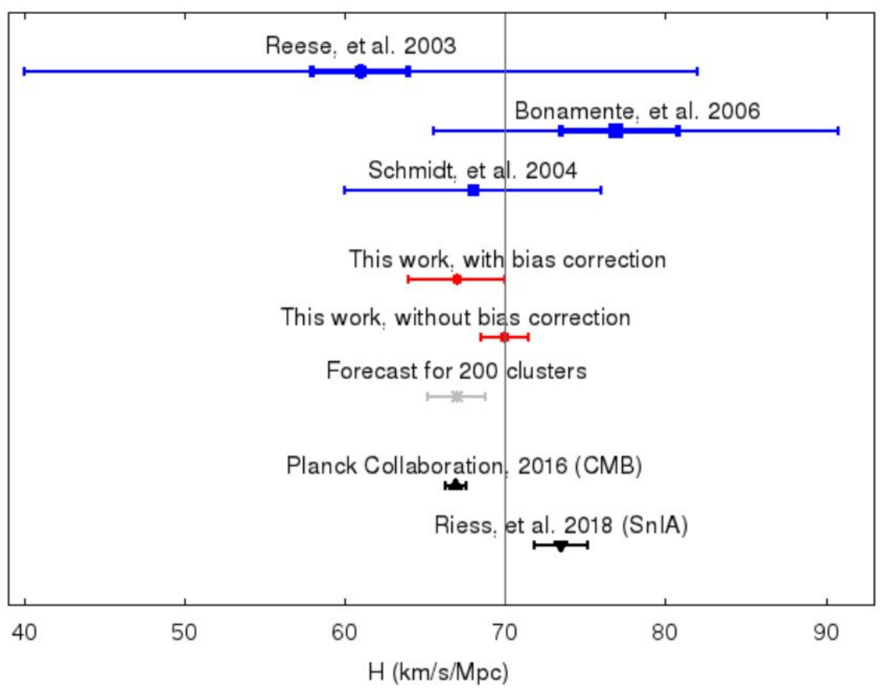

61 galaxy clusters with redshifts up to z < 0.5 observed with Planck and XMM-Newton: $H_0 = 67 \pm 3$km s^{-1} Mpc^{-1}

Kozmanyan et al. 2019

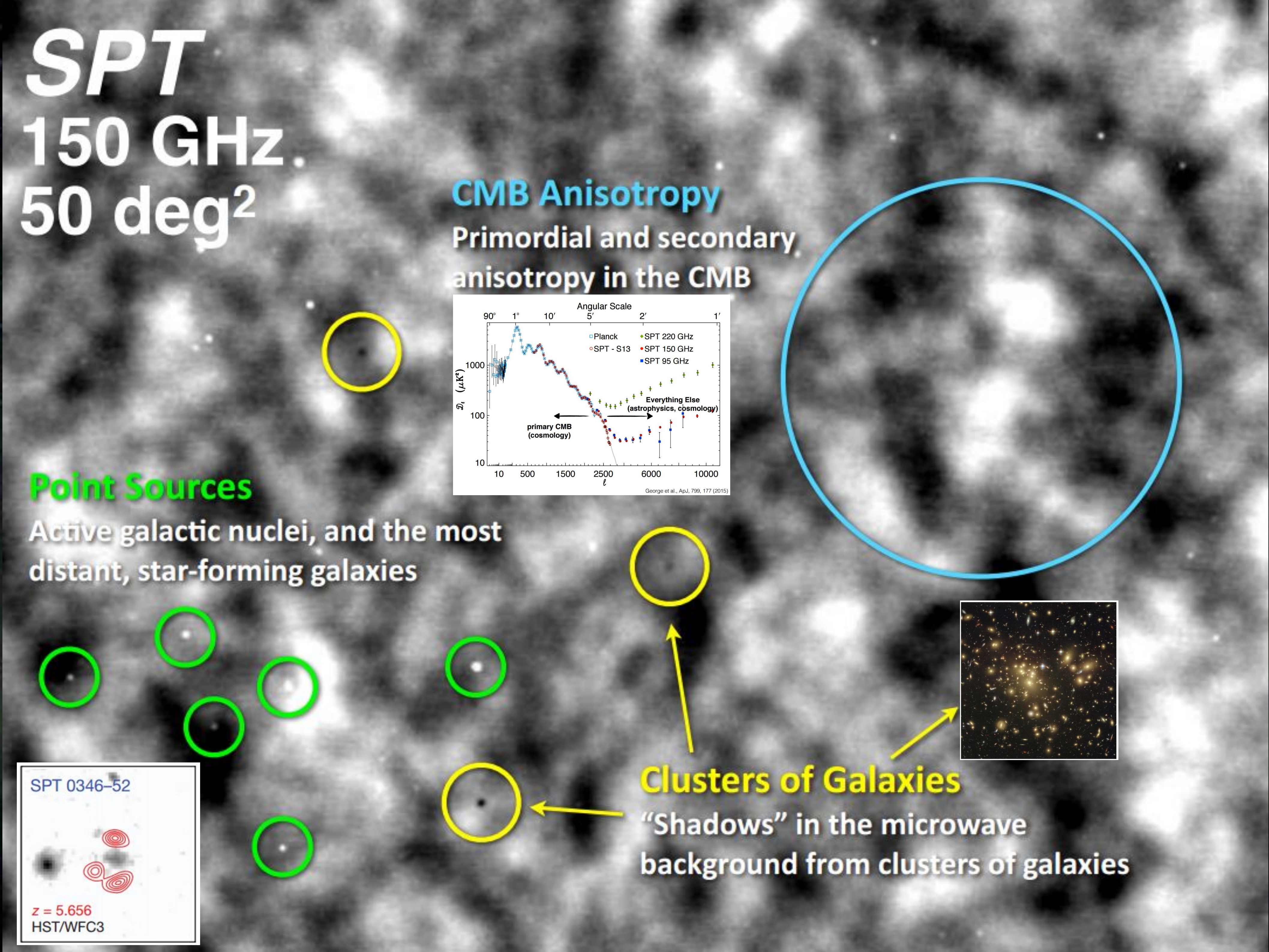
SPT
150 GHz
50 deg²
CMB Anisotropy
Primordial and secondary anisotropy in the CMB
Angular Scale
90° 1° 10′ 5′ 2′ 1′
Planck
SPT - S13
SPT 220 GHz
SPT 150 GHz
SPT 95 GHz
Everything Else
(astrophysics, cosmology)
primary CMB
(cosmology)
$\mathcal{D}_\ell$ (μK^2)
1000
100
10
10 500 1500 2500 6000 10000
ℓ
George et al., ApJ, 799, 177 (2015)
Point Sources
Active galactic nuclei, and the most distant, star-forming galaxies
SPT 0346–52
z = 5.656
HST/WFC3
Clusters of Galaxies
"Shadows" in the microwave background from clusters of galaxies

Table 1. Conversion factors for tSZ Compton parameter y to CMB temperature units and the FWHM of the beam of the *Planck* channel maps.

Frequency [GHz]	$T_{CMB}\ g(\nu)$ [K_{CMB}]	FWHM [arcmin]
100	−4.031	9.66
143	−2.785	7.27
217	0.187	5.01
353	6.205	4.86
545	14.455	4.84
857	26.335	4.63

NILC tSZ map

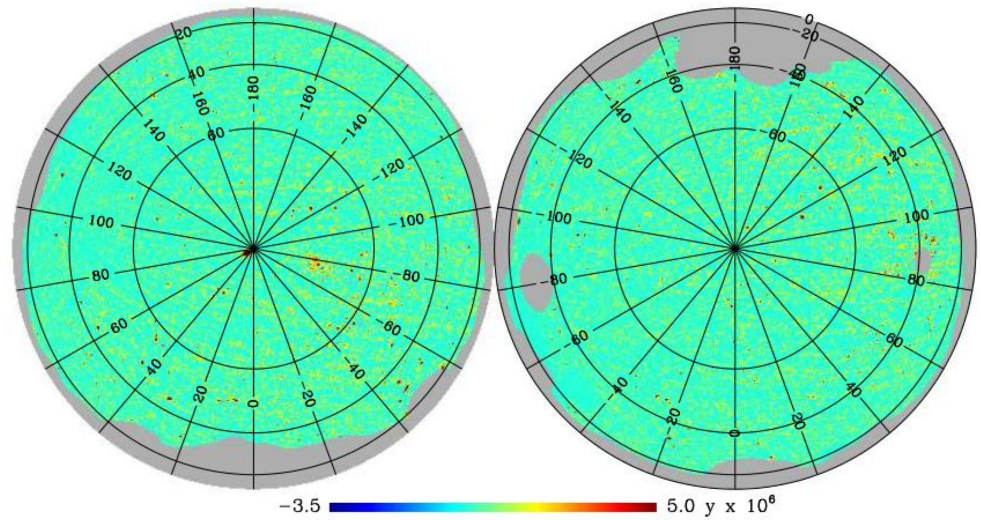

NILC tSZ map

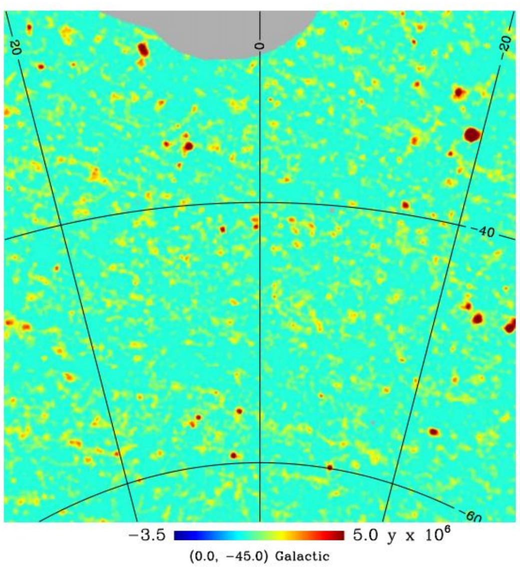

MILCA tSZ map

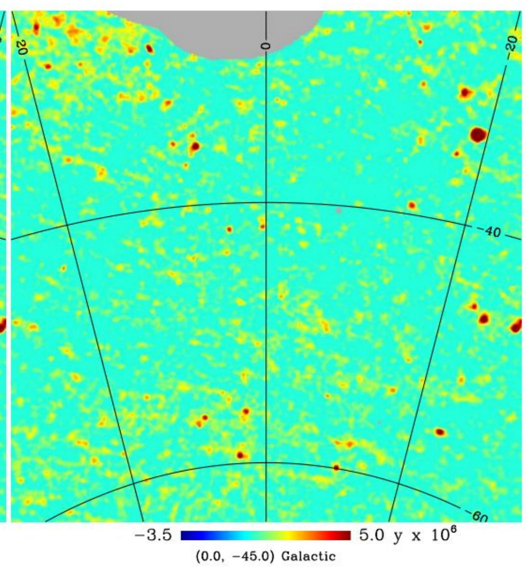

MILCA tSZ map

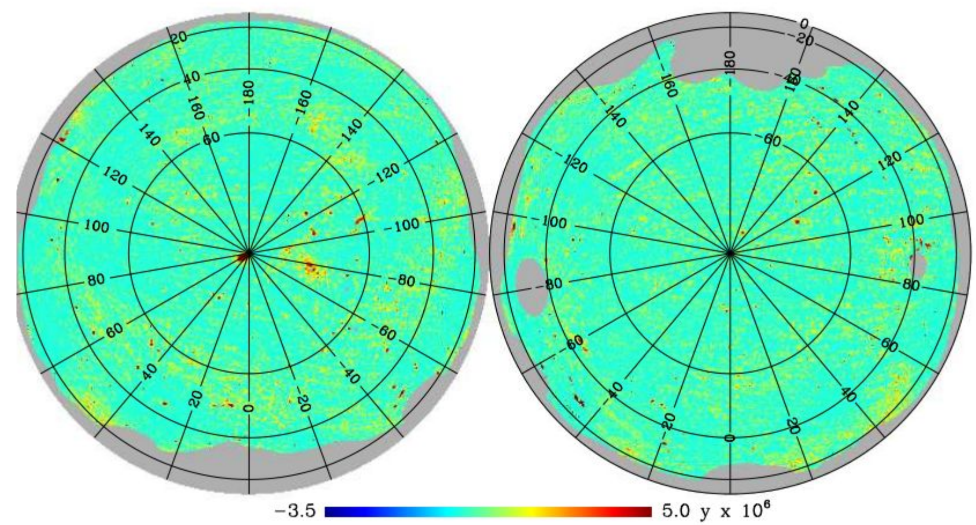

Planck 2013 results. XXI

Planck's view of galaxy clusters

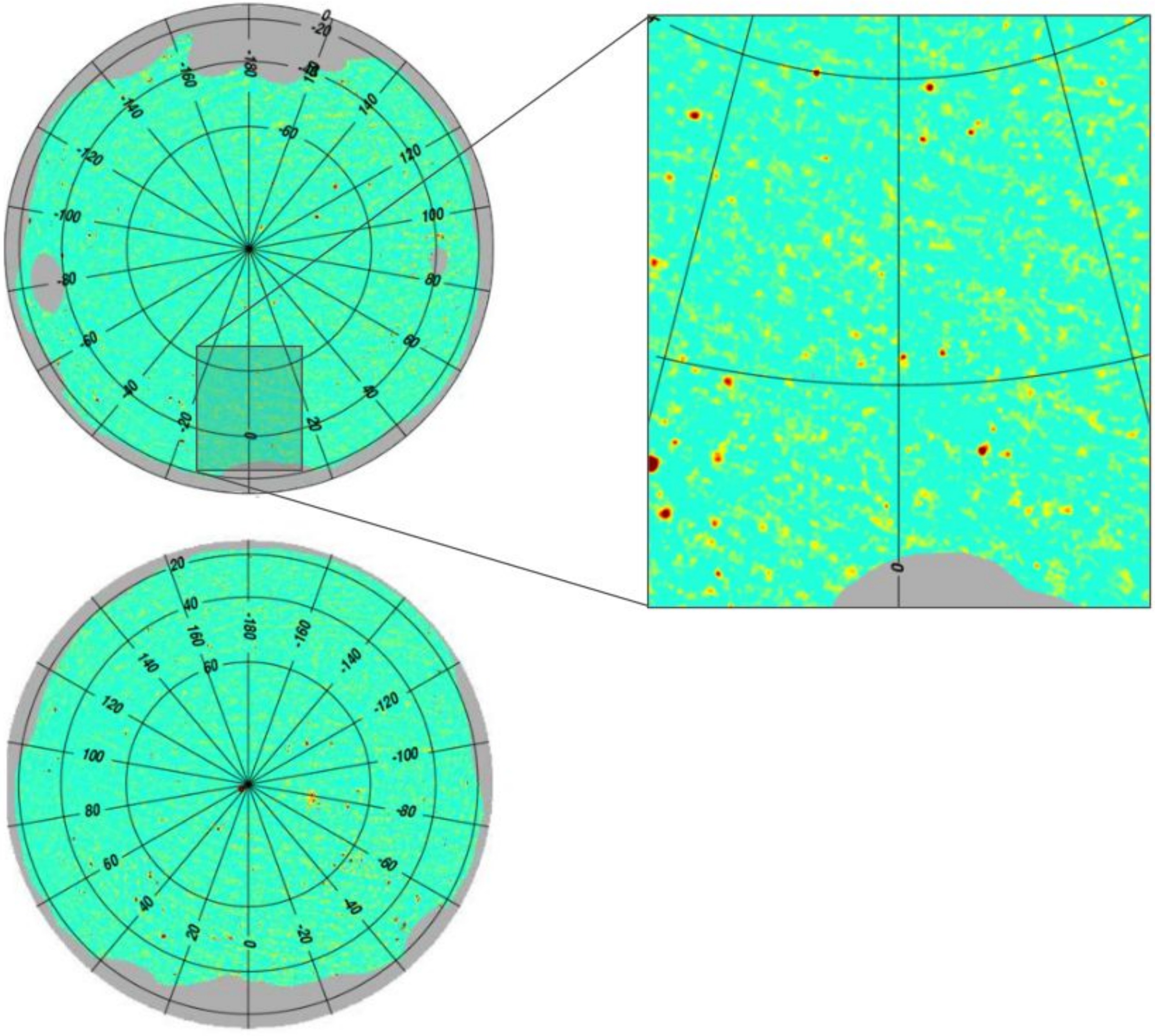

Adapted from Planck 2015 XXII

Observing the SZ effect

Planck's view of galaxy clusters

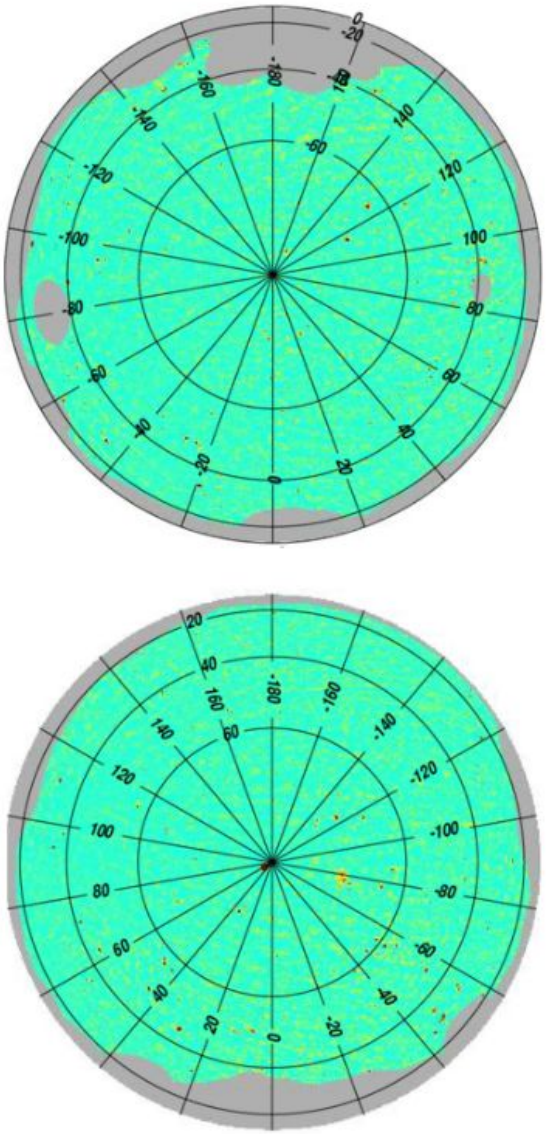

Adapted from Planck 2015 XXII

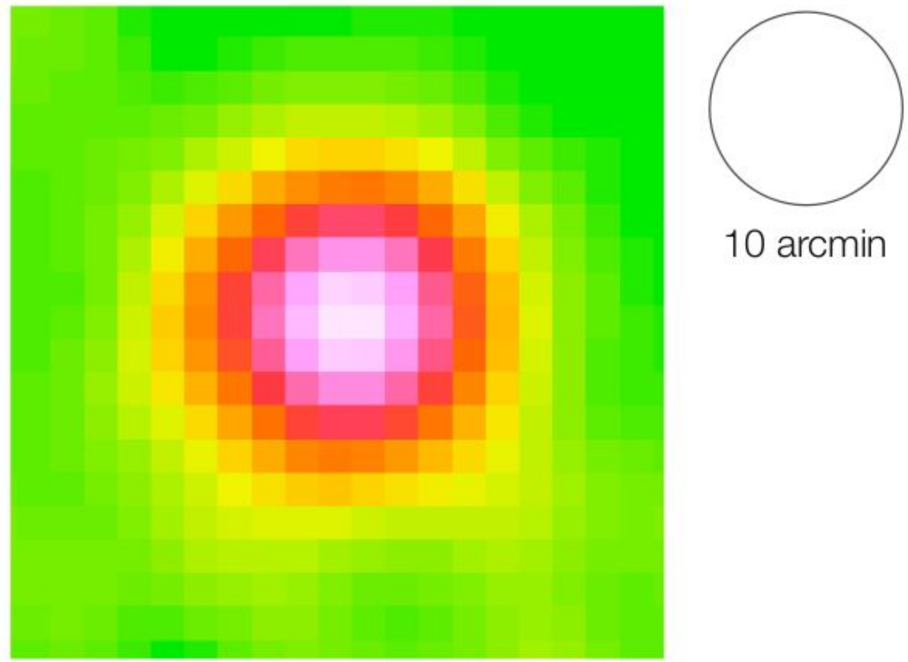

Planck Legacy Archive

Observing the SZ effect

Planck's view of galaxy clusters

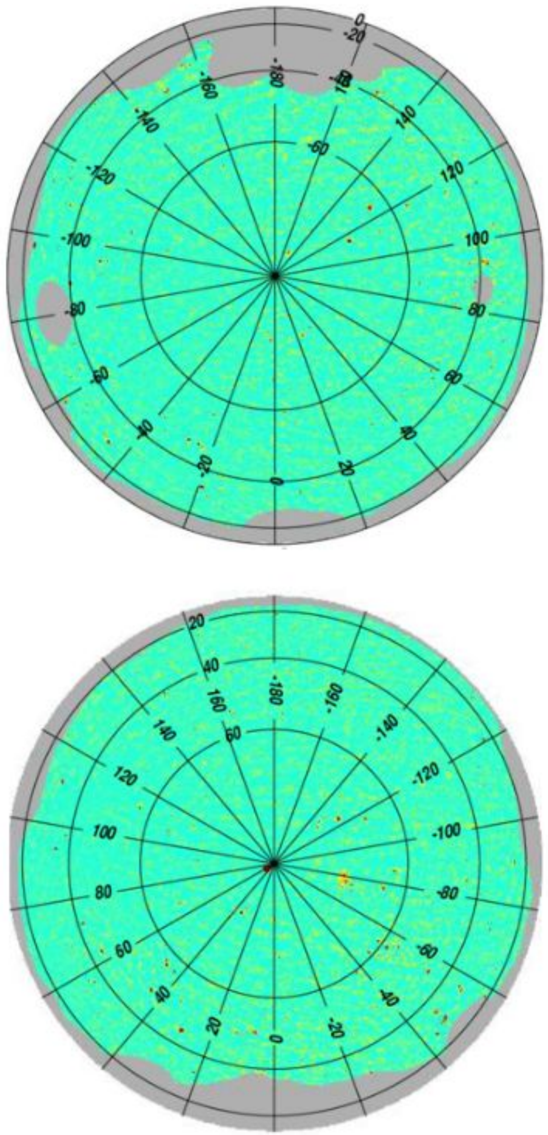

Adapted from Planck 2015 XXII

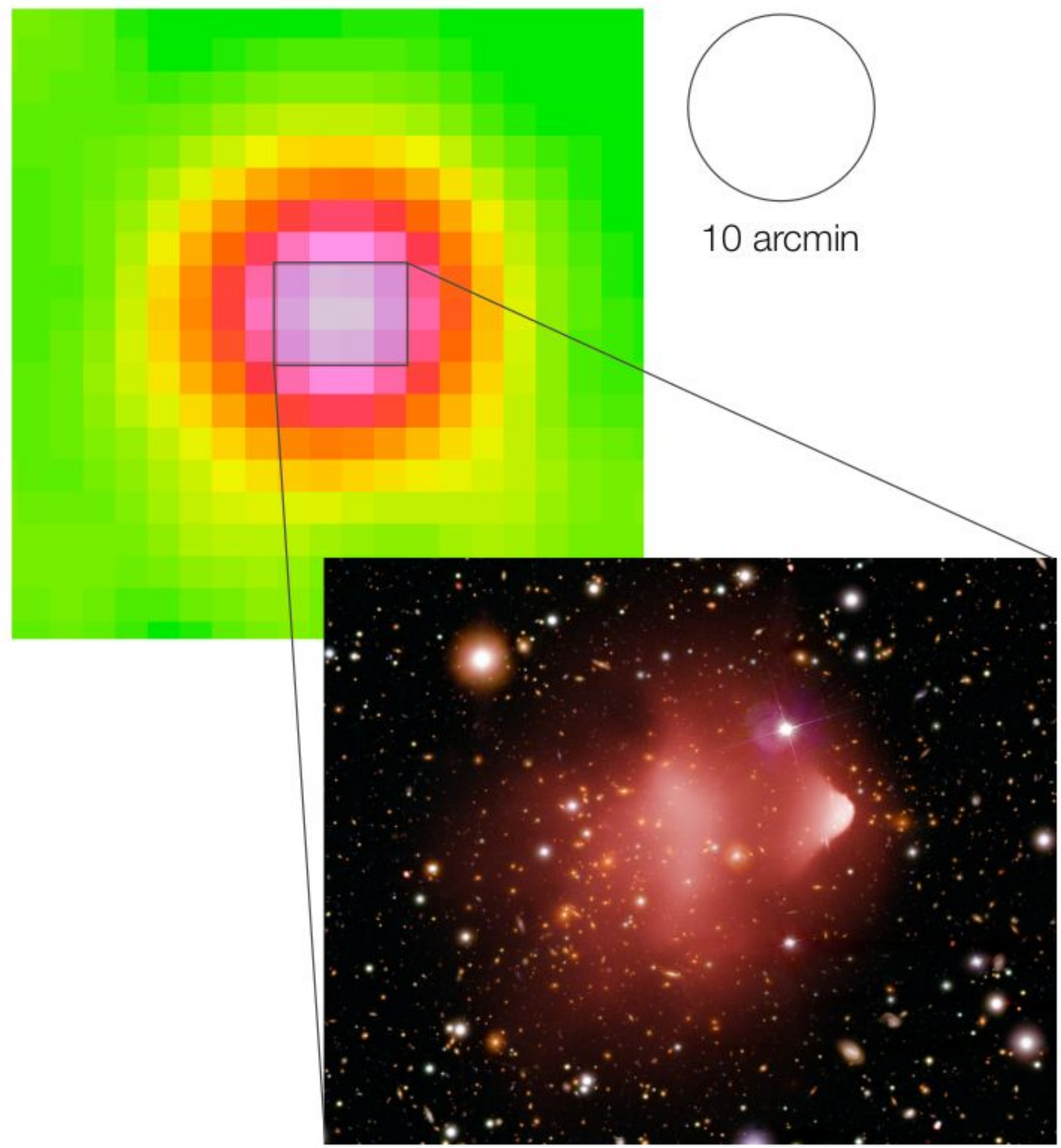

Chandra+HST

The South Pole Telescope (SPT)

10-meter
submm wave telescope

100 150 220 GHz and
1.6 1.2 1.0 arcmin resolution

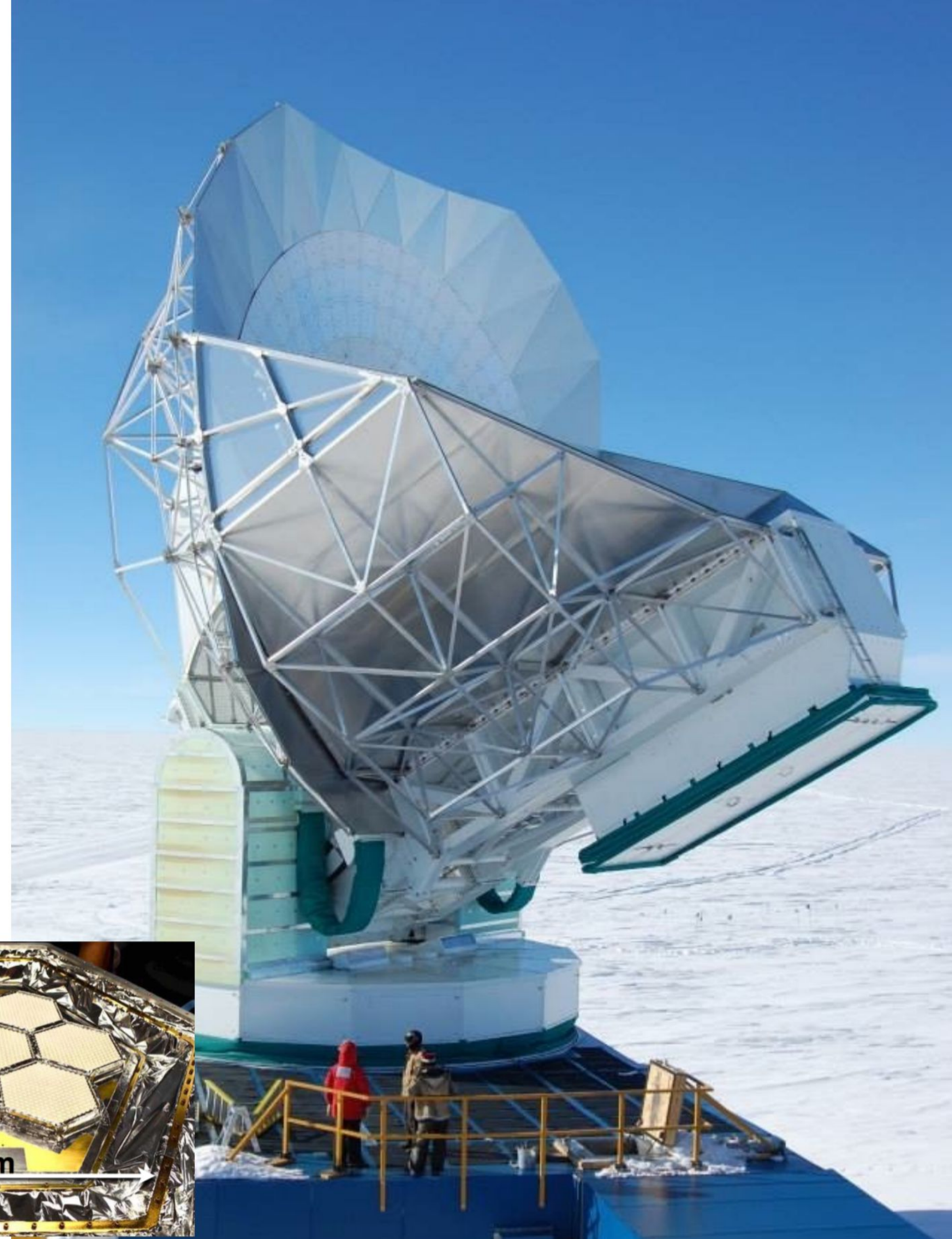

2007: SPT-SZ
960 detectors (UCB)
100,150,220 GHz

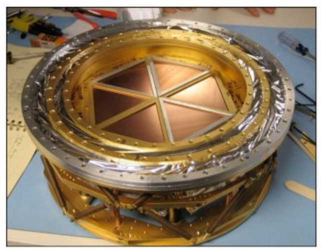

2012: SPTpol
1600 detectors
100,150 GHz
+Polarization

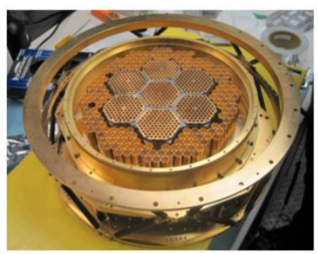

2016: SPT-3G
16,000 detectors
100,150, 220 GHz
+Polarization

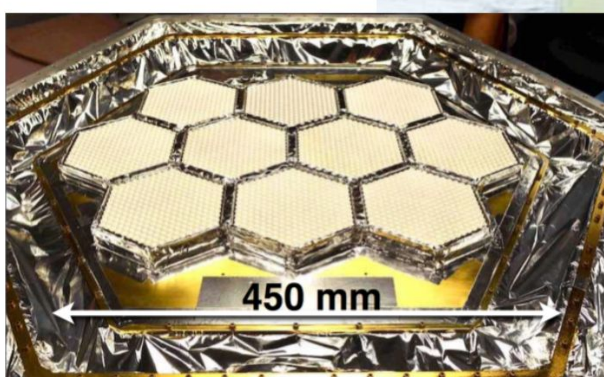

SPT Survey

The SPT Surveys 5000 deg²

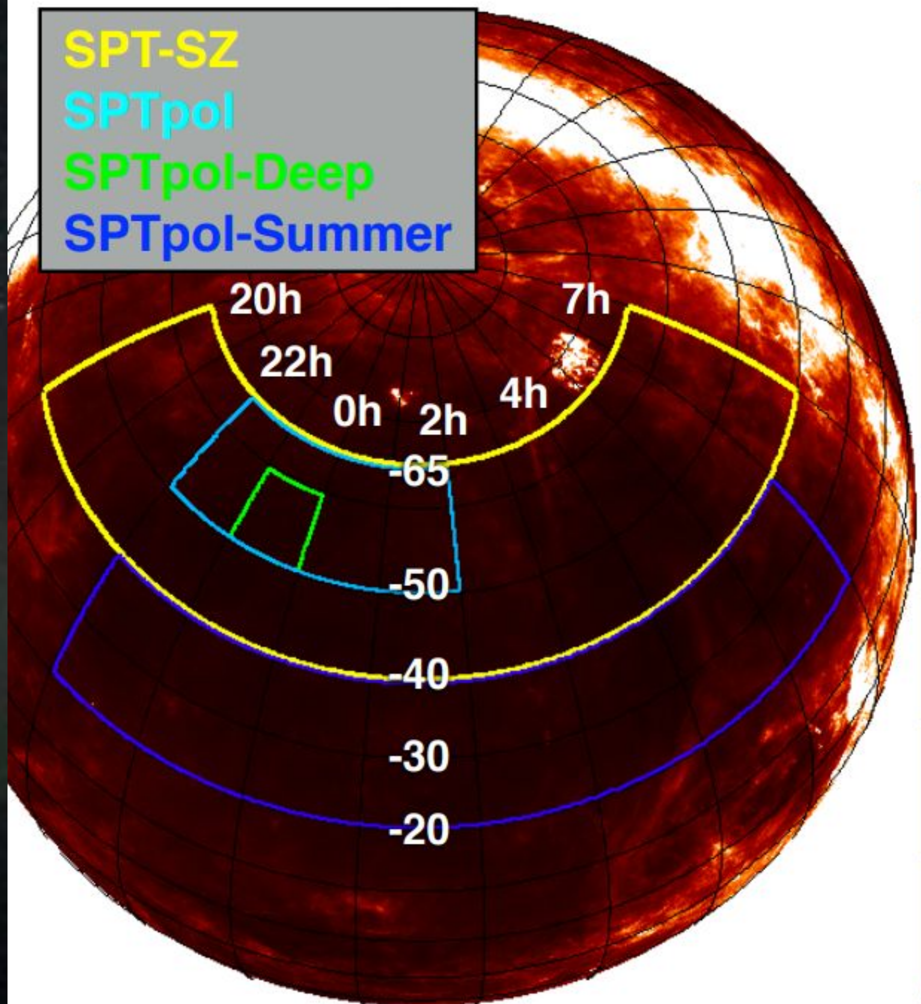

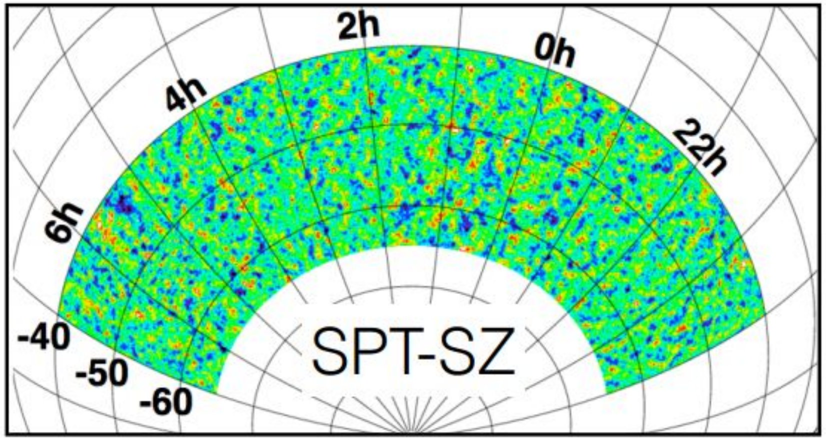

	Obs. Years	Area (deg²)	95 GHz (uK-arcmin)	150 (uK-arcmin)	220 (uK-arcmin)
SPT-SZ	2007-11	2500	40	17	80
SPTpol-Main	2012-16	500	13	5	-
SPTpol-Deep	2012-16	100	10	3.5	-
SPTpol-Summer	2012-16	2500	47	28	-
SPT-3G *(projected)*	2018-21	1500	2.8	2.6	6.6

SPT Survey

The SPT Surveys 5000 deg²

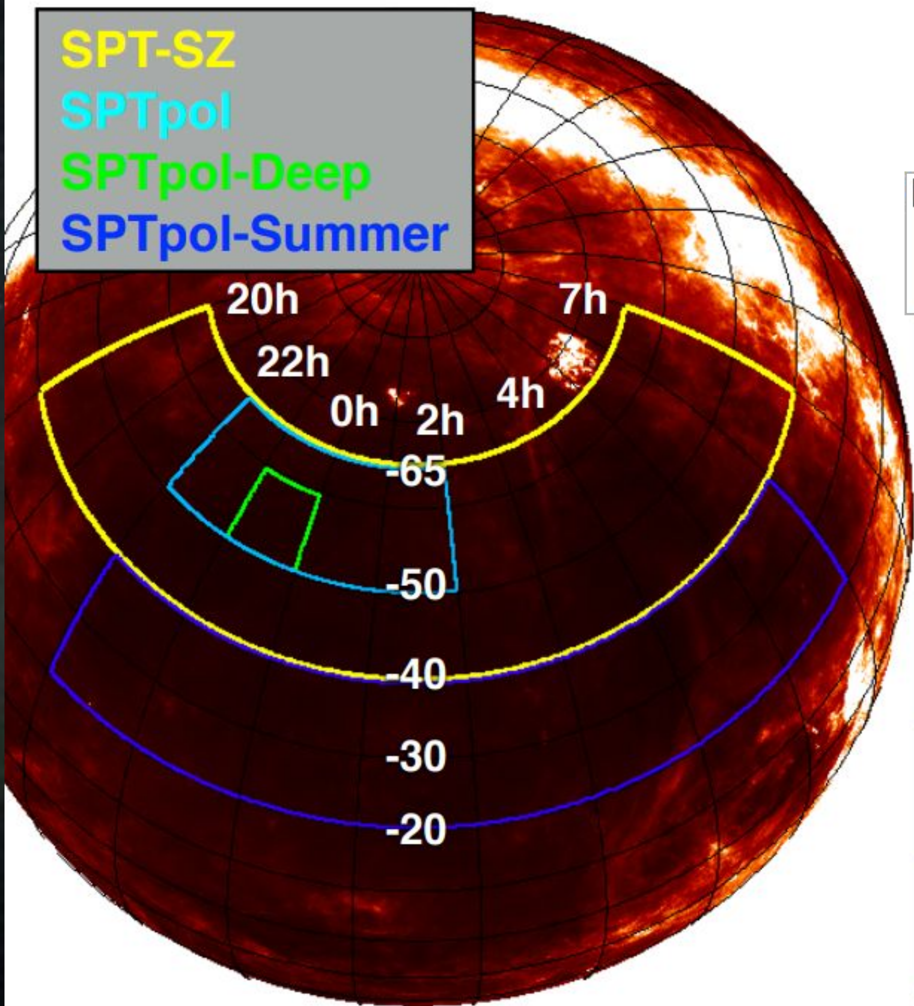

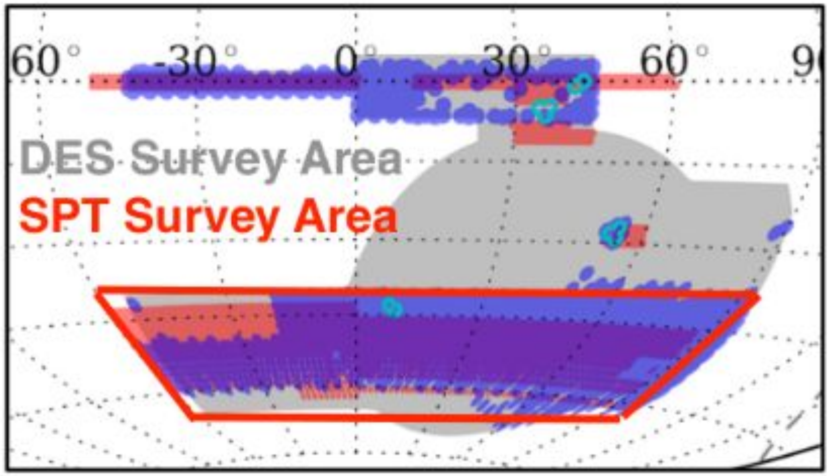

	Obs. Years	Area (deg^2)	95 GHz (uK-arcmin)	150 (uK-arcmin)	220 (uK-arcmin)
SPT-SZ	2007-11	2500	40	17	80
SPTpol-Main	2012-16	500	13	5	-
SPTpol-Deep	2012-16	100	10	3.5	-
SPTpol-Summer	2012-16	2500	47	28	-
SPT-3G *(projected)*	2018-21	1500	2.8	2.6	6.6

<date/time>

South Pole Telescope

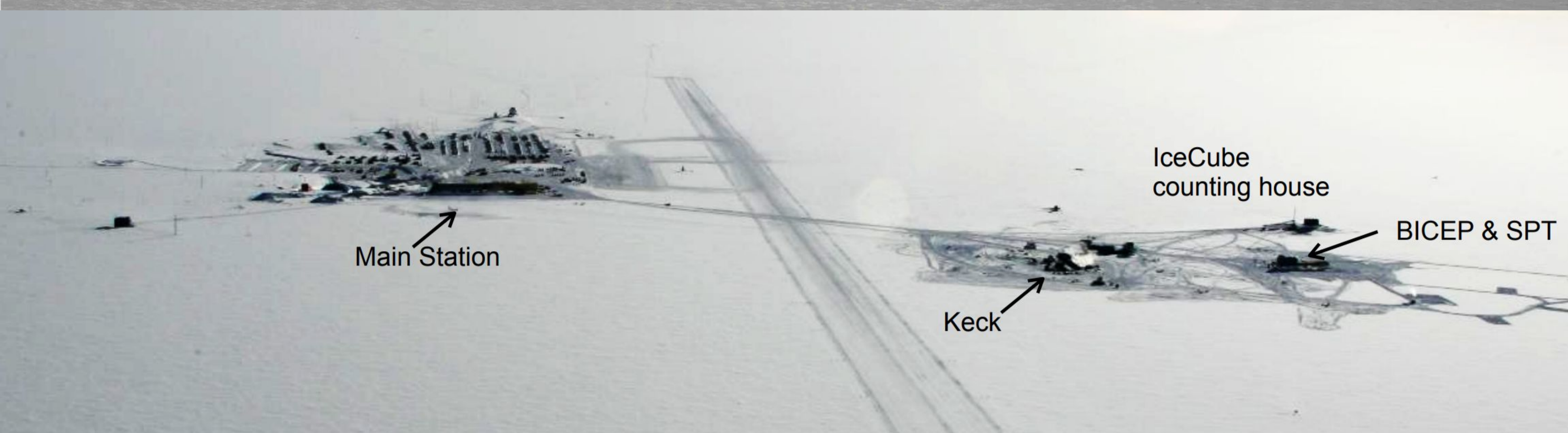

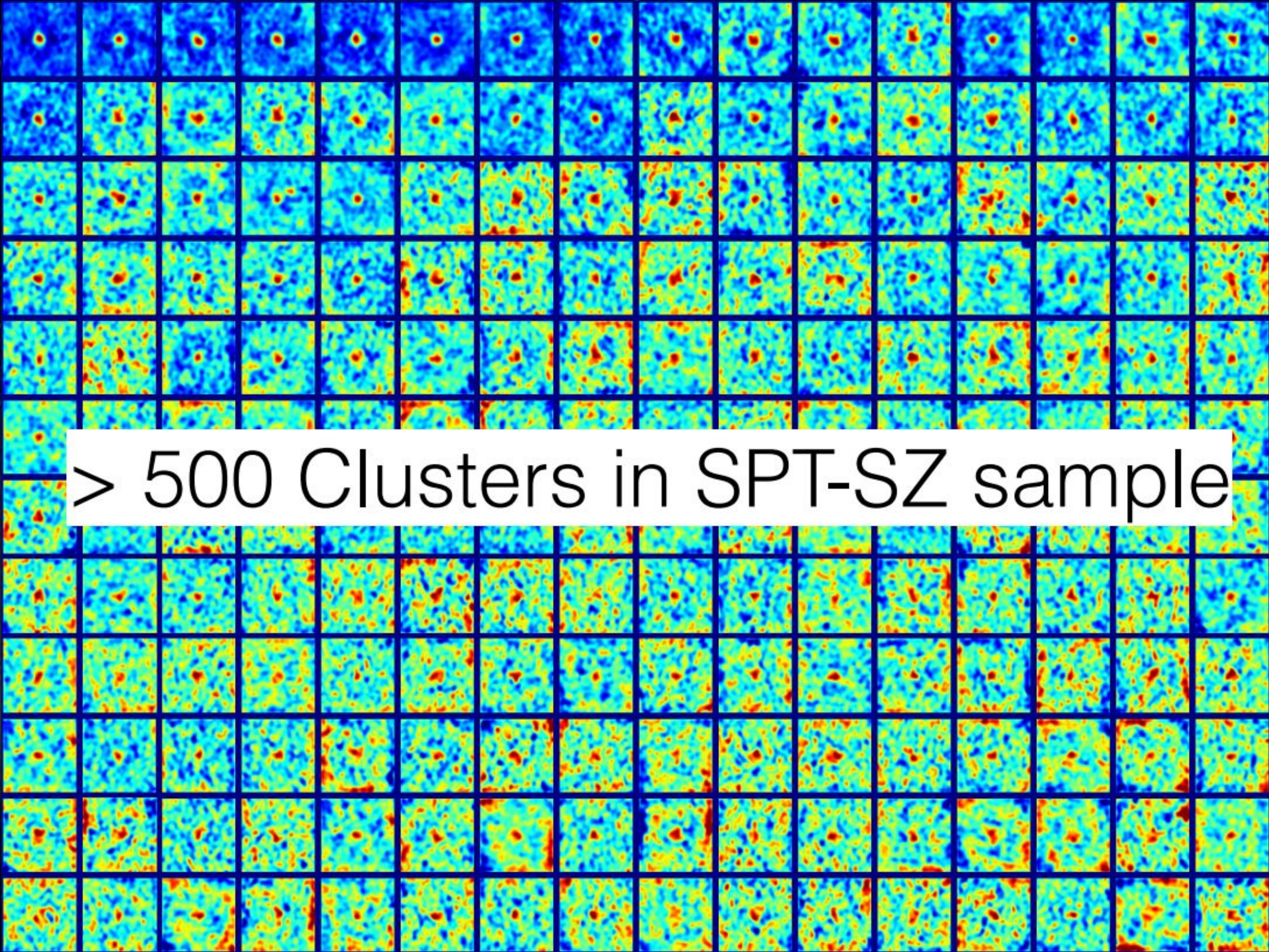
> 500 Clusters in SPT-SZ sample

SPT-SZ Sample

Song+12, Bleem+15

- 2500 deg^2 sample
  - 516 at ξ>4.5
  - 387 at ξ>5.0

Bleem+15

- High z subsample
  - ~150 (80) > 0.8
  - ~ 70 (40) at z>1
  - Max z_{spec}=1.47

Bayliss+13, Khullar+19

  - Highest phot-z

Strazzullo+19

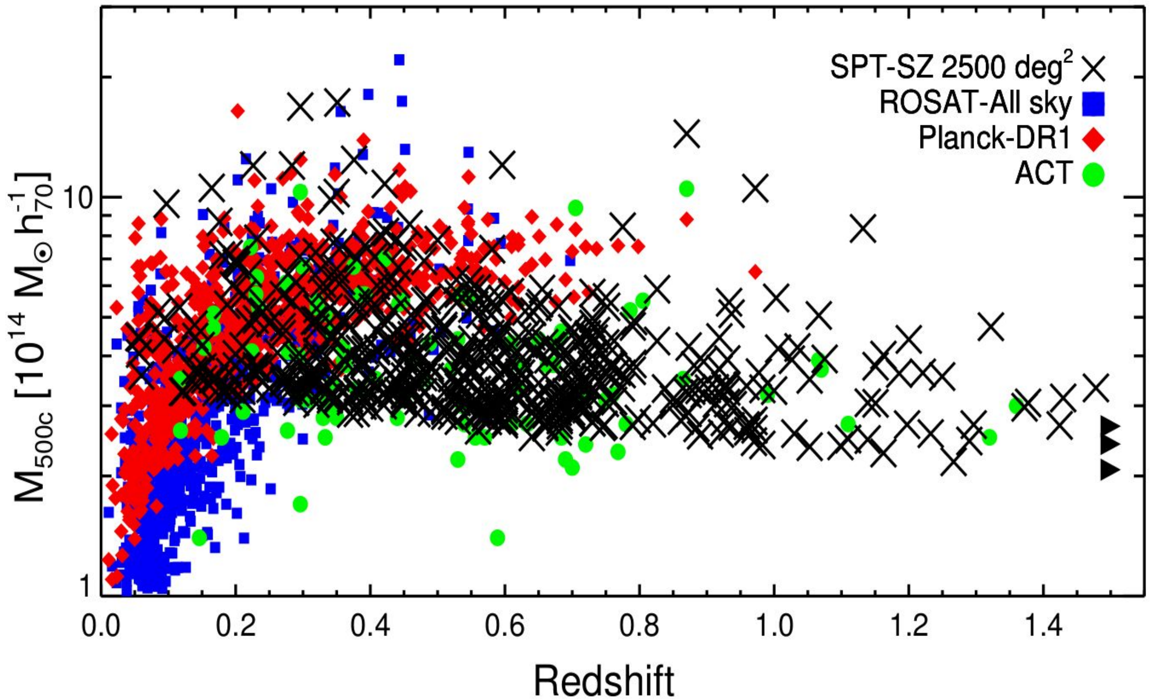

- Clean sample with M_{500}>3x10^{14} M_o to z~1.8
- Easy to use it for Cosmology and Astrophysics!!